Development of a Fast and Efficient Macromodel for Nonuniform Electromagnetic Field Excitation of Transmission Lines

by

Sina Mashayekhi

A thesis submitted to

the Faculty of Graduate Studies

in partial fulfilment of

the requirements for the degree of

Master of Science

Department of Electrical and Computer Engineering

Faculty of Graduate Studies

University of Manitoba

Winnipeg, Manitoba, Canada

Acknowledgment

To my beloved parents

Abstract

In this thesis, the problem of overvoltage calculation on multiconductor transmission lines due to nonuniform external electromagnetic field excitations, such as lightning, is investigated by introducing a field-voltage macromodel. The main purpose of this thesis is to find a fast and efficient algorithm to model the effect of the radiated electromagnetic fields on transmission lines. This is done by replacing distributed voltage and current sources along the transmission line which are as a result of external electromagnetic field radiation, by voltage and current sources at the terminals of the transmission line. For this purpose, the knowledge of electromagnetic field at every point on the transmission line is required. A transfer function based pole-residue tracing technique will be introduced in this thesis. By using the proposed algorithm, a closed form solution for the lumped sources at the terminals of transmission line in the frequency domain is obtainable. This approach will enable us to bridge the software working in frequency domain with those working in the time domain. The effect of different parameters on calculated overvoltage such as finite conductivity of the ground and lightning return stroke channel (RSC) specifications are studied. The theoretical background and extent of validity of the proposed algorithm are reviewed in this thesis.

Table of Contents

List of Figures

List of Tables

Nomenclature

2D   Two dimensional

3D   Three dimensional

DFT   Discrete Fourier Transform

DT   Discrete Time

E   Electric Field

EM   Electromagnetic

FDTD   Finite Difference Time Domain

FEM   Finite Element Method

FFT   Fast Fourier Transform

IFFT   Inverse Fast Fourier Transform

LEMP   Lightning Electromagnetic Pulse

LTI   Linear Time Invariant

M   Magnetic Field

MOR   Model Order Reduction

MTL   Multiconductor Transmission Line

MTLE   Modified Transmission Line with Exponential current attenuation

MTLL   Modified Transmission Line with Linear current attenuation

NEC   Numerical Electromagnetic Codes

RSC   Return Stroke Channel

TL   Transmission Line

TLine   Transmission Line

Chapter 1

Introduction

1.1   Motivation

The emerge of sensitive electronic equipment and devices which require highly-reliable electric power and, at the same time, are more susceptible to electromagnetic interference (EMI), gives a significant importance to the transmission line analysis research area [7]. Transmission lines are critical components of a power system from an electromagnetic point of view due to their large dimensions. One of the important external sources of interference with the transmission lines is *lightning*. A typical lightning channel consists of large amount of transient current in the range of tens of kilo Amperes and can induce voltage up to thousands Volts [8]. This induced voltage can travel on the line and harm the equipment connected to the network. Accurate knowledge of electromagnetic fields of external excitation is required to calculate the induced voltage on the line by using field-to-line coupling equations. Current methods of calculating the field-to-line effects are based on rigorous and time-consuming techniques which cannot be easily employed for the simulation of large power systems. In this thesis, the main objective is to find an

efficient way to calculate these radiated fields by using macromodel-base algorithms. Need for integration of the frequency domain software result within the time domain simulators is another motivation of this research. As an example, at the end, we will be able to use the result of NEC[1] software (in frequency-domain) to obtain time-domain transient response of an excited line in PSCAD/EMTDC[2], a commonly-used time domain power system simulator.

1.2   Problem Definition

This thesis deals with the problem of lightning return stroke channel radiation electromagnetic fields, transmission line modeling, and coupling of radiated fields to transmission lines. Although there is a massive investigation on the effect of uniform plane-wave coupling to transmission line, the nature of the most of the electromagnetic radiations are nonuniform, especially at close distances of the radiation source. The goal of this thesis is to generalize the excitation type to *nonuniform wave.* Lightning, as an important source of high power nonuniform wave radiation, is used in this work as a source of excitation. To be able to investigate the lightning effects on transmission lines, the lightning channel should be properly modeled. There have been several models proposed for lightning channel such as *Engineering Models* in the time-domain and *Electromagnetic Models* in the frequency-domain which will be used in this research.

Figure 1.1 illustrates the schematic of a lightning return stroke channel (RSC), the transmission lines, and the coupling problem. Assume a finite length transmission line over a lossy ground. During the return-stroke phase of a lightning flash, a very fast transient cur-

---

[1]Numerical Electromagnetic Code
[2]Power Systems Computer Aided Design/Electromagnetic Transients including DC
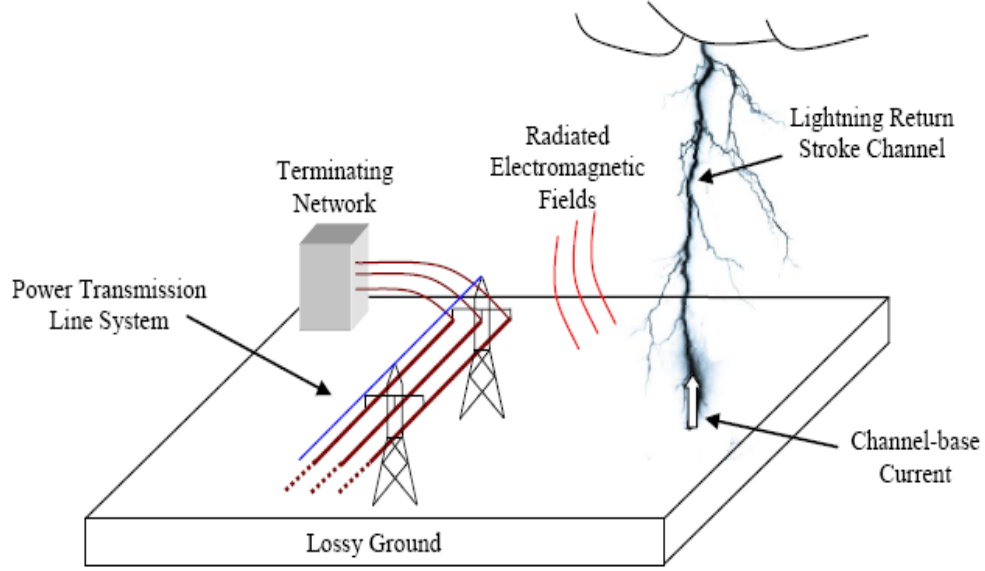
Figure 1.1: Problem definition.

rent pulse starts propagating along the already-established lightning return-stroke channel. As a result, the channel, whose length is in the order of a few kilometers, behaves like a monopole antenna and radiates electromagnetic energy in the surrounding space. Power transmission line systems, due to their expansive length, are very vulnerable to this external source of electromagnetic radiation. The coupled electromagnetic energy generates very strong transients in power distribution systems, which are capable of propagating over long distances. The ideal way of obtaining the induced voltage on a transmission line is to have the EM field information at every point on the line. If the radiated EM fields are uniform plane-wave, the only effect of propagation is delay and can be expressed analytically. However, this is not true for the case of nonuniform waves such as those radiated by lightning RSC.

In this work, the proposed approach is to obtain the transfer function of the *RSC-propagation media* system and then estimate the EM field values by tracing the poles and the residues of the transfer function in the frequency domain. Using this idea, the calculation of the

EM fields will depends on the knowledge of very few points of the propagation space. Additional calculation speed is obtainable using recursive calculations such as recursive convolution.

The validity of the proposed algorithm is verified by comparing the outcomes with measurement data. Finite Difference Time Domain (FDTD) code [4] is also used for validation of the result of plane-wave excitation of the transmission line. Further the numerical software package NEC [9,10], is used to model the lightning return stroke channel (RSC) and compare the obtained electromagnetic fields.

1.3   Thesis Outline

In chapter 2, we are doing the literature review for the problem of transmission lines responce to external electromagnetic field radiation of the lightning RSC. In the first part of this chapter, we will review the lightning phenomenon [1], along with different models proposed for the modeling of RSC [11]. In the second part of chapter 2, we will talk about different methods of analysis of transmission lines in the presence of the external excitation.

In chapter 3, the concept of macromodeling will be discussed and an efficient EM field macromodel which can be used for efficient calculation of radiated EM field of lightning, will be introduced in details. The Vector Fitting algorithm along with different effective parameters on the output of this algorithm will be explained. At the end of this chapter, several examples will follw to verify the proposed field macromodel with measurement data.

In chapter 4, governing equations in transmission lines issue will be derived and we will

see the effect of the external radiation on these equations. The second class of macro-model, voltage macromodel, in which the whole *RSC-EM field-transmission line* system is combined into one single terminal-equivalent model, will be developed. At the end of this chapter, the implementation results of the proposed technique will be compared with those results obtained by measurement. Different sources of radiation such as EMP generator and lightning RSC will be used in this section.

Chapter 5 summarizes the work done in this research and discusses the future works.

Chapter 2

Literature Review

2.1 Lightning

Lightning has been known as an important natural phenomenon which has significant effect on induced transients on cables and transmission lines [12,13]. There have been many research studies on the modeling and measuring of its effects. The interesting parameters which are being studied in measurements are the channel base current, radiated electromagnetic fields, and induced voltages on transmission lines as well as optical measurements. Generally, measurement is costly, cumbersome and time consuming, and hence, technically difficult. As a result, there has been a tendency in *simulation* research area to model the return stroke channel of lightning, calculate the EM radiated fields due to this channel as well as obtaining the induced voltage on transmission lines by using field-to-line coupling models and numerical methods. Before going through the lightning terminologies, a historical overview of lightning phenomena is discussed.

2.1.1   Historical Overview

Lightning is considered as a phenomenon whose origin is not exactly known. It is likely that lightning was present on the Earth long before life evolved on our planet and played a role in producing the organic molecules necessary for the formation of every life form. The primitive human treated it with fear and wonder. Almost all religions have mentioned lightning and storm in their religious believes as the endless power of gods. The origin of the sixth day of week, Thursday, is coming from Thor's day. Thor was believed as a god who produces lightning by throwing magic hammer toward clouds. Some believed lightning is produced by their god when he throws stone from sky, some believed it is produced when Thunderbird is diving toward Earth from clouds and opens his igneous wings [1]. The first scientific study of lightning returns to Franklin experiment in 1752 [14]. It was late in 19th century when the photography and spectroscopy became available as diagnostic tools for lightning research to identify the spectrum of lightning flash as a good source of information about physical condition inside lightning channel. Figure 2.1 shows an example of these pictures taken by Hendry 1993 [1].

 After 1960, due to increasing use of electronic devices and their susceptibility to damage because of overvoltages and induced lightning current, the research and measurement in the lightning area found a huge attention and several researchers tried to record the lightning radiated EM field by recently-developed measurement equipments. The first multiple station measurements of electromagnetic fields on the ground from close lightning were performed by Workman *et al.* (1942) [15], and Reynold and Neill (1955) [16]. The modern era of electric and magnetic field measurements relating to the lightning stroke is traced to the 1970s, when the first field records on microsecond time scales were reported. Further information on early measurement of electromagnetic fields due to lightning can be found
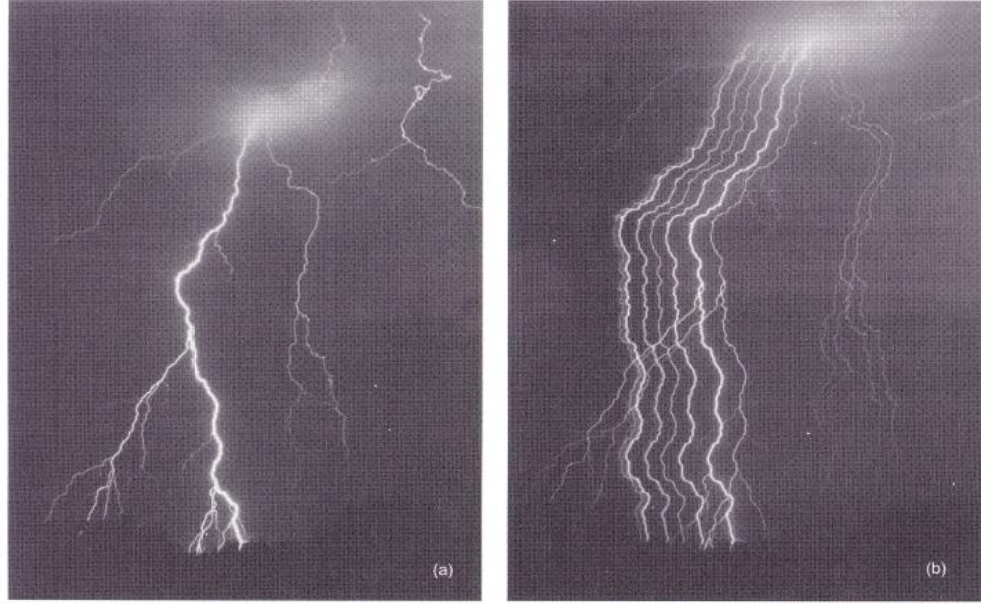
Figure 2.1: A lightning flash appears as at least seven separate ground strike points: (a) still-camera photograph, (b) moving-camera photograph. Adopted from [1].

in Uman *et al.* [17].

2.1.2 Lightning Terminologies

Natural lightning is a strong electrical discharge that typically lasts around 1 second in a length of some Kilometers. Cumulonimbus clouds are the common source of lightning phenomena. It happens whenever the electric field of a part of atmosphere due to the density of charges, breaks down the air. Usually, the distribution of charges inside clouds is in a form that negative charges are at the bottom and positive charges are at the top of the clouds, and are behaving like an electrical dipole. Figure 2.2 illustrates a typical distribution of charges in this kind of cloud. The natural lightning is categorized into two groups, cloud to cloud lightning and cloud to ground ones. Although the former consists most of the lightning cases, the latter is more interesting to researchers as it contributes in most of the damages. To give a clear picture of the way lightning happens, consider a cloud
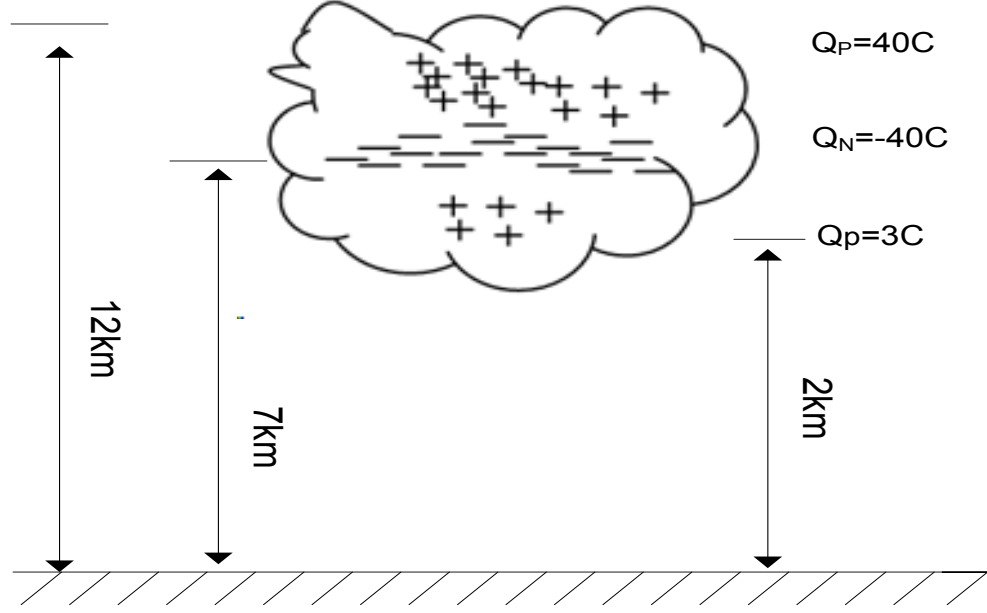
Figure 2.2: Charge distribution inside a cumulonimbus cloud.

which is electrified. If the amount of charges inside the cloud increases, it causes an *initial breakdown* because of large potential defference between the ground and cloud. Negative charges start to move toward the ground and this creates a *stepped leader* at the base of the cloud. When the stepped leader reaches close to the ground, positive charges moves from the ground toward it and contact each other. This is called the *attachment process*. After that a huge amount of current starts traveling in this established channel at a speed of one third of the speed of light and discharges the remaining charges in the cloud [1]. This is called the return *stroke phase* of lightning and the established channel is called the *lightning return stroke channel* (RSC). Evaluation of the radiated electromagnetic fields in this stage, as an external excitation of transmission lines, is one of the targets of this thesis. Figure 2.3 shows the steps mentioned in a lightning flash. There are several proposed models for the RSC which we will review in the next subsection.
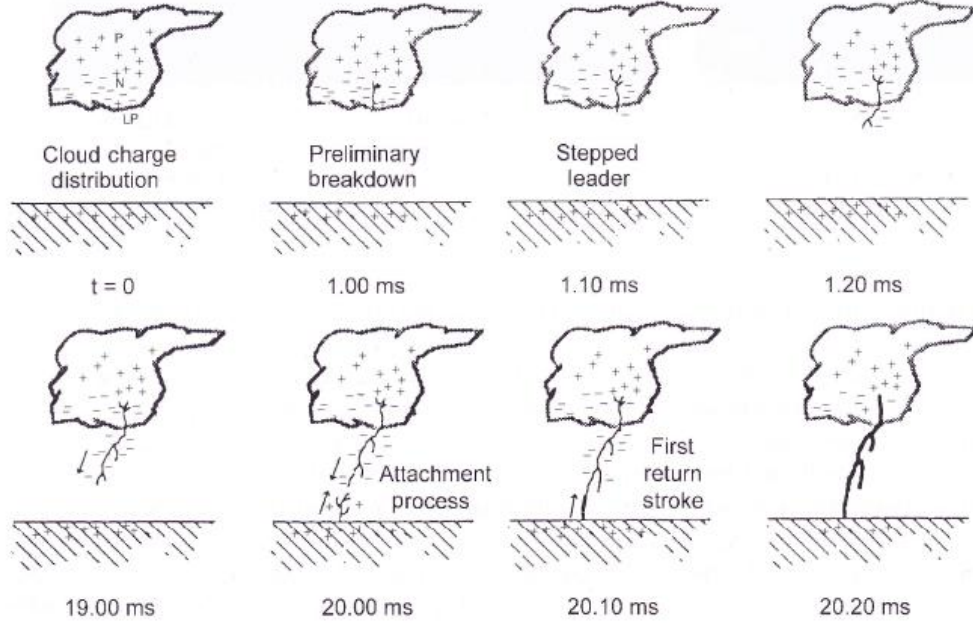
Figure 2.3: Various processes comprising a cloud-to-ground lightning flash. Adopted from [1].

2.1.3 Lightning Return Stroke Channel Models

The expression *lightning return-stroke model* is generally used to describe a specification of the time and height-dependent current in the RSC to make possible the calculation of resultant remote electromagnetic fields. Generally, there are four classes of lightning return stroke models [11]. They are distinguishable by the type of governing equation.

- The first class of models is *gas dynamic* or *physical models*. In this model, the channel is divided to short segments of cylindrical plasma column and the radius of this segments are approximated by the input current and time.

  The gas dynamic models do not consider the longitudinal evolution of the lightning channel. They also ignore the electromagnetic skin effect and corona sheath. This model has physical base and is not useful in engineering applications [18, 19].

- The second class is the *distributed circuit model*. It represents the lightning discharge

as a transient process on a vertical transmission line characterized by per unit length parameters such as resistance, inductance and capacitance. For this reason some times it is called the *R-L-C transmission line model.*

If the channel is assumed to exhibit quasi-TEM field structure, Resistance (R), Inductance (L) and Capacitance (C) are constant (e.g., Agrawal *et al.* [20]) but in general these parameters are changing with time and space due to variation in electron density and the radius of channel core. Several interesting works have been done related to this model such as Rakov [21], Baum and Baker [22,23] and Strawe in [24]. Most of these papers propose distributed-circuit models with different R, L and C variation. This model is also not useful in engineering applications as well as in this thesis.

- *Electromagnetic models* are the third class of lightning return stroke channel models first proposed by Podgorski and Landt [25]. In this model, the lightning channel is treated as a lossy thin monopole antenna. The current distribution along the lightning channel and the radiated EM fields are obtained by solving Maxwell's equations. To reduce the propagation speed of the current along the lightning channel to a value consistent with observations, a different permittivity of the medium needs to be used in the channel characteristics. As we will see in this thesis, the current wave propagation speed and attenuation is controlled by the loading of channel with a series resistance and inductance controlling the value of the permitivity.

- *Engineering models* are the last popular class of RSC models. They relate the current along the lightning channel at any height x', with the current at the base of the channel as, [26]

$$i(x',t) = u(t - \frac{x'}{v})p(x')i(0, t - \frac{x'}{v}), \tag{2.1}$$

where $u(.)$ is Heaviside function, $p(.)$ is the height-dependent current attenuation

factor, v is the current-wave propagation speed and $i(0, t)$ is called the *channel base current*.

Depending on how $p(x')$ is defined, different sub-models have been proposed in this class. Some of these sub-models are *Transmission Line model* (TL) by Uman and McLain [27], *Modified Transmission Line model with linear current decay* (MTLL) by Rakov and Dulzon [28], and *Modified Transmission Line model with exponential current decay* (MTLE) by Nucci *et al.* [29]. Table 2.1 represents different choices for $p(.)$ which are used in these sub-models.

In table 2.1, H is the channel height and λ is current decay constant (used by Nucci *et al.* [29]).

Beside the attenuation factor mentioned in 2.1, channel base current is also a determining factor for the current at any height of the lightning channel. So it directly affects the radiated electromagnetic fields. A typical lightning channel-base current, based on direct measurements performed at the top of high towers [30] or using rocket triggered lightning [2,31], is shown in Figure 2.4. Various analytical formulations have been proposed to model the measured channel base current, such as double exponential [32], modified double exponential [33, 34], Heidler [35] and a new channel-base

Table 2.1: Current attenuation factor for three simple engineering models

Model	$p(x')$
TL	1
MTLL	$1 - \frac{x'}{H}$
MTLE	$\exp\left(\frac{x'}{\lambda}\right)$
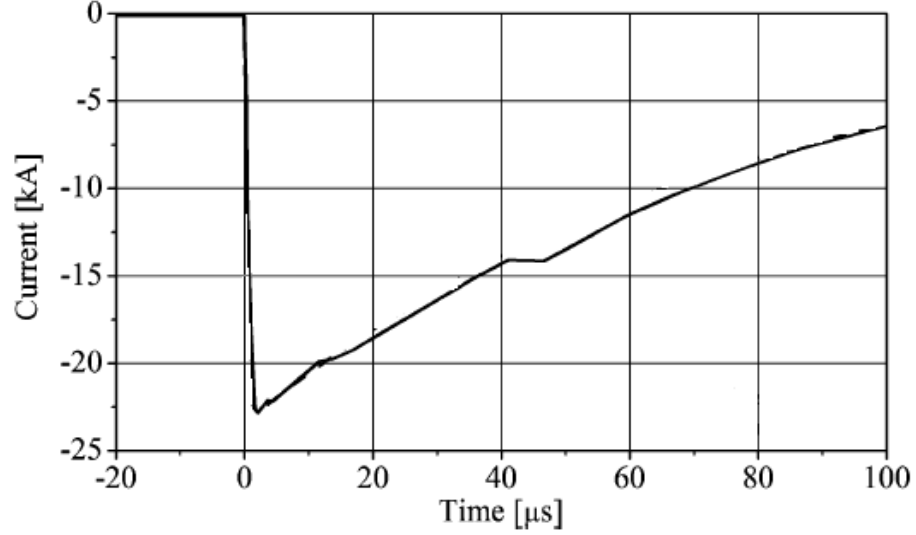
Figure 2.4: Typical measured lightning channel base current. Adopted from [2].

current function (NCBC) [36]. Improved channel-base current formulations allow controlling the rise time, the fall time, and the peak value of the waveform almost independently. Further, the formulation proposed in [36] provides analytical forms for the derivative and the integral of the waveform which are needed for calculation of the radiated EM field.

2.1.4 Radiated Electromagnetic Fields of RSC

Calculation of radiated electromagnetic fields of lightning channel is essential for obtaining induced voltage on transmission lines and cables. The electromagnetic field information is directly involved in the field-to-line coupling equations. Although the current propagating along the lightning return stroke channel attenuates due to channel characteristics, the high amplitude current in the range of Kilo-Ampere is able to create strong EM field around the channel especially at the close distance of the RSC [37]. In many studies, lightning channel has been considered as a vertical uni-dimensional antenna over perfectly-conducting
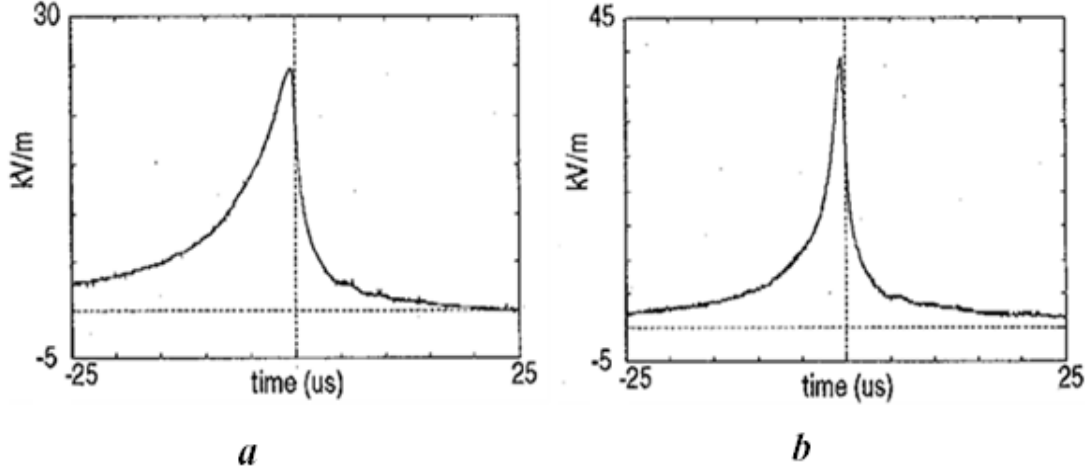
Figure 2.5: Measured vertical electric field intensity in Barker experiment at the close distance of rocket trigered lightning. a) at 110m b) at 50m from the lightning channel. Adopted from [2].

ground [38]. However the ground conductivity plays an important role in the evaluation of the radiated fields. The study of effect of ground finite conductivity was first published by Sommerfeld in 1909 [39]. Sommerfeld integrals yield the exact solution of radiated EM fields, but they are very complicated and time-consuming. Several approximations have been proposed for these integrals such as perfect ground approximation [40, 41], wavetilt formula [42], Cooray approach [43], and Rubinstein approach [44]. Barker *et al.* measured the vertical electric field radiated by a rocket-triggered lightning experiment at 50m and 110m from the RSC [2]. In this experiment, indeed the overvoltage induced on a multiconductor transmission line was measured. The measured voltages obtained in this experiment are used in this thesis for comparison purposes in chapter 4. An example of this rocket-triggered measurement is illustrated in Figure 2.5 to have an estimation about the amplitude of the electromagnetic field in a typical lightning. Furthermore several researchers have recorded lightning radiated EM field recently. These data are the most appropriate test of model validity predicted by the engineering models as well as other
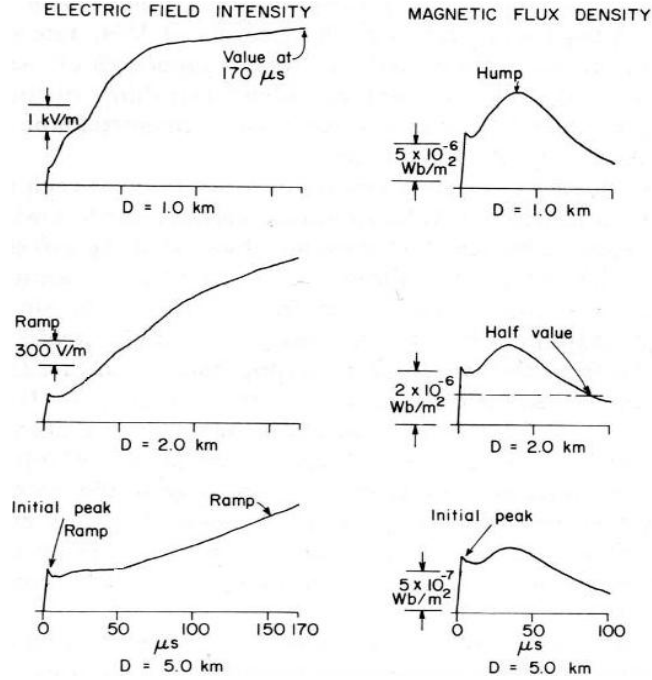
Figure 2.6: Typical vertical electric field intensity (left column) and horizontal magnetic flux density (right column) for lightning RSC at distance of 1, 2, and 5 km. Adopted from [3].

models. Measured EM fields due to natural lightning at the range of 1-200 km is presented by Lin *et al.* in [3]. Also the EM fields related to the trigered lightning is published by Uman *et al.* [45, 46] and by Rokov *et al.* [47].

One important point about lightning EM field is that it is *nonuniform*. It means that the shape of the radiated EM field dramatically changes with distance from the RSC. Figure 2.6 and Figure 2.7 show the variation of electric and magnetic fields at different distances.

Obviously, the shape of electric field is very different from magnetic field in close distances but they are similar at far distances. The reason is that in far distances the spherical waves radiated from the channel is nearly plane-wave and only difference is in their amplitude. From this figures, effect of propagation on EM fields can be parameterized as: rise time to initial peak, initial peak value, ramp starting time, ramp slope, and zero crossing time

15
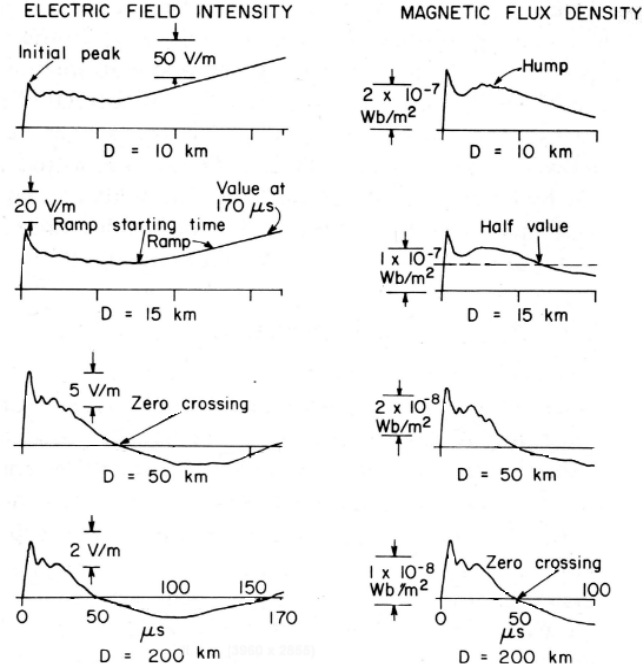
Figure 2.7: Typical vertical electric field intensity (left column) and horizontal magnetic flux density (right column) for lightning RSC at distance of 10, 15, 50, and 200 km. Adopted from [3].

for 50 and 200 km wave forms. Compare this with uniform plane wave where the shape doesn't change in different distances and the only effect of propagation is delay. So In nonuniform EM waves, the effect of propagation on these fields is remarkable and can not be neglected.

2.2 Transmission Lines

Lightning-induced voltages on overhead transmission lines have been the subject of many theoretical and experimental investigations since the first decade of the 20th century. Multiconductor transmission lines arise in application ranging from very long over-head transmission lines and cables in power transmission to tiny interconnects in VLSI[1] technology

---

[1]Very Large Scale Integration

and electronic chip packaging. Accurate and efficient simulation is important for all these applications. A fundamental difficulty arises in integrating transmission line simulation into transient circuit simulator because network nonlinearities and time-dependant components require a time-domain analysis whereas transmission line characteristics such as conductor loss and dispersion are best described in the frequency domain. The issue of mixed time-frequency domain modeling of lossy coupled multiconductor transmission lines has been studied in both power systems and electronics communities for many years. Generally the transmission line models can be divided into two groups. *Terminal-based* models and *Distributed* models.

Terminal-based models for the transmission line analysis have been considered by many researchers in simulating dispersive transmission lines in the time domain. One of the first models, referred to as the method of characteristics, can only deal with lossless transmission lines. This simple delay model was considered by Branin [48]. The issue of modelling transmission lines with frequency-dependant parameters, which has emerged as an important topic in power system area, was studied by Budner [49]. He considered a modal analysis and included the frequency-dependence of the line parameters using a convolution of the past history of the modal voltages and weighting functions where the weighting functions are the inverse transform of the two-port admittance parameters. Only symmetric transmission lines were studied, which, however, result in a frequency-independent transformation matrix. Because of the high computational cost of evaluating the convolution integrals in Budner's model, a more efficient model was proposed by Snelson [50] which is formulated using forward and backward traveling waves. Improving Budner's weighting functions, and modifying the method proposed by Snelson, J. Marti developed an equivalent circuit impedance model which is an approximation to the frequency-dependent characteristic

impedance of the line [51]. His model employs modal analysis with a frequency-independent transformation matrix, and is the progenitor of common models employed in power system simulators (such as PSCAD [52] and EMTP [53]). To avoid the inaccuracy or instability problems observed in the mode-domain models, a variety of methods in which the matrix elements of the propagation function and the characteristic admittance are directly studied and fitted in the phase domain, have been proposed (see for example [54,55]). A review of phase domain models can be found in the work of Gustavsen *et al.* [56].

Simulation software based on terminal-characteristic models, such as PSCAD and EMTP, are not capable of calculating external-field coupling, whereas one of the inherent features of distributed models is the capability of determining the response of the line to external exciting fields. For handling this problem, distributed models were developed such as those models based on FDTD method.

FDTD methods are a common way of approximating the time-domain response of transmission lines [20, 57]. The MTL equations are discretized both in time and space and the resulting difference equations are usually solved using the leap-frog scheme [4]. Basic FDTD approaches have been applied to problems with frequency-independent per-unit-length parameters. The inclusions of terminal constraints [58], lossy conductors [59], and nonlinear junctions [60] have been addressed. In [58], a first-order finite-difference approximation for one of the MTL equations was proposed to relate terminal voltages and currents, and a state-variable formulation was used to solve the whole MTL network. The skin-effect frequency dependence of the transmission-line conductors was considered in [59], where the series transmission line impedance was approximated by a rational function. A technique for incorporating the FDTD formulation in a lumped-element network simulator using modified nodal analysis (MNA) was introduced by Mardare and LoVetri [60].

They only considered frequency-independent lines. Recently Kordi *et al.* [61] developed modified version of FDTD technique (MFDTD) which is capable of considering frequency-dependence of p.u.l. The problem with distributed models is that they are time-consuming and need massive memory space to be calculated and this decreases the efficiency of these methods.

2.3   Field-to-Line EM Coupling Models

The problem of incident electromagnetic waves coupling to MTL has already been addressed in several literatures for example in [62–65]. The source of such electromagnetic fields can be, for example, a plane wave or a nearby lightning stroke. In both cases, an external source generates time-varying electromagnetic fields which surround the MTL conductors and induce voltage and current on the conductors of the line. For short transmission lines (compared to the smallest wavelength of the exciting fields), or alternatively, slow-varying fields the coupling effects of these external electromagnetic fields can be considered using lumped element sources, however, for long transmission lines (compared to the smallest wavelength of the exciting fields), or alternatively, fast-varying fields accurate simulation of the external source requires distributed sources. In [64, 66], high speed interconnection simulation algorithms based on model-reduction-based are discussed. [62] talks about time-domain macromodel for incident field coupling to MTL based on matrix-rational approximation for frequency dependant conductors. These models are capable of being incorporated into general circuit simulators such as SPICE [67]. Calculation of the time-domain equivalent source representation of incident field at transmission line's terminal, based on split representation at both ends of MTL structure, is given in [68]. Techniques such as method-of-characteristics (MoC) and matrix rational approximation

(MRA) for macromodel-base analysis of MTLs are proposed in [69, 70]. In [63], a closed form relations for equivalent sources in the time-domain accounting for EMI-induced effects based on delay extraction is provided. Furthermore the formulation of the equivalent lumped sources at the terminals of MTL, based on spectral representation of dyadic Green's function of MTLs is presented in [71]. Almost all of these works have considered uniform plane-wave excitation of line. There are few literatures discussed nonuniform cases such as [65] where a hybrid FDTD and similarity transformation technique is used to calculate the additional voltage sources due to excitation of lossless transmission line.

There are three main formulations for the field-to-transmission line coupling equations in terms of electromagnetic excitation field. In the first, the forcing functions are described in terms of electric and magnetic excitation field components [72, 73] whereas, in the second, only the vertical and horizontal electric field components are involved [20]. Finally, a third equivalent formulation of coupling equations is derived in which the forcing functions are expressed in terms of magnetic excitation field components [5]. This formulation makes it possible to evaluate field-to-transmission line coupling starting from solely the magnetic field components. The use of this formulation is particularly interesting when the exciting field is determined experimentally, as measuring the magnetic field is generally much easier than measuring the electric field.

Next chapter presents a new time-domain macromodel to handle the lossy frequency-dependant transmission line excited by a non-uniform incident EM field. The proposed technique is to overcome the problem of terminal-based models in handling non plane wave external-field coupling, and distributed models from the aspect of efficiency and speed.

Chapter 3

Electromagnetic Field Macromodel

In this chapter, we will develop an efficient algorithm to calculate the electromagnetic fields of typical radiation sources. The source of the electromagnetic radiation can be natural, such as natural lightning, or artificial sources, such as triggered lightning. In this thesis, we chose lightning channel as a source of radiation to study because there is measured data available to validate the results and is of more importance in power system simulation. The order of the sections in this chapter is as follows: we will discuss the concept of macromodel in the next section. Different approximations in calculating EM field above a lossy ground are discussed next. After that, we will introduce our proposed technique for efficient calculation of the EM fields. The idea behind this algorithm and the details are main topics of this section. In the last section of this chapter, we will show the results of the proposed macromodel and will compare them with measurement data.
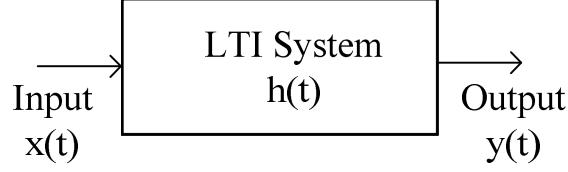
Figure 3.1: An LTI system block diagram with its input, output, and transfer function.

3.1   Concept of Macromodelling

Every linear time invariant (LTI) system can be described by its transfer function. Transfer function of a system is a relationship between input and output of that system so that for a specific input, the output can be calculated using the transfer function. Consider Figure 3.1 which shows an LTI system simple block diagram with its input and output. The relationship between these function are defined by convolution of input and transfer function in the time domain as,

$$y(t) = x(t) * h(t), \tag{3.1}$$

where $*$ represents the convolution operator. The advantage of using transfer function of a system in calculating its output is that it is independent from the input. Furthermore, by using efficient techniques such as recursive convolution, fast calculations become possible. In general, macromodeling is reducing the complexity of the transfer function of a system with model order reduction techniques (MOR) in a way that the input-output behaviour is preserved. In this chapter, we will consider the lightning RSC as the system. The input and output of this system are channel base current and radiated electromagnetic fields around the channel, respectively. Studying the transfer function of this system is the main topic of this chapter. Figure 3.2 shows the complete field macromodel with its input and
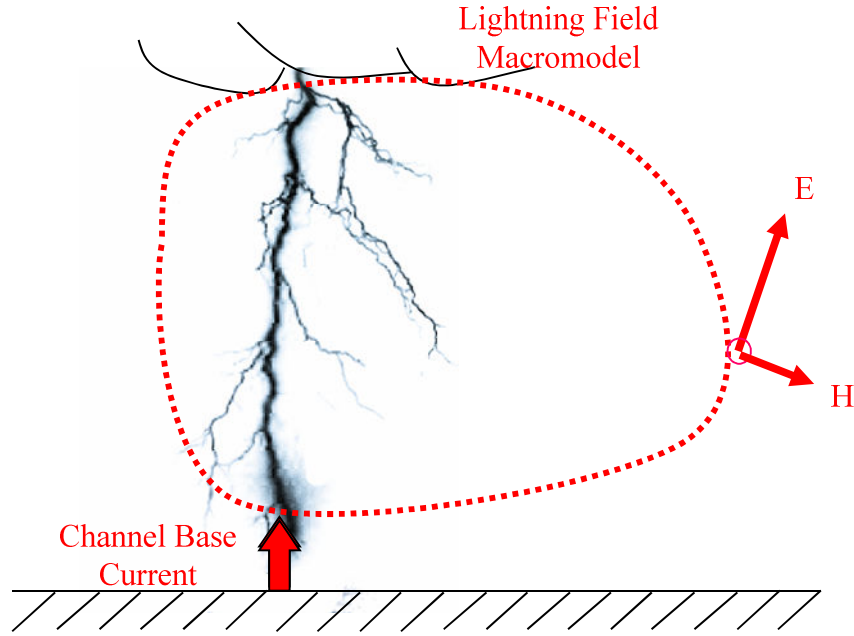
Figure 3.2: The field macromodel of lightning RSC. Channel base current as input and radiated electromagnetic fields and its output.

Figure 3.3: Equivalent block diagram representation of Figure 3.2.

output.

The equivalent block diagram representation of Figure 3.2 is shown in Figure 3.3. The idea of the electromagnetic field macromodel is to obtain electromagnetic field in an arbitrary point in the space around the radiation source by using the already-specified values of the electromagnetic field of other points in the space. To develop this idea, we need to know how to calculate the electromagnetic field over a lossy ground for those specific points. So, before going through the details of the field macromodel, in the next section we are explaining different methods and approximations to obtain electromagnetic field over a

lossy ground.

3.2 Electromagnetic Fields over a Lossy Ground

The main interest in this section is considering the effect of finite conductivity of the ground on **a**) The vertical electric field and **b**) The horizontal electric field component which are used in the calculation of induced overvoltages caused by lightning [74].

3.2.1 Effect of ground finite conductivity on the vertical electric field component

Several authors have shown that, for the frequency range of lightning studies, the vertical component of the electric filed, radiated from the RSC, is not significantly affected by ground conductivity, (e.g. [40, 41]). So for simplicity, the ground is considered to be PEC for the calculation of the vertical electric field. As shown in Figure 3.4 , using the image theory for the calculation of vertical component of the electric fields over a PEC ground we have [40],

$$
\begin{aligned}
E_x(r, x, t) = \frac{1}{4\pi\varepsilon_0} [& \int_{-H}^{H} \frac{2(x - x')^2 - r^2}{R^5} \int_{0}^{t} i(x', \tau - \frac{R}{c}) d\tau dx' \\
& + \int_{-H}^{H} \frac{2(x - x')^2 - r^2}{cR^4} i(x', t - \frac{R}{c}) dx' \\
& - \int_{-H}^{H} \frac{r^2}{c^2 R^3} \frac{\partial i(x', t - \frac{R}{c})}{\partial t} dx'],
\end{aligned}
\tag{3.2}
$$

where, r is the horizontal distance from channel base and c is the velocity of light. Equation 3.2 consists of three terms. The first term which is related to the integral of the
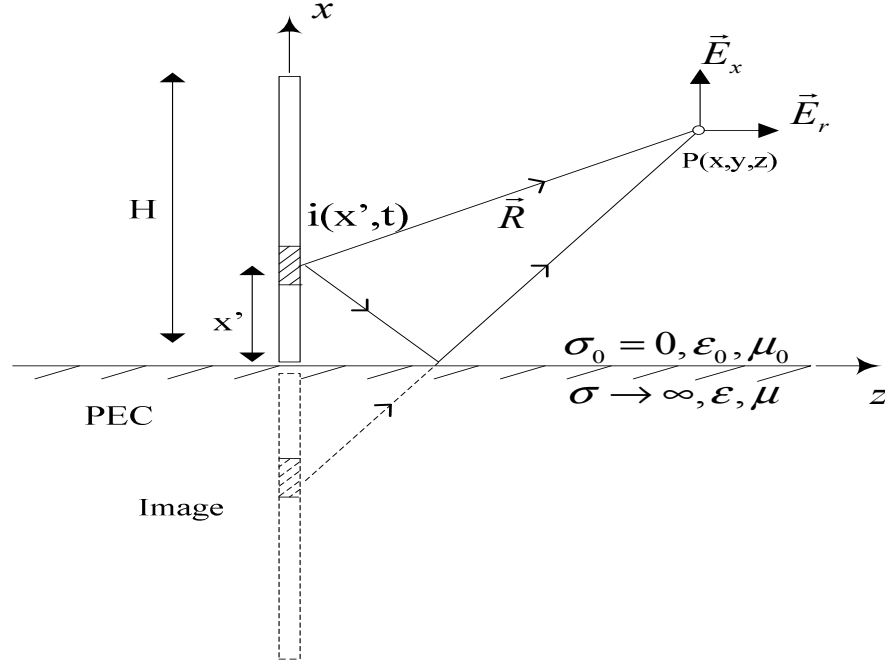
Figure 3.4: Geometry for the calculation of RSC radiated vertical electric field with PEC ground assumption.

current along the lightning channel is called the *electrostatic term.* This term is important in close distances but its role in radiated electric field decreases by moving away from the channel. The second term which is proportional to current itself is called the *induction term* and is important at mid ranges from RSC. The third term which is important at far distances is proportional to the derivative of the channel current and is called the *radiation term.* It should be mentioned that the perfect ground approximation is more valid for close distances [74], however, for far distances, the lightning radiation effects are less important.

3.2.2 Effect of ground finite conductivity on the horizontal electric field component

The horizontal component of the electric field depends on ground conductivity much more than the vertical component does. Different approaches may be used to calculate horizontal electric field of lightning RSC such as *Perfect ground assumption*, *Wavetilt formula*, *Cooray approach*, and *Rubinstein approach*.

- *Perfect ground assumption*: The radial electric field under this assumption at a height of x and a distance of r from the RSC is given by,

$$E_r(r, x, t) = \frac{1}{4\pi\varepsilon_0}\left[\int_{-H}^{H}\frac{3r(x - x')}{R^5}\int_{0}^{t}i(x', \tau - \frac{R}{c})d\tau dx' \right.$$
$$+ \int_{-H}^{H}\frac{3r(x - x')}{cR^4}i(x', t - \frac{R}{c})dx'$$
$$\left. - \int_{-H}^{H}\frac{r(x - x')}{c^2R^3}\frac{\partial i(x', t - \frac{R}{c})}{\partial t}dx'\right]. \tag{3.3}$$

To demonstrate the effect of ground conductivity on electromagnetic fields, we have plotted the horizontal electric field by using MTLL model and Cooray-Rubinstein approach (which will be described in following) for several ground conductivity. Figure 3.5 shows this for r=100m distance from the RSC and Figure 3.6 is for r=5km. The horizontal electric field on a PEC ground is zero and it changes dramatically with variation of the ground conductivity. These show that perfect ground assumption is not accurate enough for calculation of the horizontal component of electric field. There are other approximations used to calculate the horizontal electric field as follow.
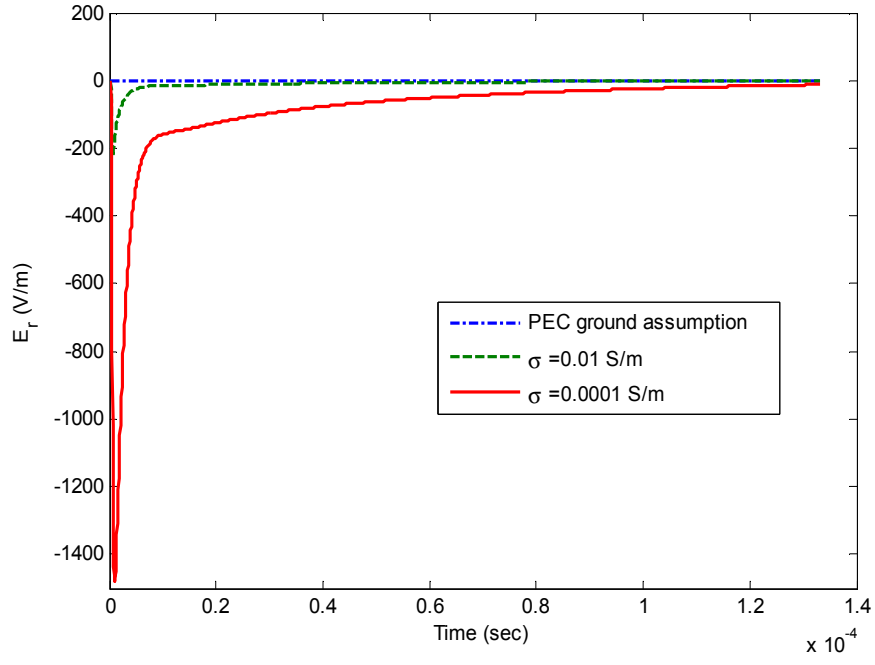
Figure 3.5: Horizontal electric field at r=100m on the ground.
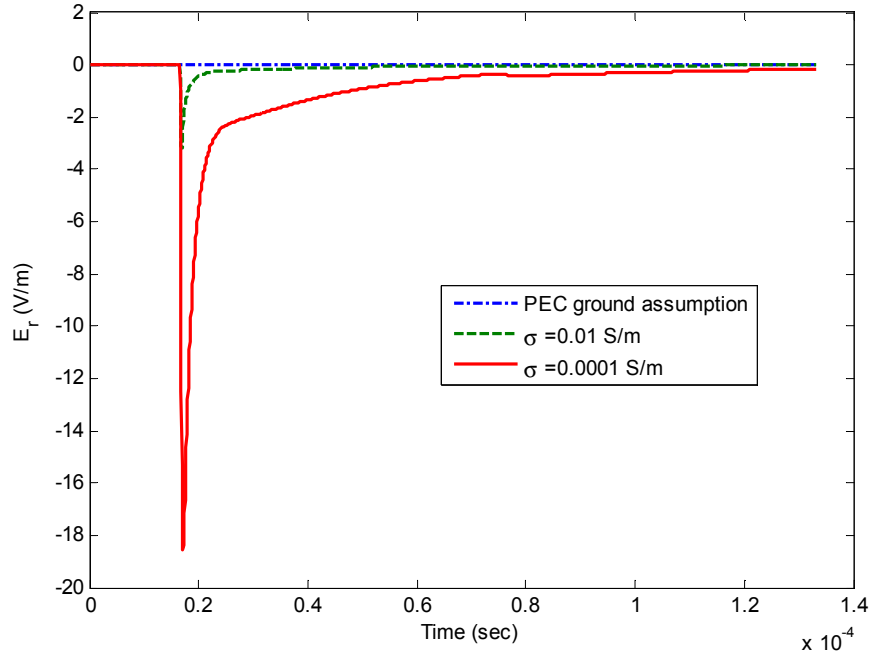
Figure 3.6: Horizontal electric field at r=5km on the ground.

- *Wavetilt Formula*: This formula expresses the ratio of the Fourier transform of the horizontal electric field $E_r(j\omega)$, to that of the vertical field $E_x(j\omega)$, and thus, allows calculating the horizontal component of the electric field over a soil of finite conductivity from the knowledge of the vertical component of the same field as,

$$w(j\omega) = \frac{E_r(j\omega)}{E_x(j\omega)} = \frac{1}{\sqrt{\varepsilon_{rg} + \frac{\sigma_g}{j\omega\varepsilon_0}}}, \tag{3.4}$$

where, σ_g and ε_{rg} are the ground conductivity and relative permittivity, respectively. $E_x(j\omega)$ can be obtained using the perfect ground assumption. According to Thomson *et al.* [42], this approach for the calculation of the radial electric field is reasonable only for far observation points and we will not use this approximation in this thesis for this reason. However, several authors have used this formula for the calculation of lightning induced voltage on transmission lines located at far, and also intermediate (about 1km) distance ranges [75–77].

- *Cooray Approach*: In [43], Cooray proposed to calculate the horizontal electric field by using the azimuthal magnetic field and surface impedance expression given by,

$$E_r(r, 0, j\omega) = B_\phi(r, 0, j\omega) \frac{c}{\sqrt{\varepsilon + \frac{\sigma_g}{j\omega\varepsilon_0}}}, \tag{3.5}$$

where, $E_r(r, 0, j\omega)$ and $B_\phi(r, 0, j\omega)$ are the Fourier transforms of the horizontal electric field and the azimuthal magnetic flux density, respectively, both at the ground level. This formula is obtained simply by writing the integral of Ampere-Maxwell equation around an infinitely long rectangle extended from ground level to $x = -\infty$ and assuming all the field components are zero at $x = -\infty$. Cooray has shown that 3.5 yields very accurate result in close distance of lightning channel up to 200m [43].

- *Rubinstein Approach*: In this approach, the horizontal electric field over a ground with conductivity of σ_g and at the height of x is given by [44],

$$E_r(r, x, j\omega) = E_{rP}(r, x, j\omega) - H_{\varphi P}(r, 0, j\omega)\frac{1+j}{\sigma_g \delta_g},\tag{3.6}$$

where, $E_{rP}(r, x, j\omega)$ and $H_{\varphi P}(r, 0, j\omega)$ are the horizontal field component over a perfect ground at the same height and azimuthal magnetic field over a perfect ground and at the ground level, respectively. δ_g is the skin-depth of the ground. In fact, $\frac{1+j}{\sigma_g \delta_g}$ acts as a correction factor similar to wavetilt formula. The basic assumption in Rubinstein formula is that $\sigma_g >> \omega \varepsilon_0 \varepsilon_{rg}{}^2$. If it is not satisfied, then the general form of Rubinstein formula becomes [44, 78],

$$E_r(r, x, j\omega) = E_{rP}(r, x, j\omega) - H_{\varphi P}(r, 0, j\omega)\frac{c\mu_0}{\sqrt{\varepsilon_{rg} + \frac{\sigma_g}{j\omega\varepsilon_0}}},\tag{3.7}$$

where, E_{rp} is same as 3.3 and,

$$H_{\varphi p}(r, 0, t) = \frac{1}{4\pi}\Big[\int_{-H}^{H} \frac{r}{R^3}i(x', t - \frac{R}{c})dx'$$
$$+ \int_{-H}^{H} \frac{r}{cR^2}\frac{\partial i(x', t - \frac{R}{c})}{\partial t}dx'\Big].\tag{3.8}$$

As the second term in 3.7 is similar to the Cooray proposed formula, 3.7 is called Cooray-Rubinstein formula. This is the formula used in this chapter to calculate the horizontal electric field along the transmission line.

3.3 Pole-Residue Representation of the EM Fields

The developed formulas for electric fields in equations 3.2- 3.7 are in the time or frequency domain. The alternate representation of electromagnetic fields is by using poles and residues of the field. Assume that we have a time domain signal, $e(t)$. Using Laplace transform we can have it in the Laplace domain $E(s)$, where, s is the complex frequency. Using Vector Fitting algorithm [79–81], a well-known technique to map the frequency domain data to corresponding poles and residues, $E(s)$ is written in the form of,

$$E(s) \cong \sum_{i=1}^{M} \frac{R_i}{s - P_i} + b + cs, \qquad (3.9)$$

where R_i and P_i are residues and poles, respectively. b and c are constant numbers and representing *proportional term* and *time derivative term*, respectively. The accuracy of this algorithm can be increased by proper choice of the number of the poles and residues required for fitting, and the number of iteration of the algorithm [82]. To convert the Laplace domain data to the frequency domain, it is enough to replace s with $j\omega$ to have,

$$E(j\omega) \cong \sum_{i=1}^{M} \frac{R_i}{j\omega - P_i} + b + cj\omega, \qquad (3.10)$$

where j is $\sqrt{-1}$ and ω is angular frequency. It should be noted that increasing M (number of poles and residues) does not necessarily increases the accuracy of fitted function and may cause unstable results. In the next section, as an example, we will obtain the *impulse response* for the vertical electric field over a PEC ground due to lightning RSC and will investigate the accuracy of the fitted function by using vector fitting algorithm. This will enable us to build the complete field-macromodel. Different parameters effective in Vector Fitting algorithm will be studied as well.
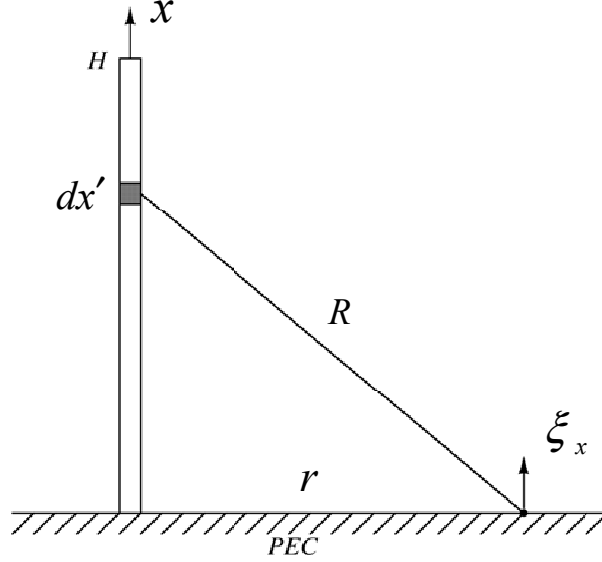
Figure 3.7: A monopole antenna representing the lightning RSC and its corresponding vertical electric field.

3.4   Vector Fitting the Electric Field Data

Assume a vertical monopole representing a lightning RSC as shown in Figure 3.7. The goal is to obtain the vertical electric field at distance r from the channel. There is an analytic formula available for this problem given in 3.2. Equation 3.2 is the general equation for vertical electric field over a PEC ground. In this section, we are dealing with engineering models. So the current function will be as given by 2.1. To obtain the impulse response of the 3.2, we need to use impulse function for channel base current. Then, combining 2.1 and 3.2, the impulse response of the vertical component of the electric field ξ_x, on the

ground level and distance r from the lightning channel will be,

$$
\begin{aligned}
\xi_x(r, \phi, 0, t)_{\text{nodelay}} = \frac{1}{4\pi\varepsilon_0}\Big[& \int_0^H \frac{2x'^2 - r^2}{R^5} P(x')u(t - \frac{x'}{v} - \frac{R}{c} + \frac{r}{c})\, dx' \\
& + \int_0^H \frac{2x'^2 - r^2}{cR^4} P(x')\delta(t - \frac{x'}{v} - \frac{R}{c} + \frac{r}{c})dx' \\
& - \int_0^H \frac{r^2}{c^2R^3} P(x')\delta'(t - \frac{x'}{v} - \frac{R}{c} + \frac{r}{c})dx'\Big],
\end{aligned}
\tag{3.11}
$$

where $u(.)$, $\delta(.)$, and $\delta'(.)$ are the unit step, unit impulse, and derivative of the unit impulse functions, respectively. In 3.11, the minimum propagation delay, (r/c) which is the time required for radiation effects to reach to the observation point, is extracted. The reason is that the field data will be fitted to poles and residues by using Vector Fitting algorithm at the end and reproducing the delay time requires a large number of poles. To discretize the system, it is assumed that the input is represented as samples of the desired waveform $i(0, t)$, sampled every Δt seconds. Our approach is to properly discretize the RSC so that in every time step, the wave travels by one segment $\Delta x'_i$ on the channel. This will remove any unreal oscillations which are created if the RSC is not discretized properly. Mathematically, we specify this condition (see Figure 3.8) as,

$$
\left(\frac{x'_{i+1}}{v} + \frac{R_{i+1}}{c}\right) - \left(\frac{x'_i}{v} + \frac{R_i}{c}\right) = \Delta t,
\tag{3.12}
$$

where $x'_{i+1} = x'_i + \Delta x'_i$ and $R_i = \sqrt{x'_i{}^2 + r^2}$. Solving 3.12 for $\Delta x'_i$ yields,

$$
\underbrace{\left(\frac{1}{v^2} - \frac{1}{c^2}\right)}_{A}\Delta x'^2_i - 2\Delta x'_i\underbrace{\left(\frac{\Delta t}{v} + \frac{x'_i}{c^2} + \frac{\sqrt{x'_i{}^2 + r^2}}{vc}\right)}_{B} + \underbrace{\Delta t\left(\Delta t + 2\frac{\sqrt{x'_i{}^2 + r^2}}{c}\right)}_{C} = 0,
$$

$$
\tag{3.13}
$$

$$
\Delta x'_i = \frac{B - \sqrt{B^2 - AC}}{A}.
\tag{3.14}
$$

32
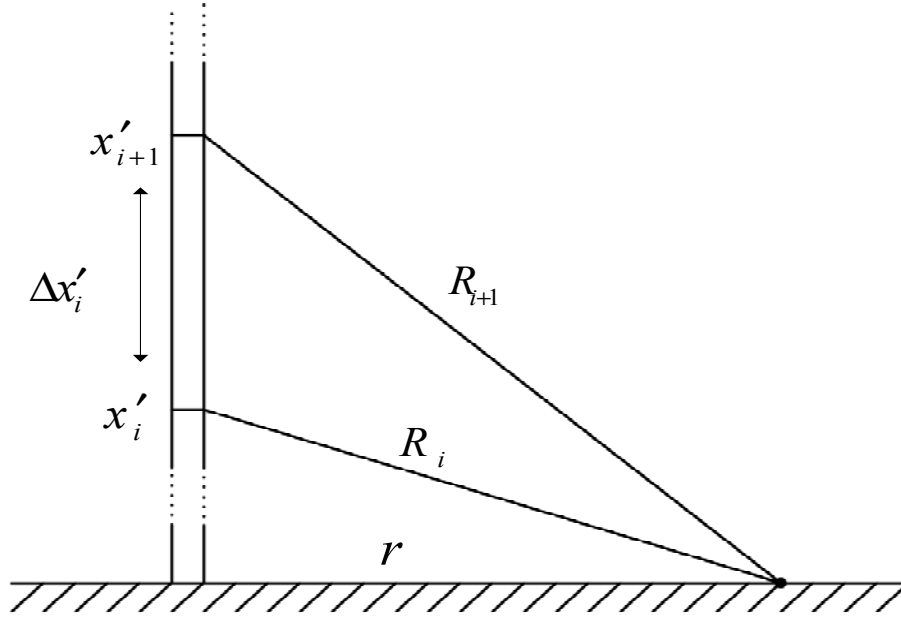
Figure 3.8: Schematic of the discretization of RSC.
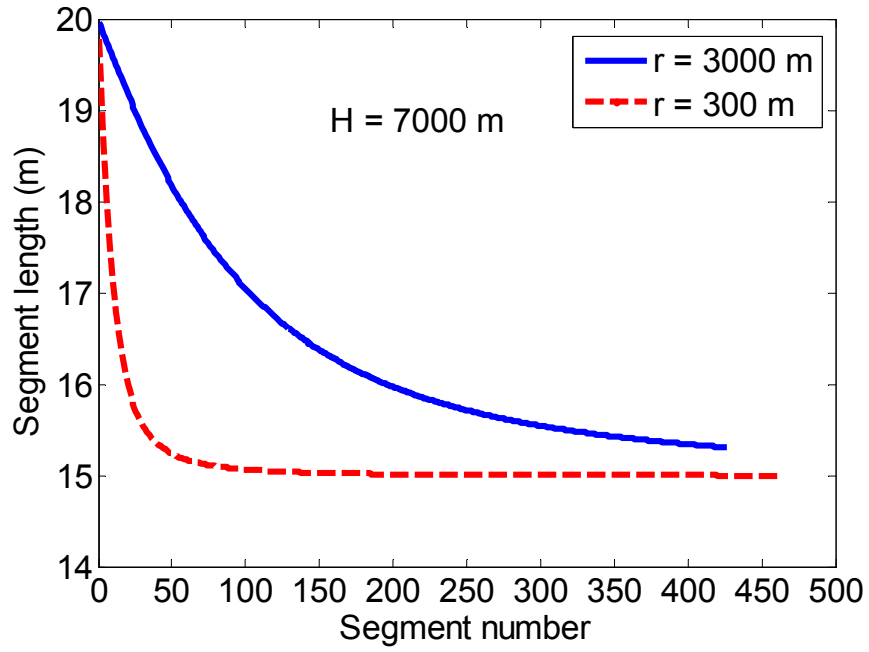
Figure 3.9: Segment length calculated by using $\Delta t = 0.2\mu s$ and $v = 100m/\mu s$.

Figure 3.9 shows the segments length as a function of the number of segments for two different values of r for a 7-km long lightning channel. The frequency response of the system is then determined by discretizing 3.11 and applying Discrete Fourier Transform (DFT) and using Discrete Time (DT) impulse function as the input. The discrete version of 3.11 becomes,

$$\xi_x(r,\phi,0,n)_{\text{nodelay}} = \frac{1}{4\pi\varepsilon_0}\Big[\sum_{i=0}^{M}\frac{2{x'}_i^2 - r_i^2}{R_i^5}P({x'}_i)\sum_{\ell=0}^{n}\delta(\ell - m_i)\,\Delta t\,\Delta {x'}_i$$

$$+\sum_{i=0}^{M}\frac{2{x'}_i^2 - r_i^2}{cR_i^4}P({x'}_i)\delta(n - m_i)\,\Delta {x'}_i$$

$$-\sum_{i=0}^{M}\frac{r_i^2}{c^2 R_i^3}P({x'}_i)\left(\delta(n - m_i) - \delta(n - m_i - 1)\right)\frac{\Delta {x'}_i}{\Delta t}\Big], \quad (3.15)$$

where m_i is the closest integer to $(R_i/c + x'_i/v - r/c)/\Delta t$, and M is the number of segments of the RSC. Figure 3.10 shows the used approximations for step, impulse and derivative of impulse function in discrete time domain where we use *zero padding* to avoid aliasing and also be able to use Fourier transform properly. The N-point DFT of 3.15 is given by,

$$\xi_x(r,\phi,0,K)_{\text{nodelay}} = \frac{1}{4\pi\varepsilon_0}\Big[\sum_{i=0}^{M}\frac{2{x'}_i^2 - r_i^2}{R_i^5}P({x'}_i)\sum_{n=m_i}^{N-1}e^{-jK\Omega_0 n}\frac{\Delta t\,\Delta {x'}_i}{N}$$

$$+\sum_{i=0}^{M}\frac{2{x'}_i^2 - r_i^2}{cR_i^4}P({x'}_i)\,e^{-jK\Omega_0 m_i}\frac{\Delta {x'}_i}{N}$$

$$-\sum_{i=0}^{M}\frac{r_i^2}{c^2 R_i^3}P({x'}_i)\,e^{-jK\Omega_0 m_i}(1 - e^{-jK\Omega_0})\frac{\Delta {x'}_i}{N\Delta t}\Big], \quad (3.16)$$

where $\Omega_0 = 2\pi/N$, K is an integer, and $0 \leq K \leq N - 1$. Evaluation of $\xi_x(r,\phi,0,K)$ provides the data needed for fitting the DT impulse response of the system into a form that is suitable for recursive convolution.
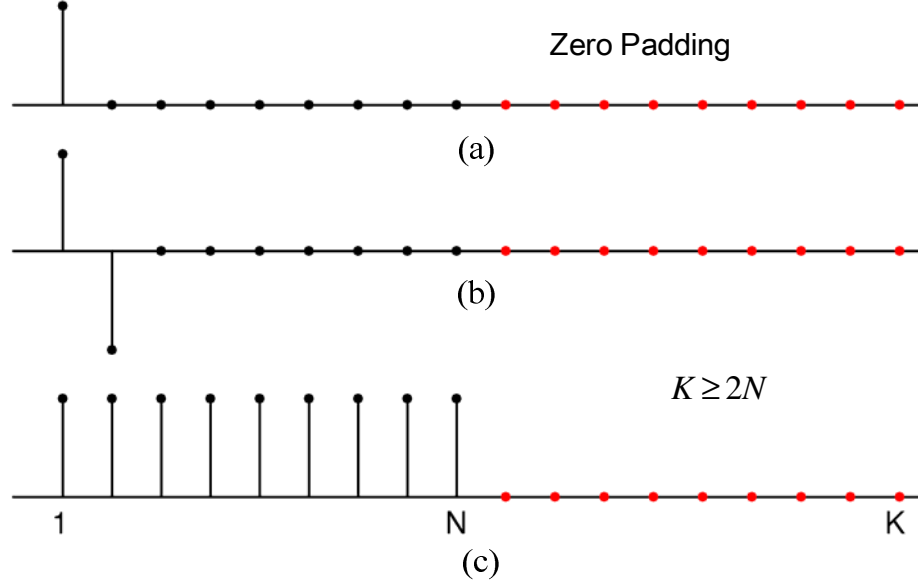
Figure 3.10: Approximation used for discretizing 3.11, a) DT Unit Impulse, b) DT Difference impulse, c) DT step function.

3.4.1 Recursive Convolution by Using Vector Fitting

To show that the form of the transfer function in 3.9 allows us to perform convolution recursively, consider a transfer function $h(t)$ with only one pole and residue given by,

$$H(s) = \frac{R}{s - P}. \tag{3.17}$$

In time domain it is in exponential function form as,

$$h(t) = \mathrm{Re}^{Pt}. \tag{3.18}$$

The system's output signal is the result of convolution of the transfer function in time domain with input signal as,

$$y(t) = x(t) * h(t) = \int_0^t x(\tau)h(t - \tau)d\tau = \mathrm{Re}^{Pt} \int_0^t x(\tau)e^{-P\tau}d\tau. \tag{3.19}$$

35

The output at the next time step will be,

$$y(t + \Delta t) = \text{Re}^{P(t+\Delta t)} \int_0^{t+\Delta t} x(\tau)e^{-P\tau}d\tau$$

$$= \text{Re}^{P\Delta t}e^{Pt} \int_0^t x(\tau)e^{-P\tau}d\tau + \text{Re}^{P(t+\Delta t)} \int_t^{\Delta t} x(\tau)e^{-P\tau}d\tau$$

$$= \underbrace{\text{Re}^{P\Delta t}}_{A} y(t) + \underbrace{R\frac{e^{P\Delta t}-1}{P}}_{B} x(t)$$

$$= \text{Ay(t)} + \text{Bx(t)}. \tag{3.20}$$

Equation 3.20 shows that the output is obtainable just by knowledge of the output at the previous time step and the input.

3.4.2 The Effect of the Number of Poles on Vector Fitted Data

To see how Vector Fitting algorithm works and what the effects of the number of poles and residues on the fitted function are, consider a 3-km RSC over a PEC ground. Using 3.16 for the vertical component of the electric field, 3.14 to discretize the RSC, and a channel base current as shown in Figure 3.11, we calculated the position of the poles and residues of the vertical component of the electric field. For the first case, we used $M{=}3$ for the number of poles to fit. Figure 3.12 and 3.13 show the position of the poles and residues of the radiation component of 3.16 at $r{=}50$m. Reconstructing the original function by using these poles and residues is shown in Figure 3.14. As expected, they do not match each other perfectly. By increasing M to 10, we can achieve a better accuracy. Figure 3.15 and 3.16 show the poles and residues position for $M{=}10$ and Figure 3.17 and 3.18 show a comparison of the amplitude and phase of the original function and fitted function by
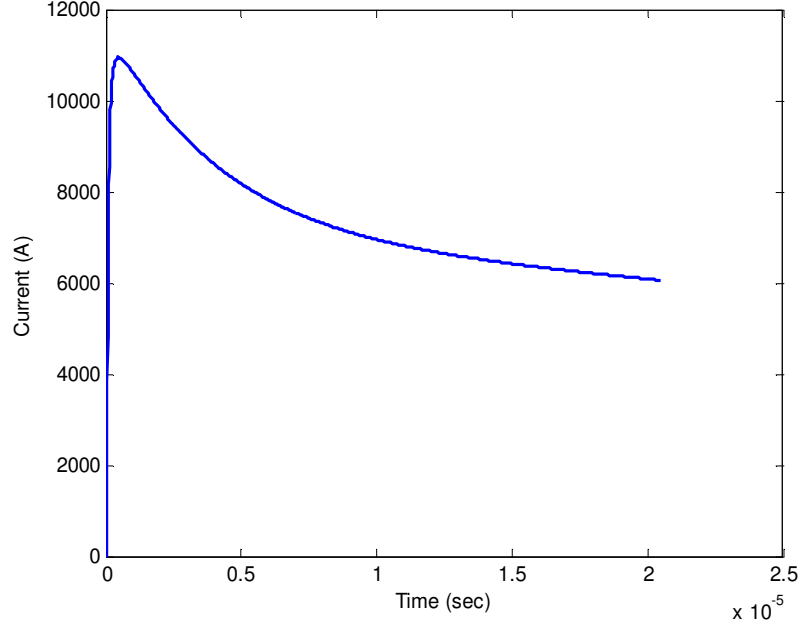
Figure 3.11: Channel base current.

using Vector Fitting, respectively. Obviously, because of increasing the number of poles there is a good agreement between the original function and the fitted one. Using obtained poles and residues and doing recursive convolution, we calculated the field information for radiation, static, and induction terms of the vertical electric field. The results are compared with direct time domain method in Figure 3.19- 3.21. Table 3.1 shows the amount of the error between different components of the electric field obtained by using Vector Fitting algorithm and direct time domain method for two different numbers of poles.The outlined procedure was done just for one specific distance from the RSC. The idea of field macromodel is repeating the above mentioned procedures for several distances, obtaining poles and residues positions and predicting the position of poles and residues for any desired distance. Next section is explaining the details of EM field macromodel.
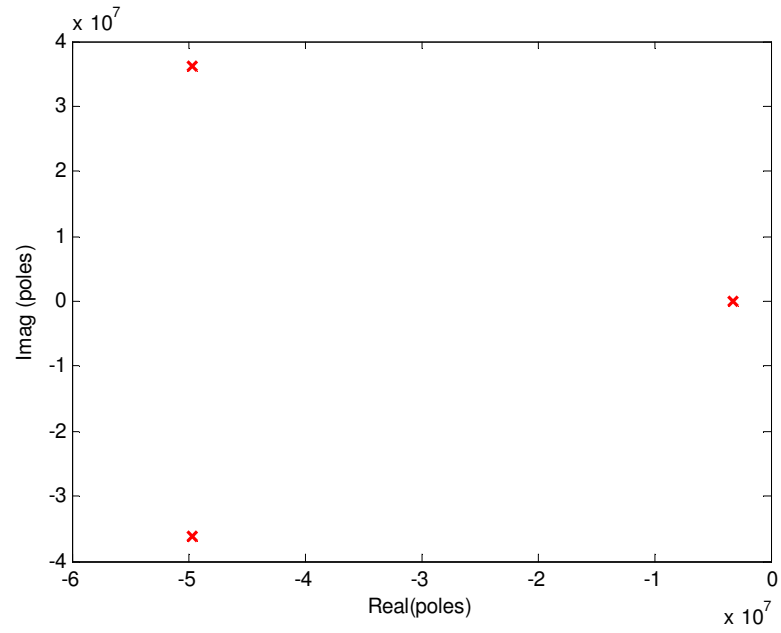
Figure 3.12: Poles location with $M{=}3$.
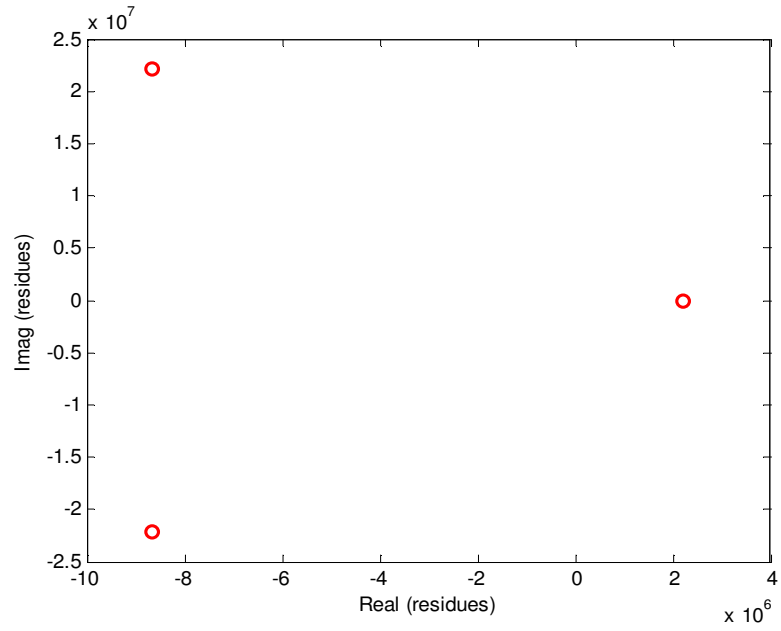
Figure 3.13: Residues location with $M{=}3$.
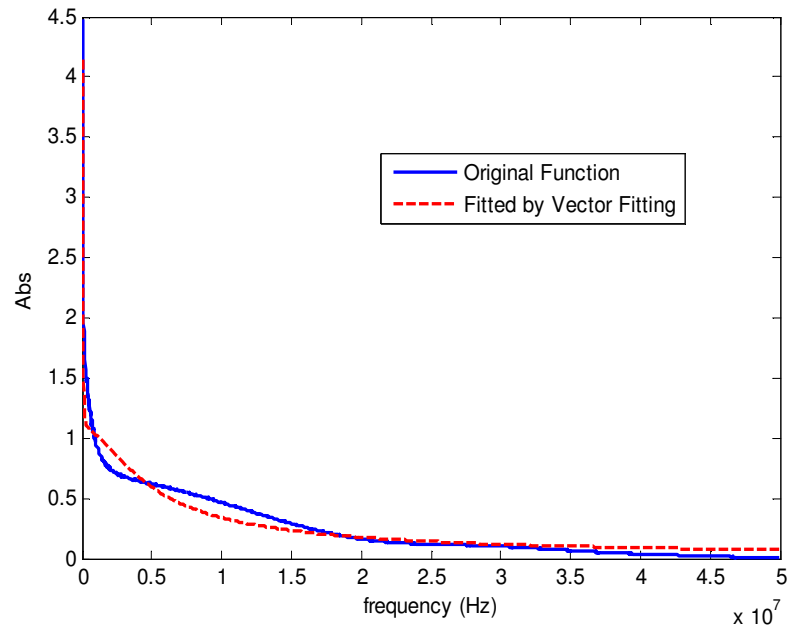
Figure 3.14: Amplitude of the original function and fitted one by using vector fitting algorithm with $M=3$.
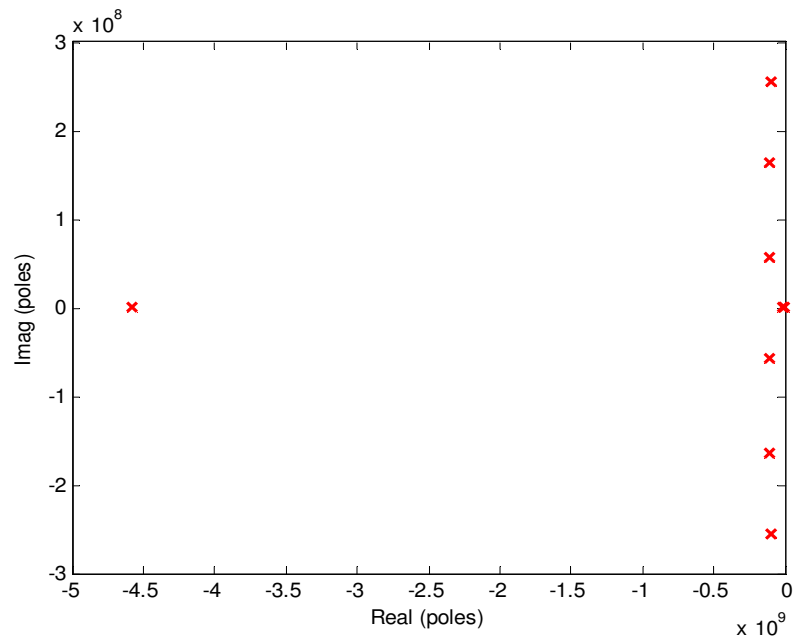
Figure 3.15: Poles location with $M=10$.
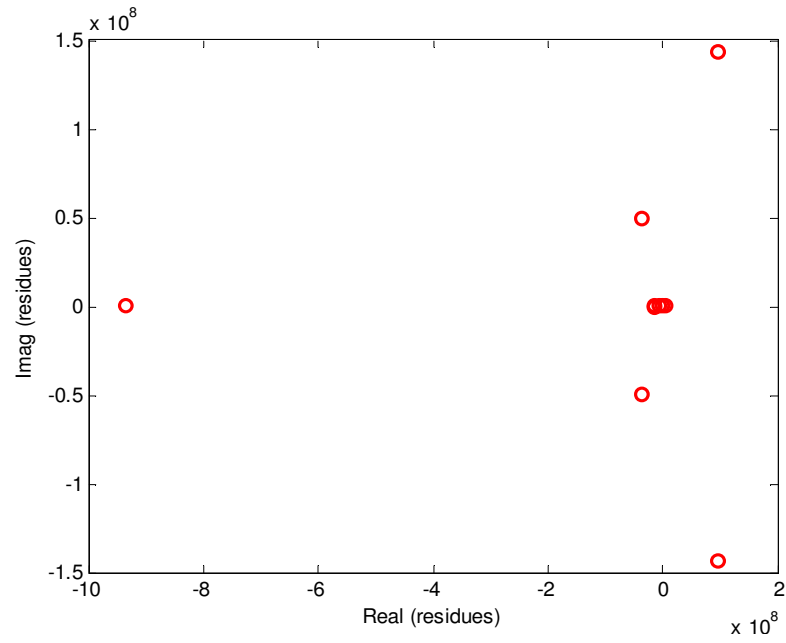
Figure 3.16: Residues location with M=10.
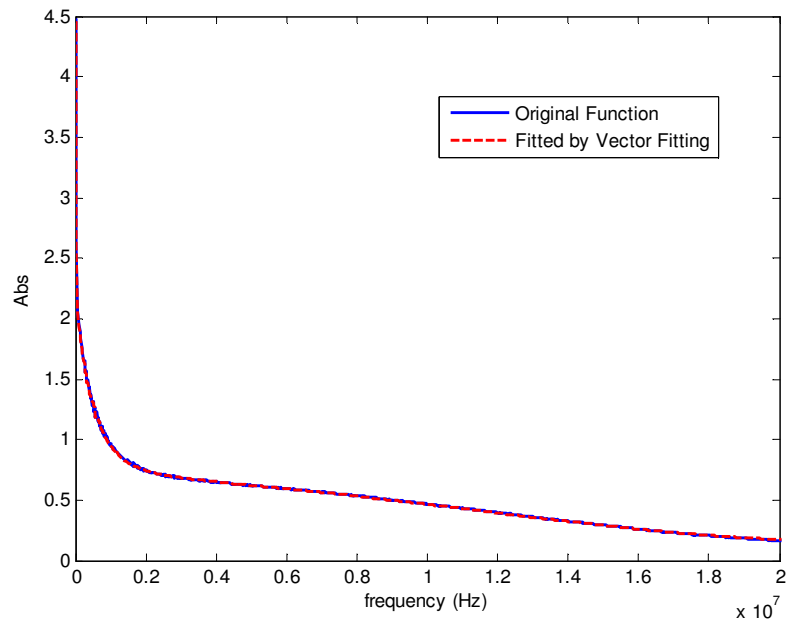
Figure 3.17: Amplitude of the original function and fitted one by using vector fitting algorithm with M=10.
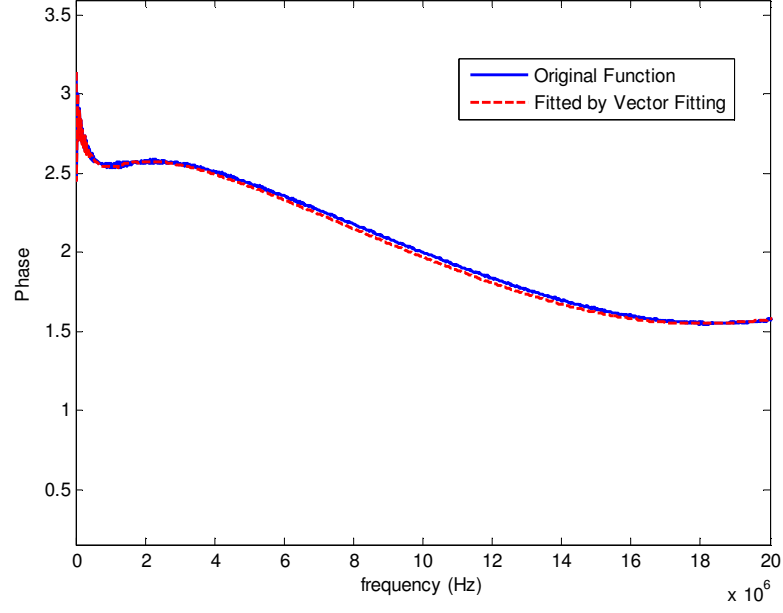
Figure 3.18: Phase of the original function and fitted one by using vector fitting algorithm with M=10.
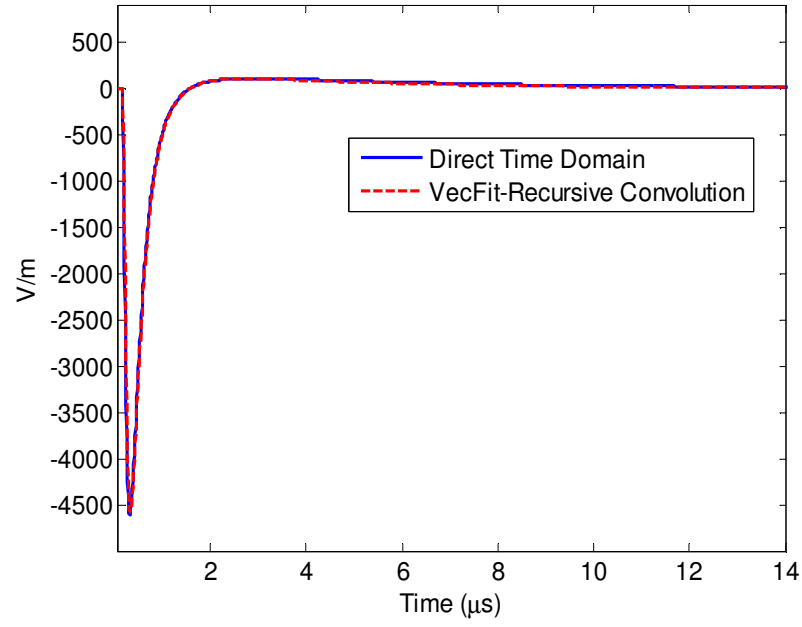
Figure 3.19: Radiation term of the electric field.
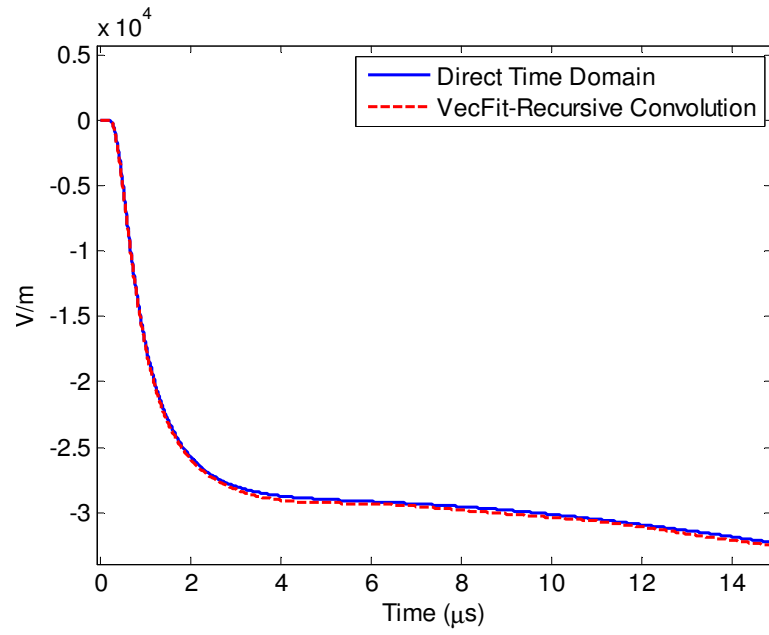
Figure 3.20: Static term of the electric field.
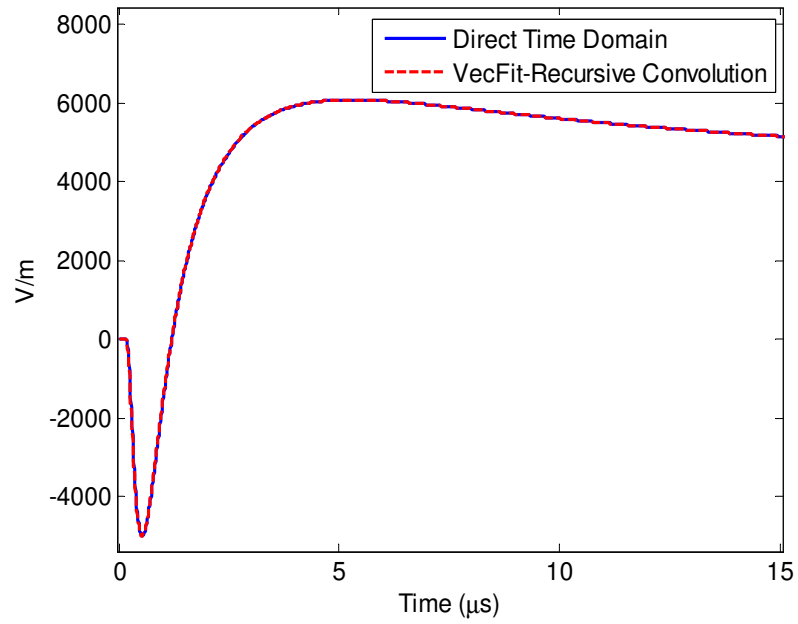
Figure 3.21: Induction term of the electric field.

Table 3.1: Error percentage of two cases of function fitting by using Vector Fitting algorithm. a)3-pole b)10-pole

Number of Poles	Induction term error	Static term error	Radiation term error
M=3	10.9%	4.32%	40.98%
M=10	0.27%	0.77%	5.79%
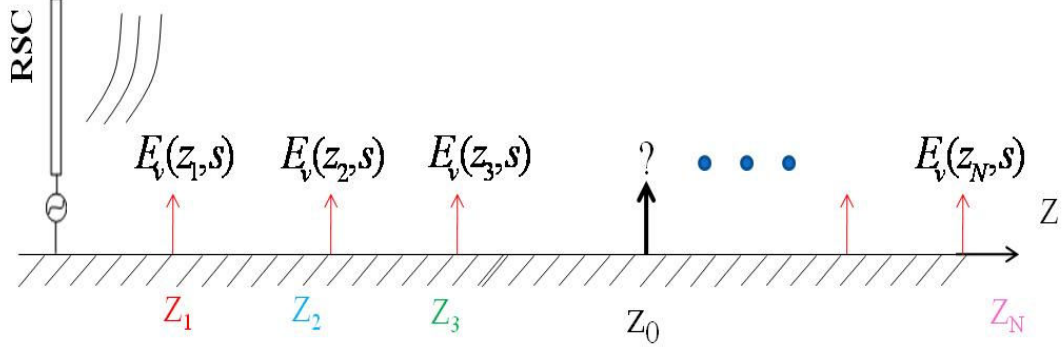
Figure 3.22: The geometry of the field macromodel problem to be solved.

3.5 Field-Macromodel's Details and Procedures

In this section, we are proposing a macromodel to calculate electromagnetic field at any arbitrary point in the space by using the knowledge of the EM field information at few other points. Figure 3.22 shows a schematic of the problem to be solved. Assume that the desired field to be calculated is the vertical component over the ground. As shown in this figure, we have the vertical components of the electric field at N points $Z_1, Z_2, ..., Z_N$, and we want to calculate the vertical electric field for an arbitrary point, z_0. Following the same procedure as we had in section 3.4 to obtain poles and residues positions, we obtain them for any of distances $Z_1, Z_2, ..., Z_N$ to form a $M \times N$ poles/residues matrix as shown in 3.21. The ith column in these matrices ($1 \leq i \leq N$), corresponds to the poles/residues
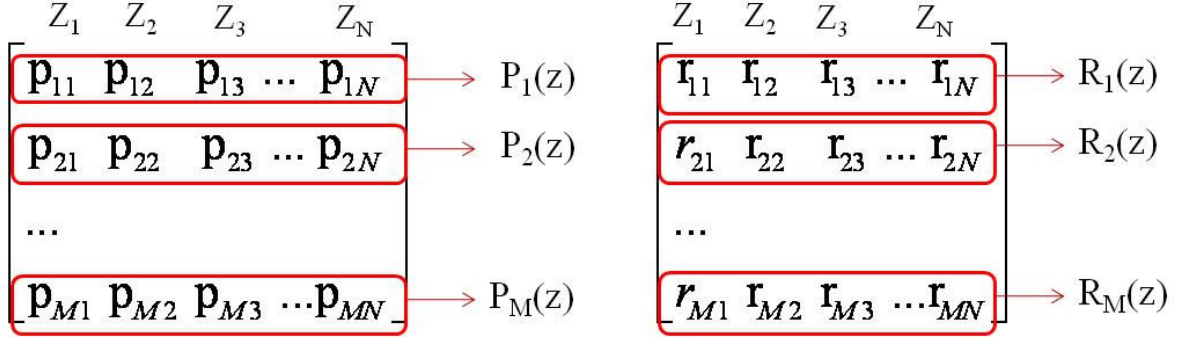
Figure 3.23: Fitting the same order poles/residues into the functions.

of distance Z_i which is obtained by Vector Fitting algorithm.

$$
P = \begin{bmatrix} p_{11} & p_{12} & p_{13} & \cdots & p_{1N} \\ p_{21} & p_{22} & p_{23} & \cdots & p_{2N} \\ \cdots & & & & \\ p_{M1} & p_{M2} & p_{M3} & \cdots & p_{MN} \end{bmatrix} , \quad R = \begin{bmatrix} r_{11} & r_{12} & r_{13} & \cdots & r_{1N} \\ r_{21} & r_{22} & r_{23} & \cdots & r_{2N} \\ \cdots & & & & \\ r_{M1} & r_{M2} & r_{M3} & \cdots & r_{MN} \end{bmatrix} . \quad (3.21)
$$

The next step is to find a relationship between the same order poles/residues as shown in Figure 3.23. In this figure the jth row ($1 \leq j \leq M$) represents the jth poles/residues of those N distances. For example, the first poles and residues are fitted to functions of z, $P_1(.)$ and $R_1(.)$, respectively. This is repeated for all M poles and residues obtained from Vector Fitting. Then for the arbitrary point z_0, we can obtain poles and residues by simply evaluating these functions.

$$
\begin{cases} p_i(z_0) = P_i(z = z_0) \\ r_i(z_0) = R_i(z = z_0) \end{cases} , i = 1, 2, ..., M \quad (3.22)
$$

44

The frequency domain data is obtained using,

$$E(z = z_0) = \sum_{i=1}^{M} \frac{r_i(z_0)}{j\omega - p_i(z_0)}. \tag{3.23}$$

Using Inverse Fourier Transform we convert it into the time domain,

$$\zeta(t, z_0) = f^{-1}(E(z_0)) = \sum_{i=1}^{M} r_i e^{p_i t} \tag{3.24}$$

where $\zeta(t, z_0)$ stands for the impulse response of the system in the time domain. Note that we obtained 3.23 by using 3.16 which was impulse response of the system. The recursive convolution is useful at this step to obtain output response by using input channel-base current as,

$$e(z_0, t) = i_{base}(t) * \zeta(t, z_0). \tag{3.25}$$

Equation 3.25 is so-called *Field Macromodel Equation*. The main challenge is to find proper functions $P_i(.)$ and $R_i(.)$ shown in Figure 3.23. In this work, we can use two types of interpolation. The first one is to use *linear interpolation* between each pole and residue to find unknown poles and residues. The second one is to *fit functions on the trace of poles and residues* and evaluate them. These functions may be polynomial, exponential, etc. This type of interpolation will be useful in Voltage Macromodel which is discussed in the next chapter.

In summary, the general procedure in the field macromodel is shown in Figure 3.24. The specific details of field macromodel is shown in Figure 3.25. As shown in Figure 3.25, the input to the macromodel is channel base current and the position of the point in the space which we need to have the electric field information at. The output is the calculated electric field in the time domain. Transfer function data required for Vector Fitting is
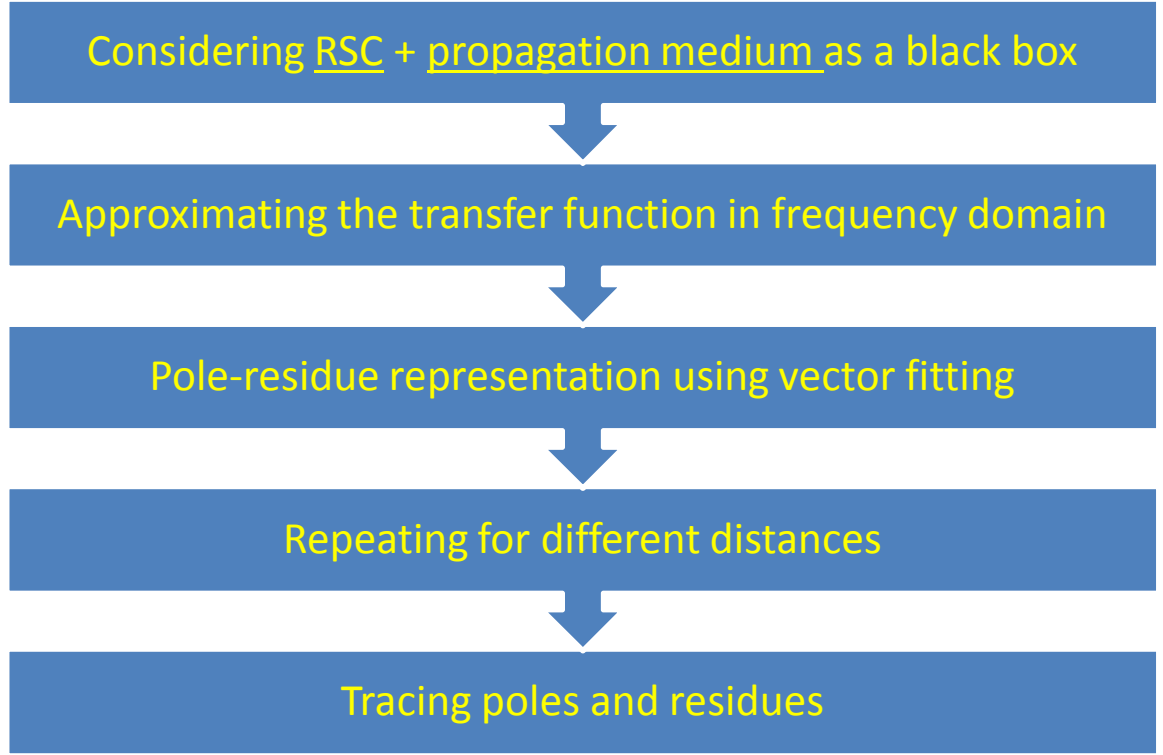
Figure 3.24: The general procedure going on in the field macromodel.

obtained either by using engineering models or NEC software (which will be explained in detail at the last section of this chapter). The former gives transfer function data in the time domain and Fourier techniques is needed to convert it into the frequency domain (as was discussed in section 3.4). NEC provides data in positive frequencies which is suitable for being used by Vector Fitting algorithm directly. The operation denoted by A is to omit the DC and negative frequencies which are due to use of FFT. It is necessary to use operation B at the end to add DC and negative frequencies data to be able apply IFFT. In the next section, we are presenting an example of lightning RSC to calculate the electric field using developed field macromodel and compare the results with those of direct time domain methods. Engineering models as well as frequency-domain software such as NEC are used to provide electric field data. Effects of different parameters such as, *different*

Figure 3.25: Solution flow of the details and procedures inside the field macromodel.

Figure 3.26: The geometry of the field macromodel example.

engineering models, different ground conductivity, different number of space segmentation, and *different number of fitting poles* are studied.

3.6 Field-Macromodel's Results

Consider a 6-km lightning flash that occurs at a distance of 50m from a 500m horizontal transmission line which is located at 10m above the ground. The geometry of this problem is shown in Figure 3.26. Efficient calculation of the horizontal electric fields along the transmission line is essential to obtain the induced overvoltage in next chapter where we will discuss the voltage macromodel. In this example, we will study the horizontal electric field component. Figure 3.27 shows the channel base current of the RSC that is used as the input of the macromodel. Time needs to be discretized in a way that there are enough data points at the rising part of the current waveform and its derivative (Figure 3.28 and 3.29). We chose $\Delta t = 20ns$ to discretize the waveform shown in Figure 3.27.

To obtain the horizontal electric field at any arbitrary point, we need to have electric field data at certain points in the space. We chose 17 equally-spaced points in the space

Figure 3.27: Channel base current for the field macromodel's input.
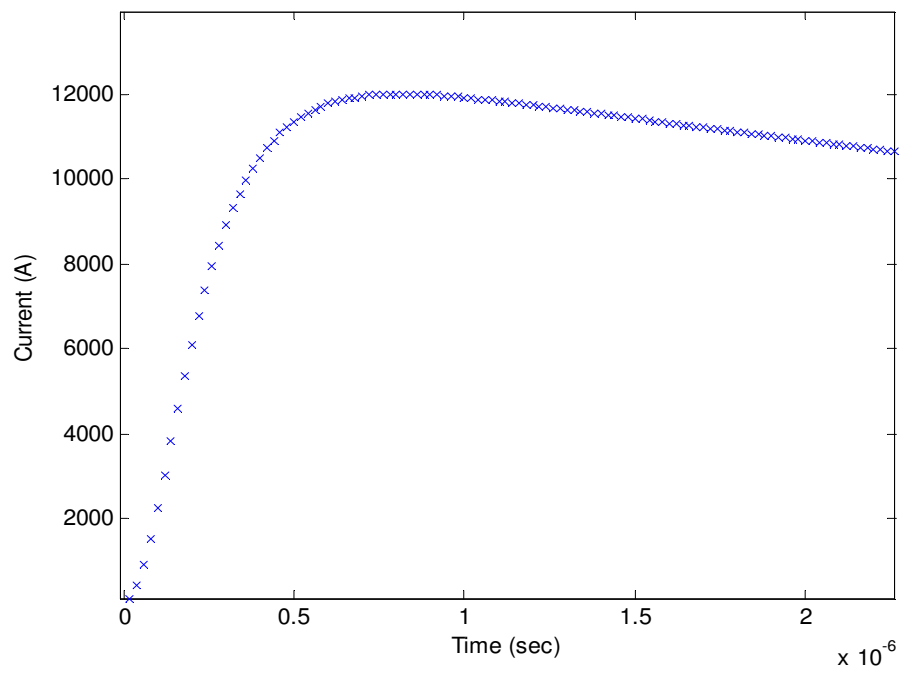
Figure 3.28: Data points on the rising part of the channel base current.

49
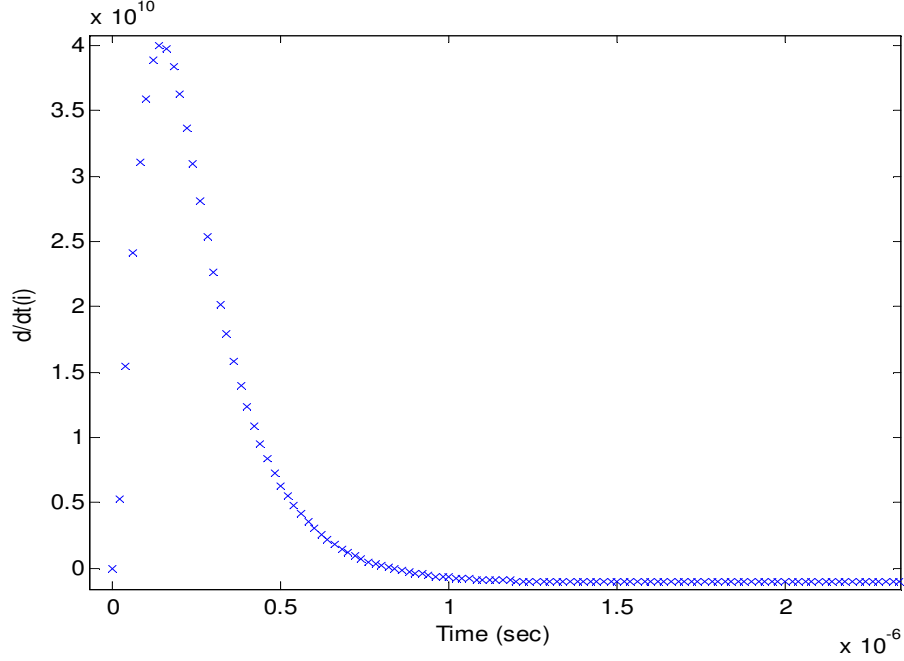
Figure 3.29: Data points on the rising part of the channel base current derivative.

with a separation of 30m. Typical values of 0.001 S/m and 10 are chosen for the ground conductivity and relative permittivity, respectively. For the 6-km lightning RSC, we use MTLL model with propagation speed along the channel equal to $1.5 \times 10^8 m/s$. Figure 3.30 shows the horizontal electric field in the time domain for 5 of 17 different segments which are obtained by using Cooray-Rubinstein formula. The frequency domain data for Vector Fitting algorithm is also provided directly by using 3.7. We used 10 poles and residues in Vector Fitting algorithm. The variation of the poles and residues of the horizontal component of the electric field for the mentioned 17 points is demonstrated as image in Figures 3.31- 3.34. In these figures, the horizontal axis is the segment's number and the vertical axis is the pole/residue's number. As expected, there is very smooth variation in the real and imaginary parts of the poles and residues. The reason is that there is no sudden change in the time variation of the electric field. This means we are able to find functions to fit into the trace of the poles and residues. This should be done for all the 10
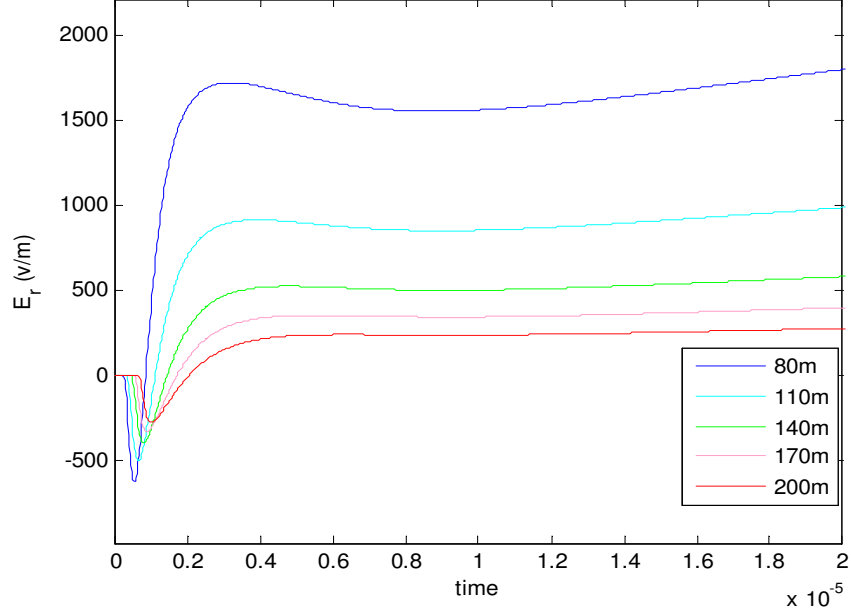
Figure 3.30: Horizontal electric field for 80, 110, 140, 170, and 200m distance from the RSC calculated by direct time domain method and RSC MTLL model

poles and residues. As samples, we plotted the position of different poles and residues and the proper fitting function in Figures 3.35- 3.42.

For example, in Figure 3.35, the positions of the real of pole number 8 for all of the 17 different segments are shown and we can see how it varies with the distance. The problem then is to find a fitting function to trace the poles. In this chapter, we are free to choose polynomial functions, exponential functions, or any other functions. Suppose we choose to fit with polynomial function. After selecting the order of the polynomial, a least square problem has to be solved to obtain the unknown coefficients of the polynomial. It should be noted that by increasing the polynomial order, the accuracy of the fitting is increased. In Chapter 4, we will see that by using first order polynomials for the poles and second order polynomials for the residues, we are able to simplify the voltage macromodel and obtain a closed form solution. Considering this fact, function $P_8(z)$ in Figure 3.35, is obtained to trace the real part of the 8th pole as, $real\{P_8\}(z) = 1.4 \times 10^3 z - 2 \times 10^6$.

51
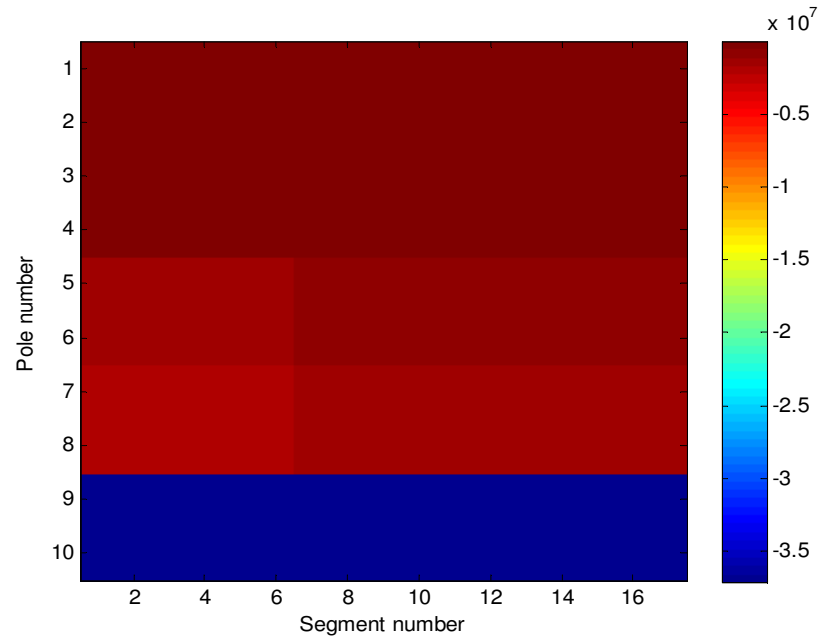
Figure 3.31: Variation of the real of the poles with segment number.
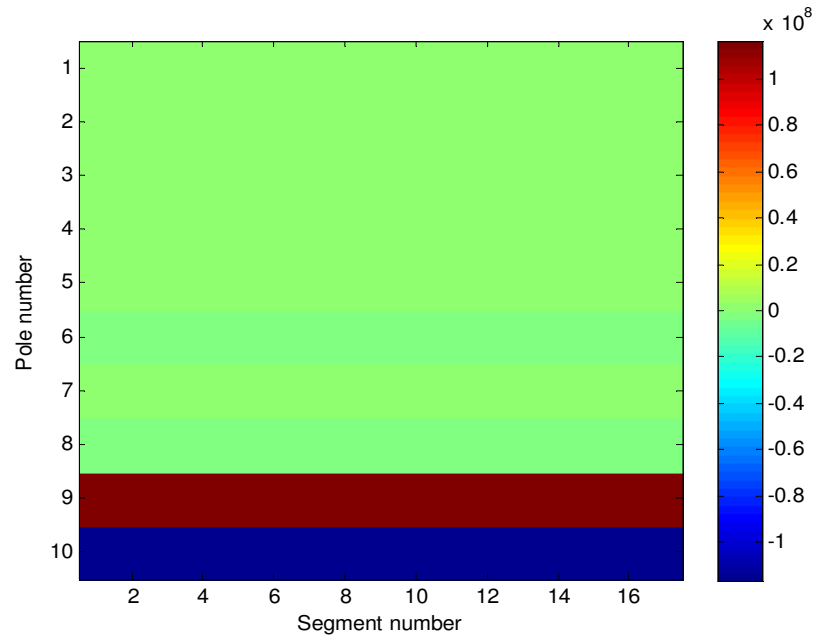
Figure 3.32: Variation of the imaginary of the poles with segment number.
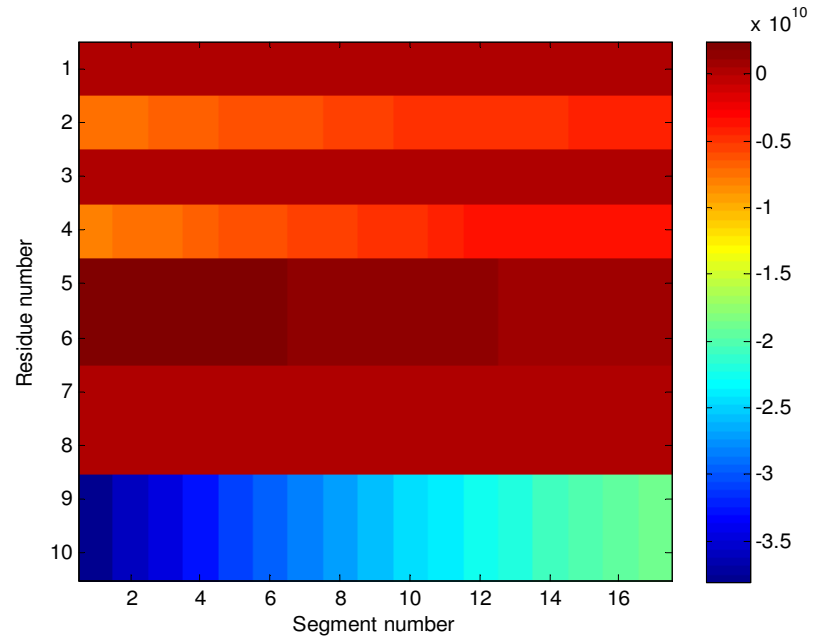
Figure 3.33: Variation of the real of the residues with segment number.
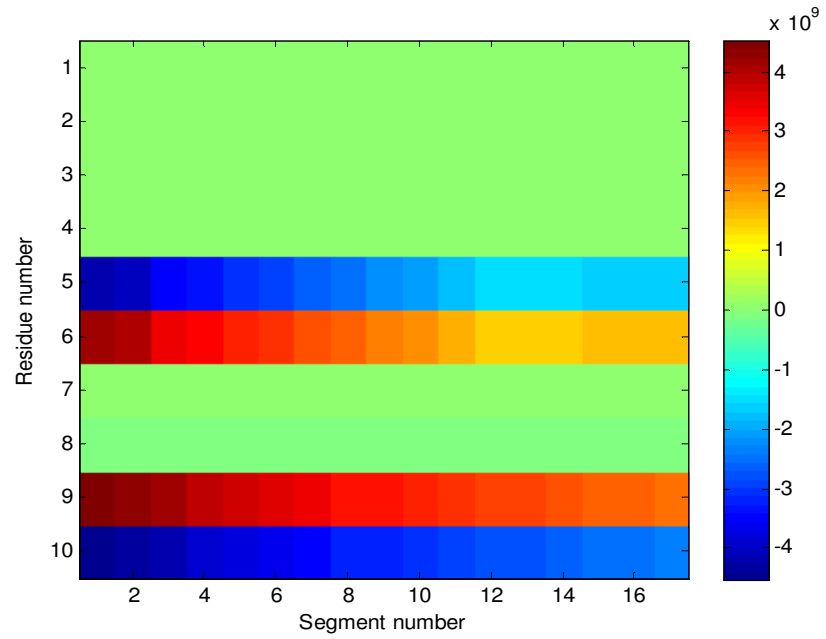
Figure 3.34: Variation of the imaginary of the residues with segment number.
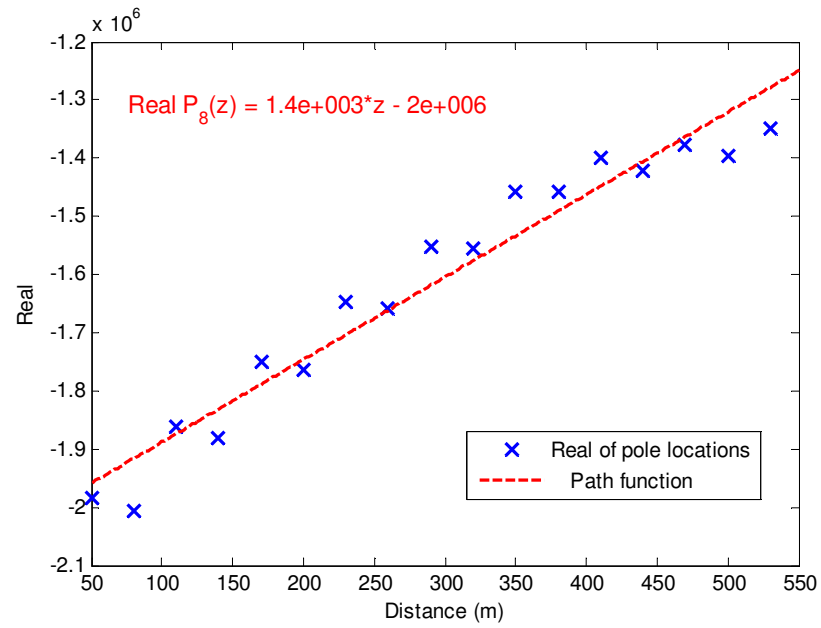
Figure 3.35: 8th pole's real part locations in different distances.
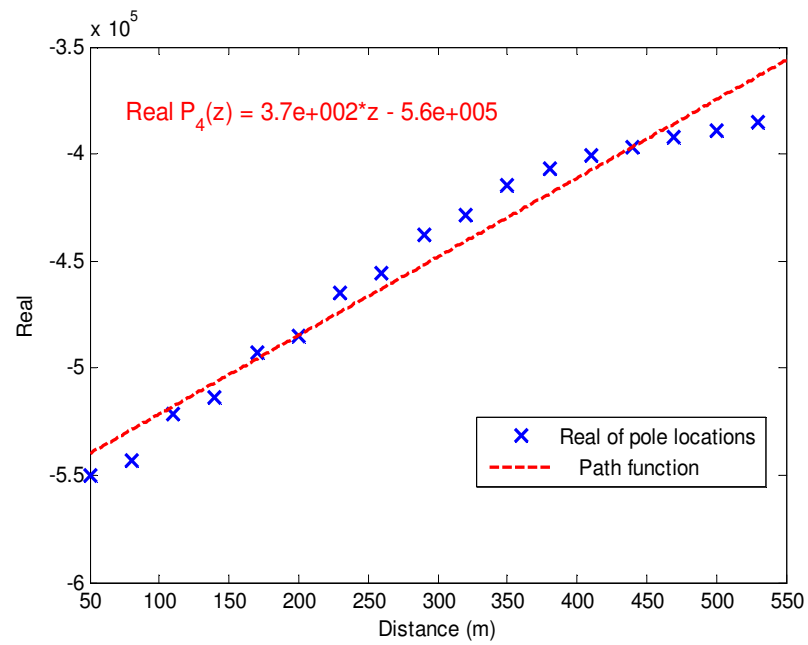
Figure 3.36: 4th pole's real part locations in different distances.

54
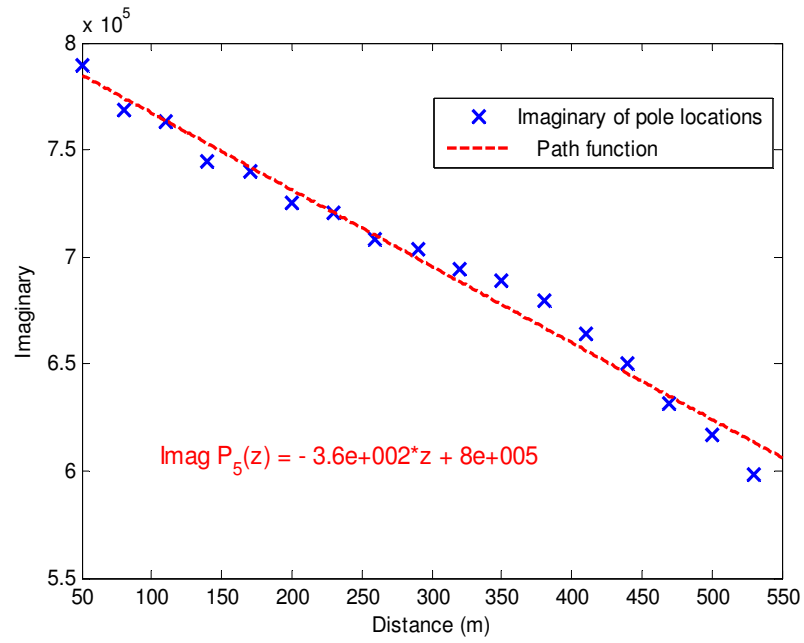
Figure 3.37: 5th pole's imaginary part locations in different distances.
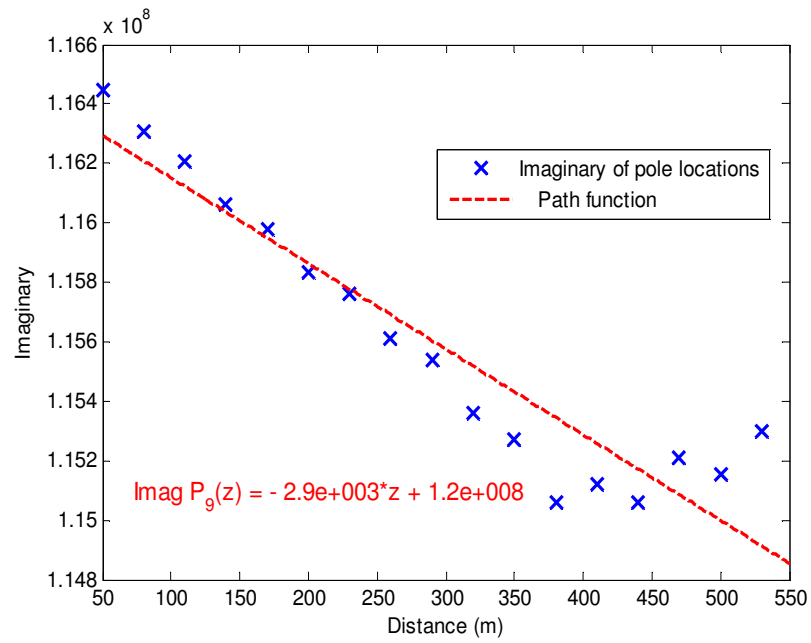
Figure 3.38: 9th pole's imaginary part locations in different distances.
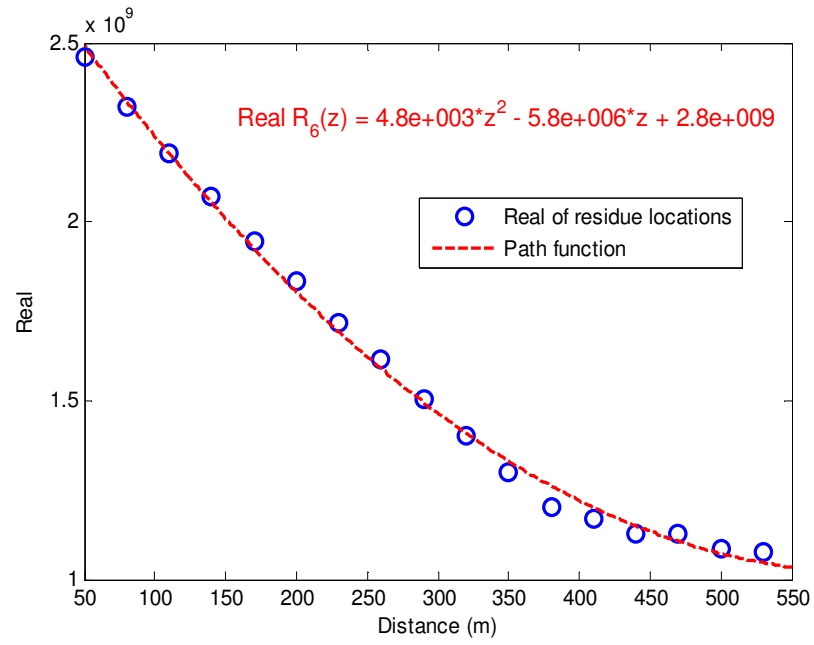
Figure 3.39: 6th residue's real part locations in different distances.
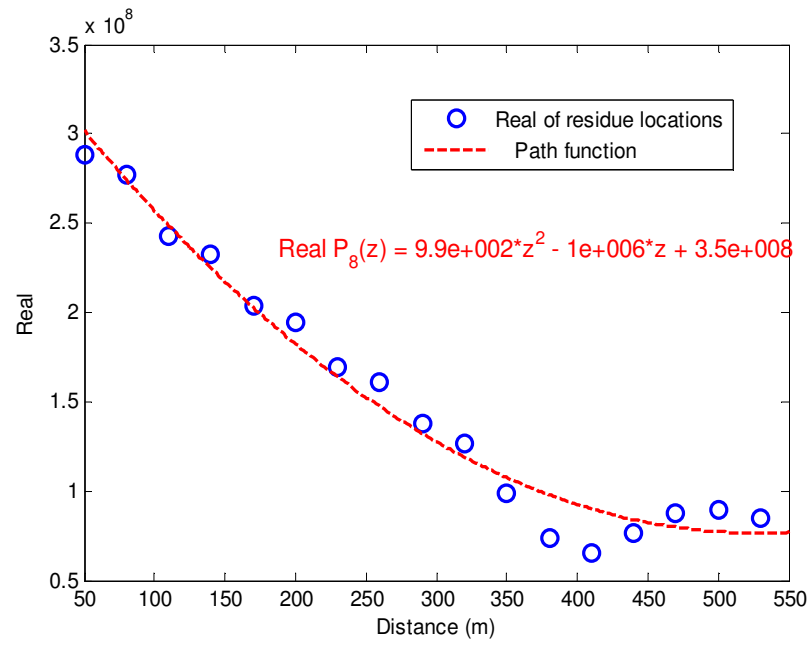
Figure 3.40: 8th residue's real part locations in different distances.
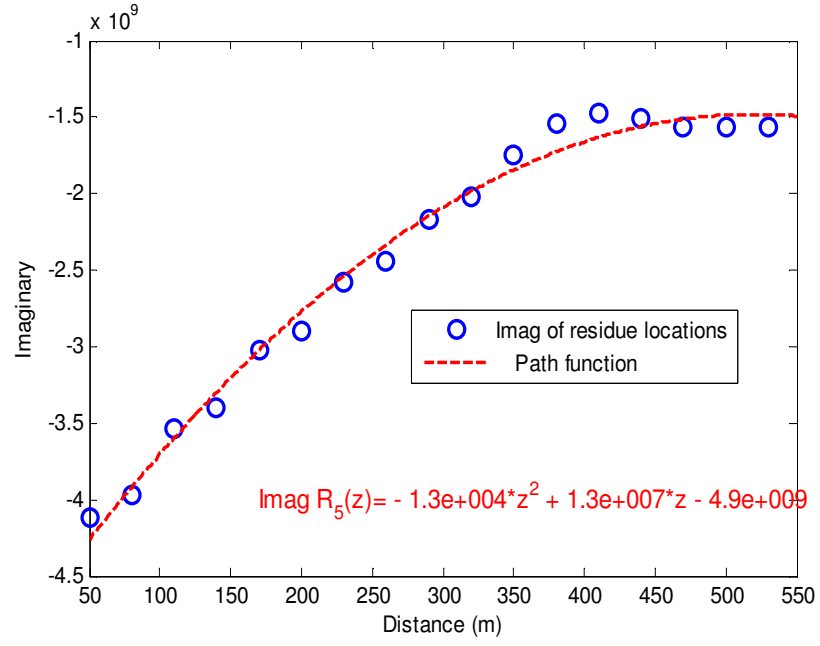
Figure 3.41: 5th residue's imaginary part locations in different distances.
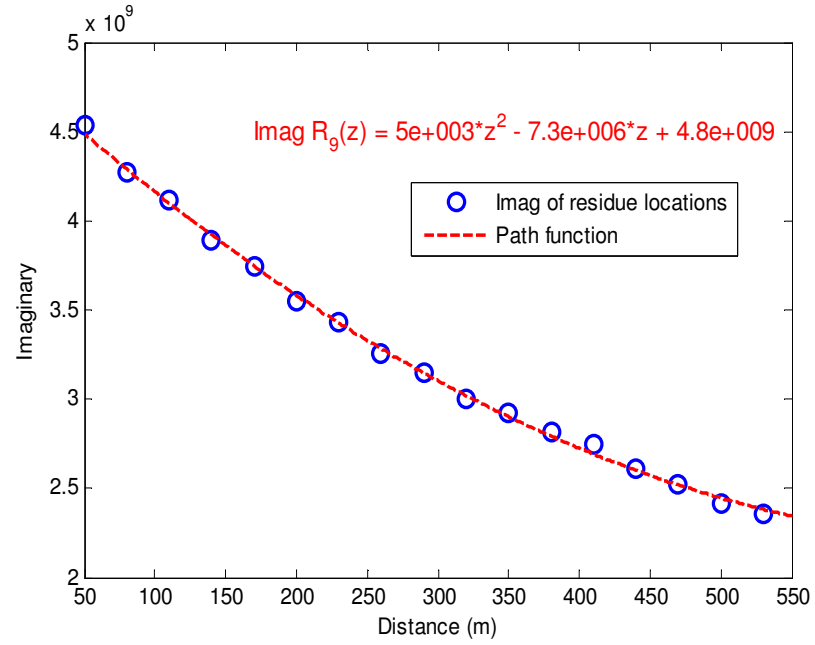
Figure 3.42: 9th residue's imaginary part locations in different distances.

57
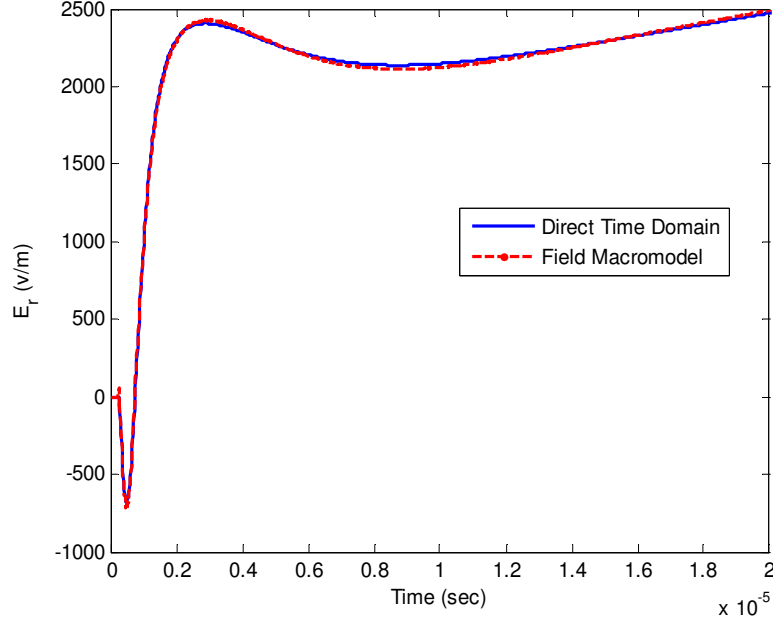
Figure 3.43: Horizontal electric field at z=70m and h=10m above the ground with $\sigma = 0.001S/m$, using MTLL model.

Same procedure needs to be taken to obtain all fitting functions. Then for any z_0, the poles and residues is calculated by these functions simply. For this section, we chose several results for z_0 such as: $z_0 = 70m, 190\text{m}, 310\text{m}, 496\text{m}$. The direct time domain result and field macromodel result is compared for mentioned distances in Figures 3.43- 3.46.

It is observed that the field macromodel results are in a very good agreement with direct time domain method results. The small difference is because of the fact that the fitted functions do not go through the exact location of poles and residues of different distances. To further examine the proposed field macromodel, different parameters are studied in next subsections.

3.6.1 The Effect of Different Engineering Models

Effect of different RSC Models such as, *MTLE*, *MTLL*, and *TL*, for a ground conductivity of 0.001 S/m and fixed distance of z=310m is studied and the results obtained using these
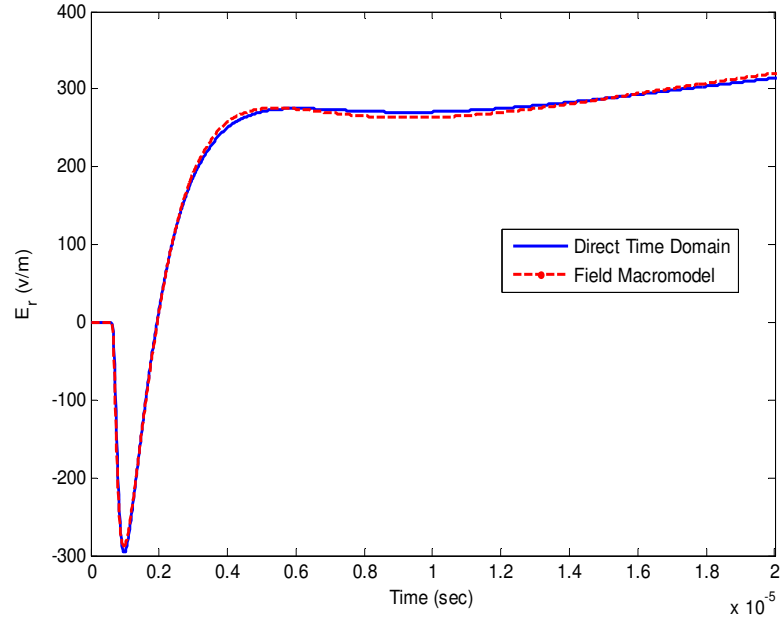
Figure 3.44: Horizontal electric field at z=190m and h=10m above the ground with $\sigma = 0.001S/m$, using MTLL model.
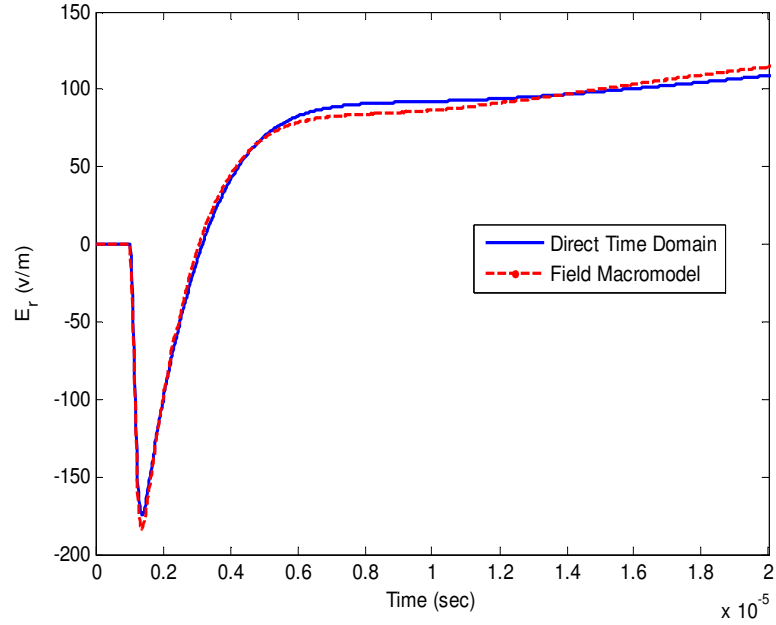
Figure 3.45: Horizontal electric field at z=310m and h=10m above the ground with $\sigma = 0.001S/m$, using MTLL model.
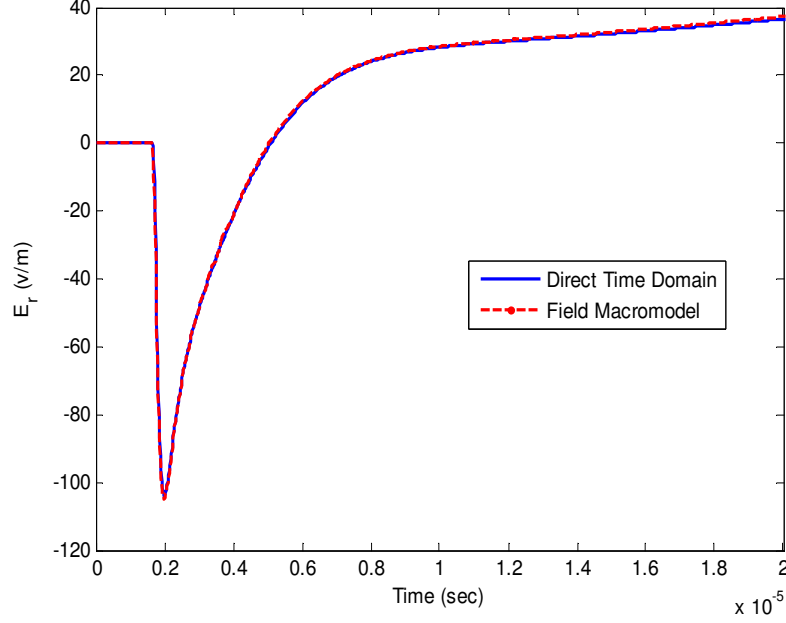
Figure 3.46: Horizontal electric field at z=495m and h=10m above the ground with $\sigma = 0.001S/m$, using MTLL model.

models are plotted in Figure 3.47. In this figure, the solid lines are direct time domain

results and the dashed lines are macromodel's output calculated by using 10 poles and

residues.

3.6.2 The Effect of Ground Conductivity

In order to study the effect of the ground conductivity on the field macromodel result and

see if the EM field macromodel is able to predict the accurate results for different values

of ground conductivities, several values of ground conductivities are studied. We used

MTLL model for RSC and obtained the horizontal electric field at z=310m for different

ground conductivities such as, $\sigma = \infty, 0.01S/m, 0.001S/m, 0.0001S/m$ and using 10 poles

and residues. A comparison of macromodel outputs and those of direct time domain results

is shown in Figure 3.48. Obviously, the ground conductivity has an important effect on

the horizontal electric field and in all the cases, field macromodel's results are in a good
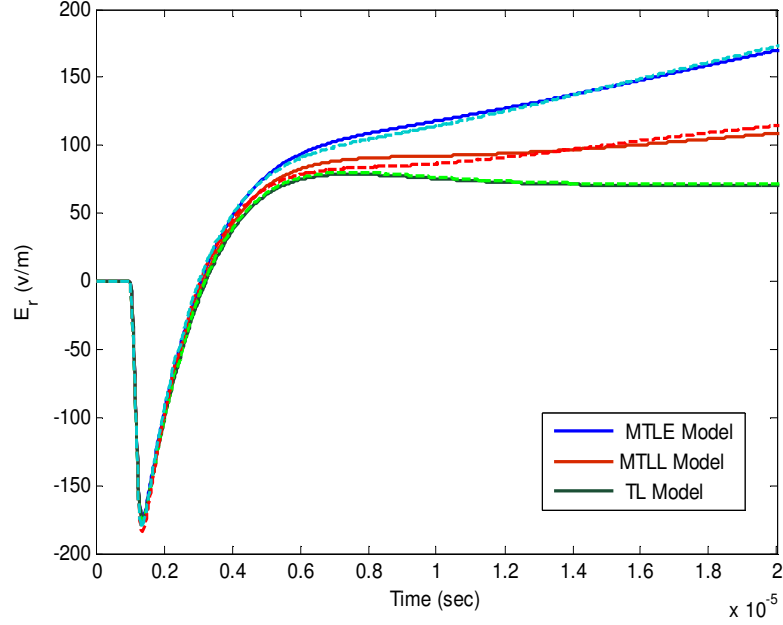
Figure 3.47: Comparison of the output of the field macromodel for three engineering models with their direct time domain solutions.

agreement with direct time domain results.

3.6.3   The Effect of the Number of Poles

This is one of the critical issues in the field macromodel and we need to choose a proper number of poles and residues to have enough accuracy. Figure 3.49 demonstrates the effect of the number of the poles on macromodel output. Similar to previous example, MTLL model is used for the RSC and the horizontal electric fields are calculated at z=310m. The results are obtained for 3, 5, 8, 10, 30, and 60 poles. As shown in Figure 3.49, small number of poles and residues makes the results inaccurate. By increasing the number of poles, the accuracy increases. But as it was mentioned before, very large number of poles makes Vector Fitting algorithm unstable. The result for 60 poles is plotted separately in Figure 3.50. Due to deficiency in performance of the Vector Fitting algorithm in large number of poles, there is a big difference between macromodel output and direct time
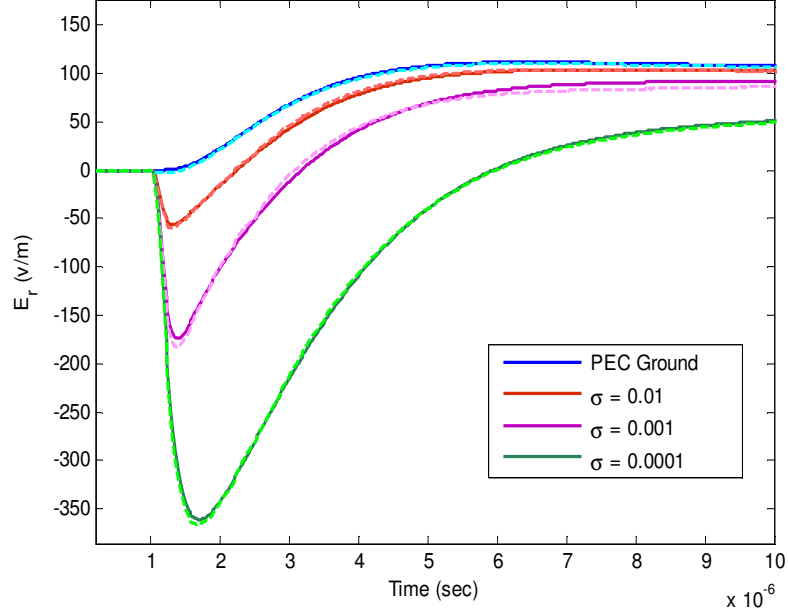
Figure 3.48: Comparison of the output of the field macromodel for different ground conductivities with their direct time domain solutions.

domain method's result.

3.6.4 The Effect of the Number of Segmentation

We need to have the knowledge of the electric field in some points in the space. In this thesis, we chose N_z points in the space, linearly separated with Δz, $(N_z - 1$ segments). In the above mentioned example, we had 17 points from 50m up to 550m distance from RSC location which is equivalent to $\Delta z = 30m$. Figure 3.51 shows the field macromodel output for different numbers of segmentation. Expectedly, by increasing the segments length, the accuracy of the poles and residues tracing will decrease and the output will be inaccurate. It should be noted that having very small segment length means increasing the calculation time. For our cases, $\Delta z = 30m$ was accurate enough.
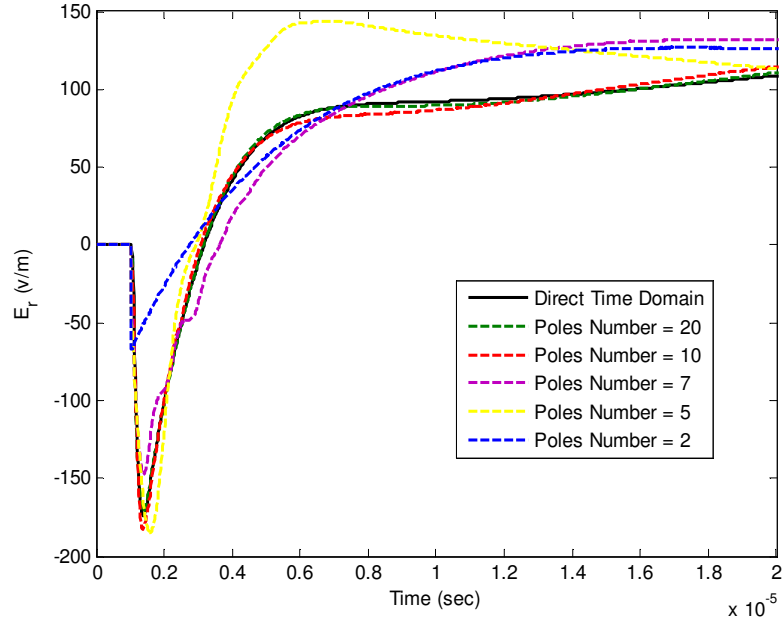
Figure 3.49: Comparison of the output of the field macromodel for different poles number with their direct time domain solutions.
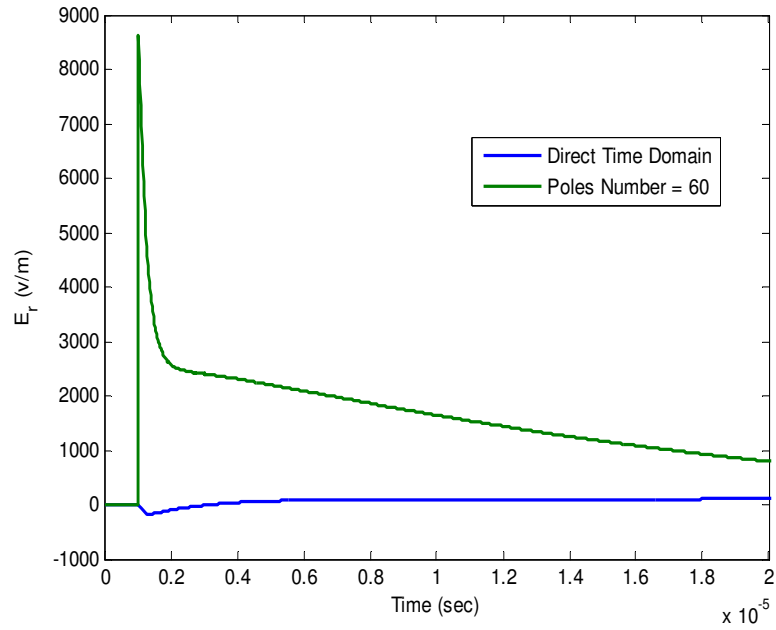
Figure 3.50: Comparison of the output of the field macromodel for a high number of poles for fitting with its direct time domain solution.
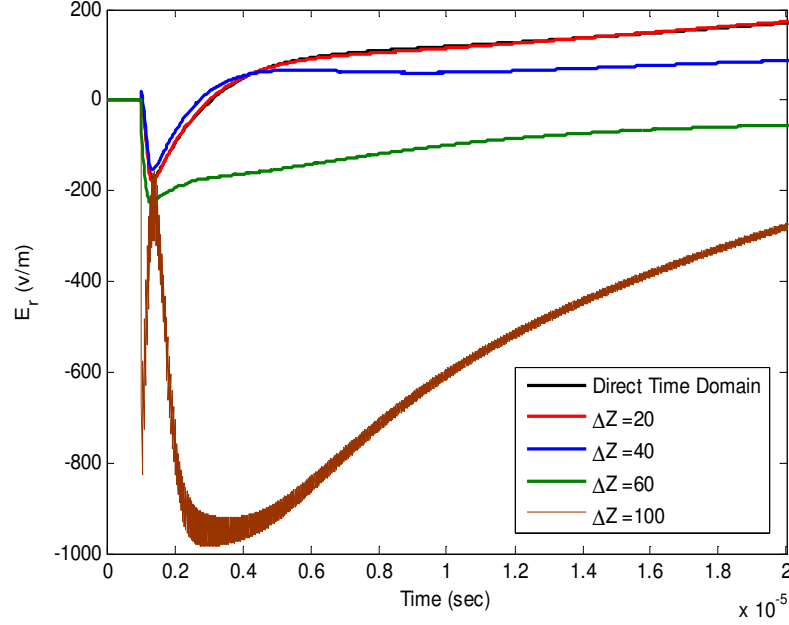
Figure 3.51: Comparison of the output of the field macromodel for different segmentation length with their direct time domain solution.

3.6.5 NEC

As shown in Figure 3.25, the input data for Vector Fitting algorithm can be from any algorithm or software that calculates the electromagnetic frequency domain information. In this work, Numerical Electromagnetic Code (NEC) is also used for this purpose besides the engineering models. There are several considerations in working with NEC which will be discussed in this subsection. At the end, we will show the field macromodel output for the data provided by NEC.

NEC is a standard tool for numerical analysis of electromagnetic field around wire antennas and can be applied to analysis of lightning transient voltages. This code solves 3-dimentional boundary problems by using electric field integral equation. This program provides the EM field data in positive frequencies. It means it doesn't give any information about the DC frequency. In this thesis, the DC component of the electric field produced

by NEC are considered to be zero. As mentioned in chapter 2, in electromagnetic models of RSC, the lightning channel is modeled as a monopole antenna which is discretized in space and frequency. For this purpose, the conductors are modeled with cylindrical wire segments which are defined by their two end points and radiuses. Geometrically, the segments should follow the path of conductors as close as possible by using a piece-wise linear fit on curves. The main electrical consideration is on the segment length Δx, relative to the wavelength λ, as, [83,84]

$$10^{-3}\lambda < \Delta x < 0.1\lambda. \tag{3.26}$$

Careful considerations should be taken in determining the time step Δt, and the duration of analysis T (or equivalently the highest frequency f_{high}, and the lowest frequency f_{low}, in the frequency domain analysis). The frequencies of the output must be coincided with the frequencies analyzed by NEC software. In our example, the time step Δt, is chosen $20ns$ with respect to the channel base current shape and to have enough data points on the rise time of the current derivative and 2049 time steps is considered ($T = N_t \times \Delta t = 40.98\mu s$). The sampling frequency is, $f_s = \frac{1}{\Delta t} = 50MHz$. So the bandwidth is, $Bw = \frac{f_s}{2} = 25MHz$. This is the upper frequency which should be considered in NEC. Because of using Discrete Fourier Transform, the number of frequency points should be half of the time points ($N_f = 1024$). The lowest frequency then is obtainable by dividing the highest frequency over number of frequency points ($f_{lowest} = \frac{25MHz}{1024} = 24.4kHz$). Next, proper RSC channel segments length must be selected. Equation 3.26 should be satisfied so that, $10^{-3}\lambda_{max} < \Delta x$ and $\Delta x < 0.1\lambda_{min}.(\lambda_{max} = \frac{c}{f_{min}} = 12.3km$ and $\lambda_{min} = \frac{c}{f_{max}} = 12m$). This means the ideal segment length should satisfy $12.3m < \Delta x < 1.2m$ which is impossible. In lightning case, most of the energy presents in the frequencies lower than 1MHz. So lower frequency constrain is more important in segment length determination. We chose
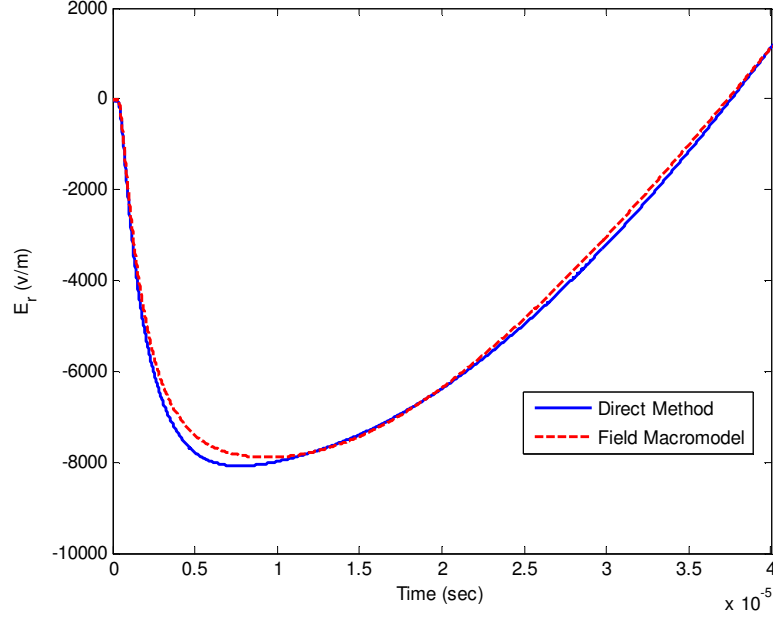
Figure 3.52: Horizontal electric field at z=100m and h=10m above the ground with $\sigma = 0.001 S/m$, by using NEC.

$\Delta x = 15m$ and the 6-km lightning flash is divided into 400 segments to be analysed by NEC. In order to control the current propagation velocity along the antenna, we add electrical components in series along the antenna. To reach a velocity of half of the velocity of light, we used $R = 1\Omega/m$ and $L = 3\mu H/m$ for RSC channel loading. The reason of the presence of the resistor is to decrease the oscillations due to inductor. The procedure to obtain the horizontal electric field at any arbitrary point after using the Vector Fitting algorithm is the same as the case we used the engineering model. Figures 3.52 and 3.53 show the field macromodel's output by using NEC analysis. The results are obtained at 10m above a ground with $\sigma = 0.001 S/m$ at z=100m and z=370m, respectively. Similar to previous cases, macromodel's results are in good agreement with those obtained using Inverse Fourier Transform of the frequency domain EM field data.

In summary, in this chapter, we introduced an efficient macromodel to calculate the electromagnetic field at any arbitrary point in the space around a source of EM radiation.
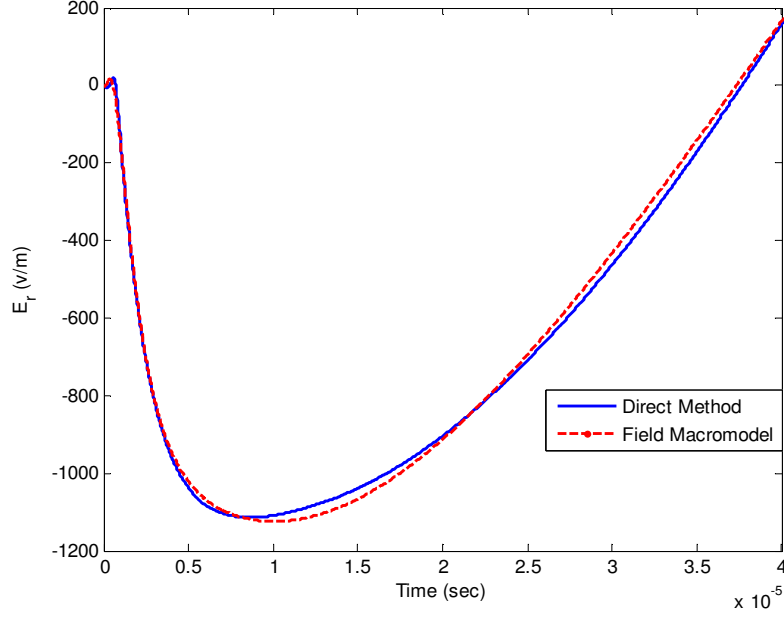
Figure 3.53: Horizontal electric field at z=370m and h=10m above the ground with $\sigma = 0.001 S/m$, by using NEC.

Because of the importance of the lightning-induced voltage in power system simulations and the availability of measurement data, we studied lightning RSC as the radiation source. A discretized channel-base-current-to-radiated-field transfer function was developed using the engineering models of the lightning return-stroke channel. Applying Discrete Time Fourier transform, the channel-base-current-to-field transfer function was evaluated in the frequency domain and was fitted to a pole-residue form by using the Vector Fitting algorithm. Time-domain fields were then determined using the actual and approximate formulations. By repeating these procedures for some other points in the space and interpolating the poles and residues trace of the electric field, we were able to obtain location of any point's poles and residues and subsequently its electromagnetic field information. We did several parametric studies to test our proposed macromodel. The efficiency of the proposed macromodel can be studied by comparing the time required for direct time domain method and our EM field macromodel. In the next chapter we will see that for ob-

taining the induced overvoltage due to external radiation, the space needs to be discretized into 1m segments and field information is needed in these segments. By using direct time-domain formulations to calculate the horizontal electric field at each 1m segments for a 500m transmission line, 8370sec is required while this time reduces to 284sec by using the EM field macromodel (nearly 30 times faster)[1]. As a further advantage, by using field macromodel we just need to calculate the EM field information at certain points only once and for any input, the output signal can be calculated, efficiently.

The Next chapter is focused to explain one of the applications of the proposed EM field macromodel in power system simulators and introduce the voltage macromodel.

---

[1]These results are obtained by using a computer with 2GB RAM and 2.5GHz Dual Core CPU

Chapter 4

Voltage Macromodel

In this chapter, we will develop an efficient macromodel to calculate the induced overvoltages on transmission lines due to external electromagnetic radiations. In fact, this chapter is demonstrating an application of the proposed EM field macromodel. Besides, we will see how this macromodel relates the frequency domain software and time domain simulators. In one hand, complicated power network simulators need to work in the time domain due to time variant and nonlinear electrical components. In the other hand, transmission line characteristics such as conductor loss and dispersion are best described in frequency domain. By using proposed macromodel, we will be able to get advantage of both time and frequency domains.

The organization of this chapter is as follows. In the first section, we will present the telegrapher's equations and the effect of the external excitation on these equations. The second section is dedicated to obtain a closed form solution for coupling equations in frequency domain by using the EM field macromodel concept. The last sections comprises of a number of examples to verify the performance of the developed voltage macromodel.
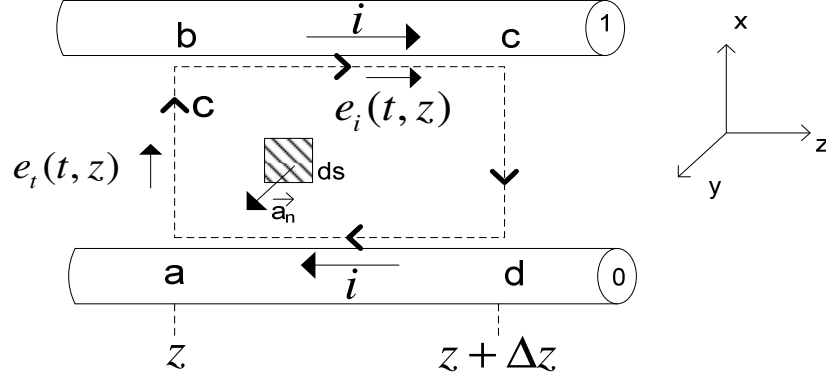
Figure 4.1: Definition of the contour c and the associated surface s for derivation of the first transmission line equation - longitudinal view along the z axis.

4.1 Governing Equation in Transmission Lines

4.1.1 Unexcited Transmission Line

Figure 4.1 shows a general schematic of a two-conductor transmission line. An open surface s between the two conductors which are uniform in cross section along the longitudinal, is shown and it is bounded by a closed contour c. In this figure, $e_t(t,z)$ denotes the transverse electric field and $e_i(t,z)$ denotes the longitudinal electric field. Without loss of the generality of the problem, we assume a frequency independent transmission line. By writing the Faraday's law around the contour c, the first transmission line equation is obtained as [4],

$$\frac{\partial v(z,t)}{\partial z} = -ri(z,t) - l\frac{\partial i(z,t)}{\partial t} \tag{4.1}$$

where, r and l are per unit length resistance and inductance, respectively. In order to derive the second transmission line equation, consider placing closed surface s' around the top conductor, as shown in Figure 4.2. By simply writing the continuity equation or equation of the conservation of charge, the second transmission line equation is derived
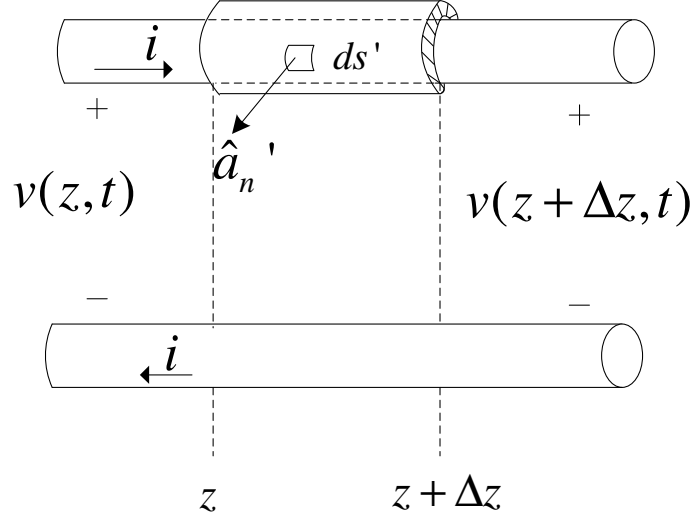
Figure 4.2: Definition of surface s' for derivation of the second transmission line equation - longitudinal view along the z axis.

as [4],

$$\frac{\partial i(z,t)}{\partial z} = -gv(z,t) - c\frac{\partial v(z,t)}{\partial t}, \tag{4.2}$$

where, g and c are per unit length conductance and capacitance respectively. Equations 4.1

and 4.2 can be generalized for the case of multiconductor transmission lines. The general

form of the telegrapher's equations are given by [4],

$$\frac{\partial \mathbf{v}(z,t)}{\partial z} = -\mathbf{r}\mathbf{i}(z,t) - \mathbf{l}\frac{\partial \mathbf{i}(z,t)}{\partial t},$$
$$\frac{\partial \mathbf{i}(z,t)}{\partial z} = -\mathbf{g}\mathbf{v}(z,t) - \mathbf{c}\frac{\partial \mathbf{v}(z,t)}{\partial t}. \tag{4.3}$$

where, $\mathbf{v}$ and $\mathbf{i}$ are the $n \times 1$ voltage and current vectors, respectively, and n is the number

of conductors. $\mathbf{r}$, $\mathbf{l}$, $\mathbf{g}$ and $\mathbf{c}$ are $n \times n$ per-unit length resistance, inductance, conductance

and capacitance matrices, respectively.

4.1.2 Excited Transmission Line

In order to find the effect of external electromagnetic field excitation on Telegrapher's equation and obtaining the coupling-to-line equations, let's consider Figures 4.1 and 4.2 in the presence of external electromagnetic fields. The derivation of transmission line equations for an excited line is similar to the unexcited line but as this chapter relies on the fundamental results of this section, the whole procedure is shown below. Writing the Faraday's law around the contour of the flat surface between the two conductor, as shown in Figure 4.1, gives, [4]

$$\int_a^b \mathbf{e} \cdot \mathbf{dl} + \int_b^c \mathbf{e} \cdot \mathbf{dl} + \int_c^d \mathbf{e} \cdot \mathbf{dl} + \int_d^a \mathbf{e} \cdot \mathbf{dl} = \frac{d}{dt}\psi_n, \tag{4.4}$$

where, $\mathbf{e}$ represents the incident electric field. The total magnetic flux penetrating the flat surface is,

$$\psi_n = \int_s \mathbf{b} \cdot \mathbf{ds} = \int_s \mathbf{b} \cdot \hat{\mathbf{a}}_n ds, \tag{4.5}$$

where, $\hat{\mathbf{a}}_n$ is unit normal vector to the surface. The magnetic flux density $\mathbf{b}$, consists of two components. The scattered field, denoted as $\mathbf{b}^{scat}$, and the incident field component, denoted as $\mathbf{b}^{inc}$. Equation 4.5 becomes,

$$\psi_n = \int_s \mathbf{b}^{scat} \cdot \hat{\mathbf{a}}_n ds + \int_s \mathbf{b}^{inc} \cdot \hat{\mathbf{a}}_n ds \tag{4.6}$$

The line voltages are defined as,

$$v(z,t) = -\int_a^b \mathbf{e}(x,y,z,t) \cdot \mathbf{dl},$$

$$v(z+\Delta z, t) = -\int_d^c \mathbf{e}(x,y,z+\Delta z,t) \cdot \mathbf{dl}. \tag{4.7}$$

If the per-unit-length resistance of conductors are r_1 and $r_0 \Omega/m$, respectively, then,

$$-\int_b^c \mathbf{e} \cdot \mathbf{dl} = -\int_b^c e_z dz = -r_1 \Delta z i(z,t),$$

$$-\int_d^a \mathbf{e} \cdot \mathbf{dl} = -\int_d^a e_z dz = -r_0 \Delta z i(z,t), \tag{4.8}$$

where, we used e_z as the longitudinal electric field. Combining 4.6, 4.7, 4.8, and 4.4 and dividing both sides by Δz gives,

$$\frac{v(z + \Delta z, t) - v(z,t)}{\Delta z} + r_1 i(z,t) + r_0 i(z,t)$$

$$- \frac{1}{\Delta z} \frac{d}{dt} \int_s \mathbf{b}^{scat} \cdot \hat{\mathbf{a}}_n ds = \frac{1}{\Delta z} \frac{d}{dt} \int_s \mathbf{b}^{inc} \cdot \hat{\mathbf{a}}_n ds. \tag{4.9}$$

The per-unit-length magnetic flux penetrating the flat surface which is due to the currents of the conductors, is related to the per-unit-length inductance of the line l, as,

$$\psi = -\lim_{\Delta z \to 0} \frac{1}{\Delta z} \int_s \mathbf{b}^{scat} \cdot \hat{\mathbf{a}}_n ds = -\int_a^b \mathbf{b}^{scat} \cdot \hat{\mathbf{a}}_n dl = l i(z,t). \tag{4.10}$$

Taking the limit of 4.9 and using 4.10, gives the first transmission line equation as,

$$\frac{\partial v(z,t)}{\partial z} + r i(z,t) + l \frac{\partial i(z,t)}{\partial t} = \frac{\partial}{\partial t} \int_a^b \mathbf{b}^{inc} \cdot \hat{\mathbf{a}}_n dl, \tag{4.11}$$

where, r represents the total per-unit-length resistance of the line and $r = r_1 + r_0$. For obtaining the second coupling equation, consider Figure 4.2 in the presence of an incident electromagnetic field. The portion of the surface over the caps is denoted as S_e whereas the

portion over the side is denoted as S_s. According the equation of conservation of charge,

$$\oiint_S \mathbf{J} \cdot \mathbf{ds} = -\frac{\partial}{\partial t} Q_{enc}, \qquad (4.12)$$

Where S is the total enclosed surface. Over the end caps we have,

$$\oiint_{S_e} \mathbf{J} \cdot \mathbf{ds} = i(z + \Delta z, t) - i(z, t). \qquad (4.13)$$

Defining the per-unit-length conductance g between the two conductors as the ratio of conduction current flowing between the two conductors in the transverse plane per unit of line length i_t, to the voltage between the two conductors, we have,

$$i_t(z, t) = \lim_{\Delta z \to 0} \frac{1}{\Delta z} \oiint_{S_s} \mathbf{J} \cdot \mathbf{ds} = -g \int_a^b \mathbf{e}^{scat} \cdot \mathbf{dl}$$

$$= \mathrm{gv}(\mathrm{z}, \mathrm{t}) + \mathrm{g} \int_a^b \mathbf{e}^{inc} \cdot \mathbf{dl}. \qquad (4.14)$$

The per-unit-length capacitance is defined as,

$$\lim_{\Delta z \to 0} \frac{Q_{enc}}{\Delta z} = -c \int_a^b \mathbf{e}^{scat} \cdot \mathbf{dl} = cv(z, t) + c \int_a^b \mathbf{e}^{inc} \cdot \mathbf{dl}. \qquad (4.15)$$

Substituting 4.13, 4.14, and 4.15 into 4.12, dividing by Δz and taking the limit when $\Delta z \to 0$, gives,

$$\frac{\partial i(z, t)}{\partial z} + gv(z, t) + c \frac{\partial v(z, t)}{\partial t} = -g \int_a^b \mathbf{e}^{inc} \cdot \mathbf{dl} - c \frac{\partial}{\partial t} \int_a^b \mathbf{e}^{inc} \cdot \mathbf{dl}. \qquad (4.16)$$

So, the transmission line equations can be written as,

$$\frac{\partial v(z,t)}{\partial z} + ri(z,t) + l\frac{\partial i(z,t)}{\partial t} = v_F(z,t),$$
$$\frac{\partial i(z,t)}{\partial z} + gv(z,t) + c\frac{\partial v(z,t)}{\partial t} = i_F(z,t), \qquad (4.17)$$

where,

$$v_F(z,t) = \frac{\partial}{\partial t}\int_a^b \mathbf{b}^{inc}\cdot\hat{\mathbf{a}}_n dl,$$
$$i_F(z,t) = -g\int_a^b \mathbf{e}^{inc}\cdot\mathbf{dl} - c\frac{\partial}{\partial t}\int_a^b \mathbf{e}^{inc}\cdot\mathbf{dl}. \qquad (4.18)$$

$v_F(.)$ and $i_F(.)$ are called time-domain distributed force functions due to external electromagnetic fields. It is shown that the voltage source in 4.18, which is in terms of the magnetic field, can be written in terms of incident electric field by using Faraday's law around contour c in Figure 4.1 as, [4].

$$v_F(z,t) = [e_z^{inc}(conductor\#1,z,t) - e_z^{inc}(reference conductor,z,t)] - \frac{\partial}{\partial z}\int_a^b \mathbf{e}^{inc}\cdot\mathbf{dl}. \qquad (4.19)$$

According to equations 4.18 and 4.19 we only need to know the components of incident electric field, 1) along the surface of the conductors, and 2) transverse to the line between two conductors.

Considering distributed current-voltage sources as the effect of external excitation, equivalent circuit representation with incident field illumination is shown in Figure 4.3. v_F and i_F are representing the effect of external excitation as distributed sources along the line. An interesting work is to summarize the effects of all of these distributed sources at the terminal of transmission line which is topic of the next section.
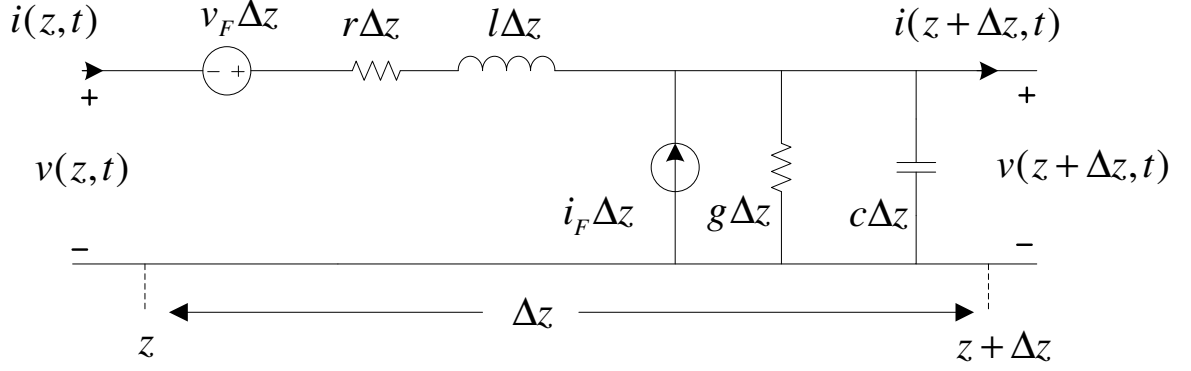
Figure 4.3: The per unit length equivalent circuit for a transmission line with an incident field illumination.

4.1.3 Equivalent of source representations

In order to find equivalent sources that can be placed at the terminal of a two-conductor transmission line, we need to transfer equation 4.17 into the frequency domain as,

$$\frac{dV(z)}{dz} + \underbrace{(r + j\omega l)}_{z} I(z) = V_F(z),$$

$$\frac{dI(z)}{dz} + \underbrace{(g + j\omega c)}_{y} V(z) = I_F(z), \tag{4.20}$$

where, the frequency domain sources are,

$$V_F(z) = [E_z^{inc}(conductor\#1, z) - E_z^{inc}(referenceconductor, z)] - \frac{\partial}{\partial z}\int_a^b \mathbf{E}^{inc} \cdot \mathbf{dl}$$

$$I_F(z) = -(g + j\omega c)\int_a^b \mathbf{E}^{inc} \cdot \mathbf{dl}, \tag{4.21}$$

where, $\mathbf{E}^{inc}$ represents the frequency domain incident field. The per-unit-length impedance and admittance are $z = (r + j\omega l)$ and $y = (g + j\omega c)$, respectively. Equation 4.20, which is a set of a first-order ordinary differential equations, needs to be solved. They are similar

76

to *state variable equations* which are in the form of,

$$\frac{d}{dt}X(t) = AX(t) + W(t). \tag{4.22}$$

The solution of 4.22 is given by,

$$X(t) = \varphi(t - t_0)X(t_0) + \int_{t_0}^{t} \varphi(t - \tau)W(\tau)d\tau, \tag{4.23}$$

where,

$$\varphi(t) = e^{At}. \tag{4.24}$$

Similarly, by defining,

$$X(z) = \begin{bmatrix} V(z) \\ I(z) \end{bmatrix},$$

$$W(z) = \begin{bmatrix} V_F(z) \\ I_F(z) \end{bmatrix},$$

$$A = \begin{bmatrix} 0 & -z \\ -y & 0 \end{bmatrix}, \tag{4.25}$$

Then the solution of the Tline equations in the frequency domain for a line of a total length of L is given by,

$$\begin{bmatrix} V(L) \\ I(L) \end{bmatrix} = \varphi(L) \begin{bmatrix} V(0) \\ I(0) \end{bmatrix} + \begin{bmatrix} V_{FT}(L) \\ I_{FT}(L) \end{bmatrix}, \tag{4.26}$$

where $\varphi(.)$ is called chain parameter matrix in transmission line studies and can be calculated by using,

$$\varphi(L) = e^{AL}. \tag{4.27}$$

In general, for a n-conductor transmission line, 4.27 will be a $n \times n$ matrix but for a two-conductor transmission line it is shown that the chain parameter matrix can be written as, [4]

$$\varphi(L) = \begin{bmatrix} \varphi_{11}(L) & \varphi_{12}(L) \\ \varphi_{21}(L) & \varphi_{22}(L) \end{bmatrix}, \tag{4.28}$$

where,

$$\varphi_{11}(L) = \cosh(\gamma L),$$

$$\varphi_{12}(L) = -Z_C \sinh(\gamma L),$$

$$\varphi_{21}(L) = -\frac{1}{Z_C} \sinh(\gamma L),$$

$$\varphi_{22}(L) = \cosh(\gamma L). \tag{4.29}$$

Z_C is the line characteristic impedance and γ is the propagation constant given by,

$$Z_C = \sqrt{\frac{z}{y}} = \sqrt{\frac{r + j\omega l}{g + j\omega c}},$$

$$\gamma = \sqrt{zy} = \sqrt{(r + j\omega l)(g + j\omega c)}. \tag{4.30}$$

In equation 4.26,

$$\begin{bmatrix} V_{FT}(L) \\ I_{FT}(L) \end{bmatrix} = \int_0^L \varphi(L - \tau) \begin{bmatrix} V_F(\tau) \\ I_F(\tau) \end{bmatrix} d\tau. \tag{4.31}$$
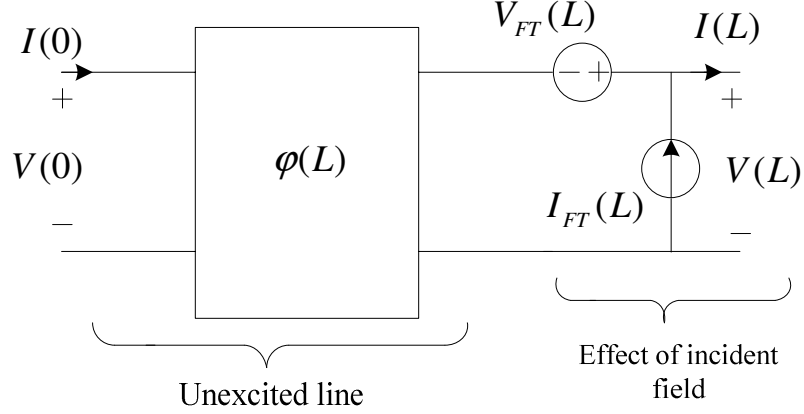
Figure 4.4: Illustration of the representation of a transmission line with incident field illumination as a two-port having lumped sources that represents the effect of the incident field, being put at $z=L$.

Using the chain parameter matrix properties and the definition of V_F and I_F as given in 4.21 and 4.31, the expanded form of V_{FT} and I_{FT} becomes, [4]

$$V_{FT}(L) = \int_0^L \varphi_{11}(L-\tau)[E_z^{inc}(conductor\#1, \tau) - E_z^{inc}(reference conductor, \tau)]d\tau$$

$$-[\int_a^b \mathbf{E}^{inc} \cdot \mathbf{dl}]|_{z=L} + \varphi_{11}(L)[\int_a^b \mathbf{E}^{inc} \cdot \mathbf{dl}]|_{z=0},$$

$$I_{FT}(L) = \int_0^L \varphi_{21}(L-\tau)[E_z^{inc}(conductor\#1, \tau) - E_z^{inc}(reference conductor, \tau)]d\tau$$

$$+ \varphi_{21}(L)[\int_a^b \mathbf{E}^{inc} \cdot \mathbf{dl}]|_{z=0}. \tag{4.32}$$

Equation 4.32 represents lumped sources due to incident electromagnetic field that are located at the end terminal of the Tline and replace the distributed sources. Figure 4.4 illustrates these lumped sources at the far end terminal. Following similar procedure, one can derive lumped sources that are placed at the beginning of the transmission line as
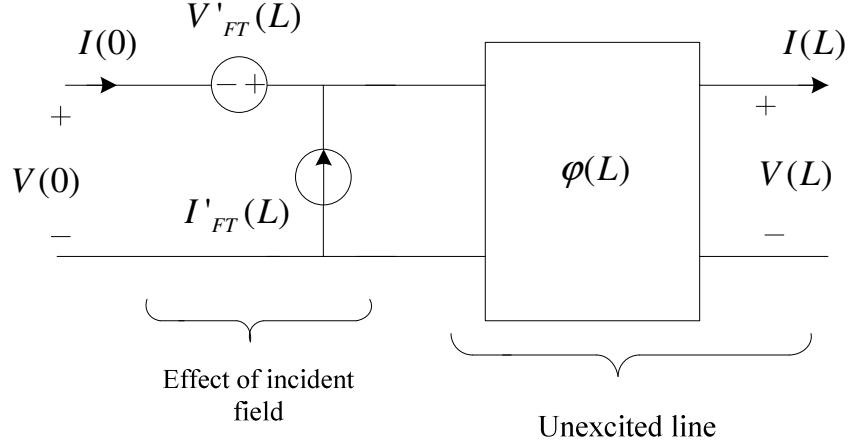
Figure 4.5: Illustration of the representation of a transmission line with incident field illumination as a two-port having lumped sources that represents the effect of the incident field, being put at $z=0$.

given by, [4]

$$V'_{FT}(L) = \int_0^L \varphi_{11}(z)[E_z^{inc}(conductor\#1, z) - E_z^{inc}(reference conductor, z)]dz$$

$$+ [\int_a^b \mathbf{E}^{inc} \cdot \mathbf{dl}]|_{z=0} - \varphi_{11}(L)[\int_a^b \mathbf{E}^{inc} \cdot \mathbf{dl}]|_{z=L},$$

$$I'_{FT}(L) = -\int_0^L \varphi_{21}(z)[E_z^{inc}(conductor\#1, z) - E_z^{inc}(reference conductor, z)]dz$$

$$+ \varphi_{21}(L)[\int_a^b \mathbf{E}^{inc} \cdot \mathbf{dl}]|_{z=L}. \tag{4.33}$$

Figure 4.5 shows the lumped sources which are placed at the near end terminal. The main

advantage of using these lumped voltage and current sources at the terminals instead of

having distributed sources along the Tline is that the transmission line can be treated

as an unexcited line and commonly-used time domain simulators are able to handle this

configuration in the time domain to solve the problem for the terminal voltages.

Following the similar procedure, the lumped sources for a multiconductor transmission line

will be, [4]

$$\mathbf{V}'_{FT}(L) = \int_0^L \varphi_{11}(z) \begin{bmatrix} \dots \\ E_z^{inc}(ith\text{conductor}, z) - E_z^{inc}(\text{referenceconductor}, z) \\ \dots \end{bmatrix} dz$$

$$+\mathbf{I}_n \begin{bmatrix} \dots \\ \int_a^b \mathbf{E}^{inc} \cdot \mathbf{dl} \\ \dots \end{bmatrix} |_{z=0} - \varphi_{11}(L) \begin{bmatrix} \dots \\ \int_a^b \mathbf{E}^{inc} \cdot \mathbf{dl} \\ \dots \end{bmatrix} |_{z=L},$$

$$\mathbf{I}'_{FT}(L) = -\int_0^L \varphi_{21}(z) \begin{bmatrix} \dots \\ E_z^{inc}(ith\text{conductor}, z) - E_z^{inc}(\text{referenceconductor}, z) \\ \dots \end{bmatrix} dz$$

$$+\varphi_{21}(L) \begin{bmatrix} \dots \\ \int_a^b \mathbf{E}^{inc} \cdot \mathbf{dl} \\ \dots \end{bmatrix} |_{z=L}, \tag{4.34}$$

where, I_n is a $n \times n$ identity matrix and the chain parameter matrix can be obtained using 4.27.

In the next section, it is shown that in the case of a *plane-wave excitation* of line, there is a closed form solution for lumped sources as defined in 4.32 and 4.33.

4.1.4 Uniform Plane-Wave Excitation of the Line

The electromagnetic fields from a far radiation structure can be assumed as a local uniform plane wave. Consider a two-conductor transmission line terminated by loads Z_S and Z_L, which is being illuminated by a uniform plane wave radiation as shown in Figure 4.6. The
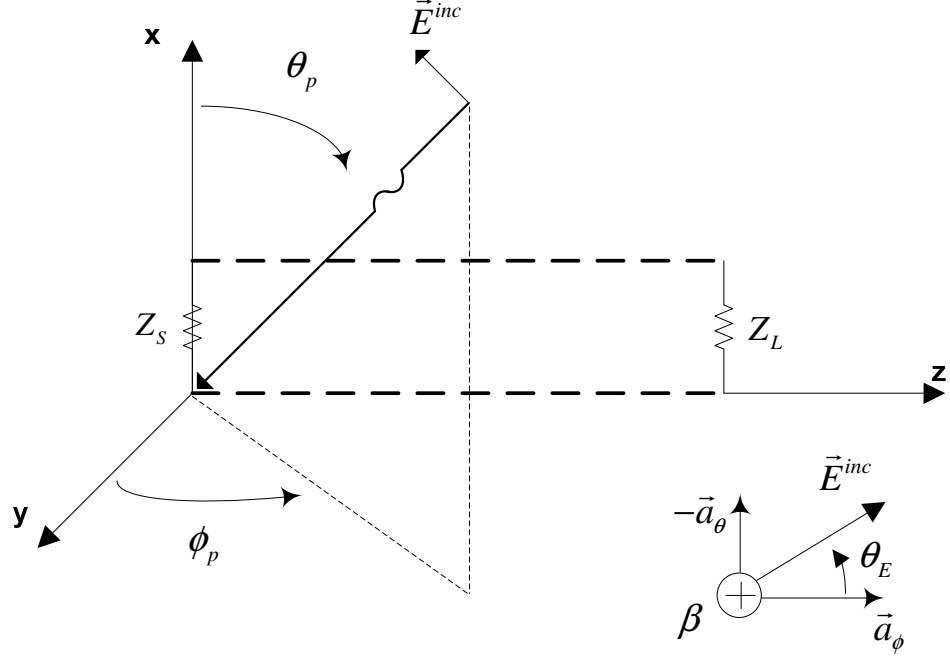
Figure 4.6: Definition of the parameters characterizing the incident field as a uniform plane wave. Adapted from [4].

general expression for electric field in the frequency domain can be written as, [4]

$$\mathbf{E}^{inc} = E_0[e_x\hat{\mathbf{a}}_x + e_y\hat{\mathbf{a}}_y + e_z\hat{\mathbf{a}}_z]e^{-j\beta_x x}e^{-j\beta_y y}e^{-j\beta_z z}, \qquad (4.35)$$

where, the components of the incident field vector along x, y and z axis are,

$$e_x = \sin\theta_E \sin\theta_p,$$

$$e_y = -\sin\theta_E \cos\theta_p \sin\phi_p - \cos\theta_E \sin\phi_p,$$

$$e_z = -\sin\theta_E \cos\theta_p \sin\phi_p + \cos\theta_E \cos\phi_p, \qquad (4.36)$$

and,

$$\beta_x = -\beta \cos \theta_p,$$

$$\beta_y = -\beta \sin \theta_p \cos \phi_p,$$

$$\beta_z = -\beta \sin \theta_p \sin \phi_p, \tag{4.37}$$

where, β is the phase constant and is defined as,

$$\beta = \omega \sqrt{\mu \varepsilon}. \tag{4.38}$$

To show that for the uniform plane wave, as defined in 4.35, there is a closed form solution for the lumped source functions, it is enough to consider the integrals introduced in 4.32. The transverse electric field component in the plane of the transmission line conductors (y=0) becomes,

$$E_T^{inc} = E_0 e_x e^{-j\beta_x x} e^{-j\beta_z z} \hat{\mathbf{a}}_x. \tag{4.39}$$

The contribution of this component in the integrals of 4.32 becomes,

$$\int_a^b \mathbf{E}^{inc} \cdot \mathbf{dl} = \int_{x=0}^d E_0 e_x e^{-j\beta_x x} e^{-j\beta_z z} dx = E_0 d e_x e^{-j\beta_z z} e^{-j\beta_x \frac{d}{2}} \frac{\sin(\beta_x \frac{d}{2})}{\beta_x \frac{d}{2}} \tag{4.40}$$

The contribution from longitudinal electric field component becomes,

$$\int_0^L \phi_{11}(L-z)[E_z^{inc}(conductor\#1, z) - E_z^{inc}(reference conductor, z)]dz =$$
$$\int_0^L \cosh(L-z)[-j\beta_x E_0 d e_z e^{-j\beta_z z} e^{-j\beta_x \frac{d}{2}} \frac{\sin(\beta_x \frac{d}{2})}{\beta_x \frac{d}{2}}]dz \tag{4.41}$$

In 4.41, by writing the *cosh(.)* in terms of exponential functions, the integral can be calculated easily in a closed form solution. Equations 4.41 and 4.40 imply that for uniform plane wave there is a closed form solution to obtain lumped sources representing the effect of excitation. Similar procedure is applicable for the multiconductor case to find the closed form solution for 4.34. In the case of a non-uniform electromagnetic wave, because we cannot write it in the form of 4.35, equations 4.32 and 4.33 do not have a closed form solution.

4.1.5   Field-to-Transmission Line Coupling Equations

In this section, we will review different, but equivalent formulations of the field-to-transmission line coupling equations. There are three main formulations to calculate the external EM field coupling to Tlines.

- The first model which described transmission lines excited by an external electromagnetic source, was presented in 1965 by Taylor, Satterwhite, and Harrison [72], for the case of a two-wire system. In this model, the forcing functions in coupling equations are in terms of vertical-electric and transverse-magnetic excitation fields. Consider a single wire transmission line above a lossy ground at a height of h and with a length of L, illuminated by an external transient nonuniform electromagnetic field as shown in Figure 4.7. The excitation field components E^e and B^e, are the sum of the incident fields E^{inc}, B^{inc} and the ground-reflected fields E^{ref}, B^{ref}, both in the absence of the wire. The total EM fields $\mathbf{E}$ and $\mathbf{B}$, are the sum of the excitation field E^e, B^e, and of the scattered fields E^s, B^s, which represent the reaction of the wire to the excitation EM fields [5]. Applying Maxwell's equations to the Tline shown in Figure 4.7 and using the transmission-line approximation, it is possible to derive the two
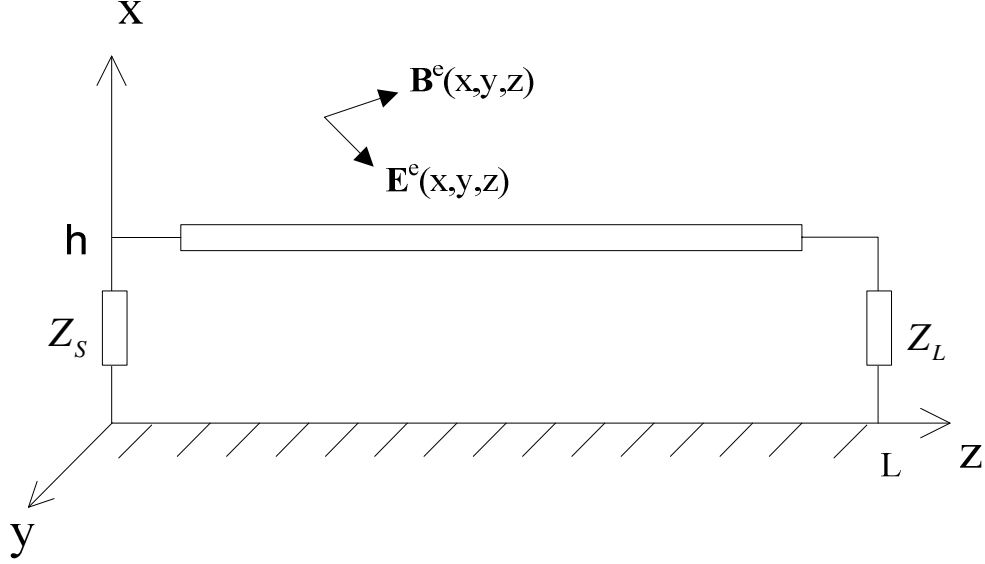
Figure 4.7: Geometry of a single wire illuminated by an external nonuniform electromagnetic field. Adopted from [5].

equations describing the coupling of external electromagnetic field to transmission line as, [85–87]

$$\frac{dV(z)}{dz} + Z'I(z) = j\omega \int_0^h B_y^e(x,z)dx,$$

$$\frac{dI(z)}{dz} + Y'V(z) = -Y' \int_0^h E_x^e(x,z)dx, \qquad (4.42)$$

which is similar to 4.20 and Z' and Y' represent the distributed per-unit-length longitudinal impedance and transverse admittance of the transmission line, respectively. The boundary condition for this kind of formulation is given by,

$$V(0) = -Z_S I(0),$$

$$V(L) = Z_L I(L). \qquad (4.43)$$

The source terms in the right hand side of 4.42 are expressed in terms of the transverse

component of the magnetic field B_y^e, and the vertical component of the electric field E_x^e. Paul in 1976, presented the extension of this model to the case of multiconductor lines [73].

- In 1980, Agrawal, Price, and Gurbaxani [20], derived a new equaivalent formulation of coupling equations in which the forcing functions are expressed only in terms of electric excitation field. This was done by decomposing the total voltage $V(z)$, into scattered voltage $V^s(z)$ and exciting voltage $V^e(z)$. The formulation given in 4.42 then turns into,

$$\frac{dV^s(z)}{dz} + Z'I(z) = E_z^e(h, z),$$
$$\frac{dI(z)}{dz} + Y'V^s(z) = 0. \tag{4.44}$$

The source function in 4.44 is in term of tangential exciting electric field only. The terminal conditions in terms of the scattered voltage and the total current, are described as, [5]

$$V^s(0) = -Z_S I(0) + \int_0^h E_x^e(x, 0)dx,$$
$$V^s(L) = Z_L I(L) + \int_0^h E_x^e(x, L)dx, \tag{4.45}$$

where, the integral terms represents the exciting voltage.

- c) Rachidi in [5], derived a new formulation of the forcing sources which are solely in

terms of magnetic excitation field components as,

$$\frac{dV(z)}{dz} + Z'I(z) = j\omega \int_0^h B_y^e(x,z)dx$$

$$+ \frac{1}{\mu_0(\sigma_{air} + j\omega\varepsilon_0)} \cdot [\frac{\partial B_y^e(0,z)}{\partial x} - \frac{\partial B_x^e(0,z)}{\partial y}],$$

$$\frac{dI(z)}{dz} + Y'V(z) = -\frac{Y'}{\mu_0(\sigma_{air} + j\omega\varepsilon_0)} \cdot \int_0^h [\frac{\partial B_z^e(x,z)}{\partial y} - \frac{\partial B_y^e(x,z)}{\partial z}]dx. \qquad (4.46)$$

The boundary conditions for this formulation are similar to 4.43. This formulation is useful when the exciting field data is determined experimentally as it is generally easier to measure the magnetic field rather than electric field. In this thesis, specifically in this chapter, we are using the extended version of the formulation presented by Taylor and Satterwhite, and Harrison [4] which is mentioned in 4.32 and 4.33. Next section will describe details of the proposed voltage macromodel.

4.2 The Voltage-Macromodel

In this section, the goal is to find a closed form solution in the frequency domain for the formulation given by 4.33 for the case of nonuniform electromagnetic excitation of Tline. In this work, we are using the proposed EM field macromodel as the core of the calculations. Figure 4.8 shows the geometry of the problem and the relationship between these two macromodels. The input to the voltage macromodel is the channel base current and the output is the induced voltages on the transmission line. This macromodel employs the field macromodel that was proposed in Chapter 3. Figure 4.9 shows a simple block diagram of the macromodel.

To calculate the induced voltage on this line within the framework of a time domain power system/circuit simulator, we need to represent the excitation effect with electri-
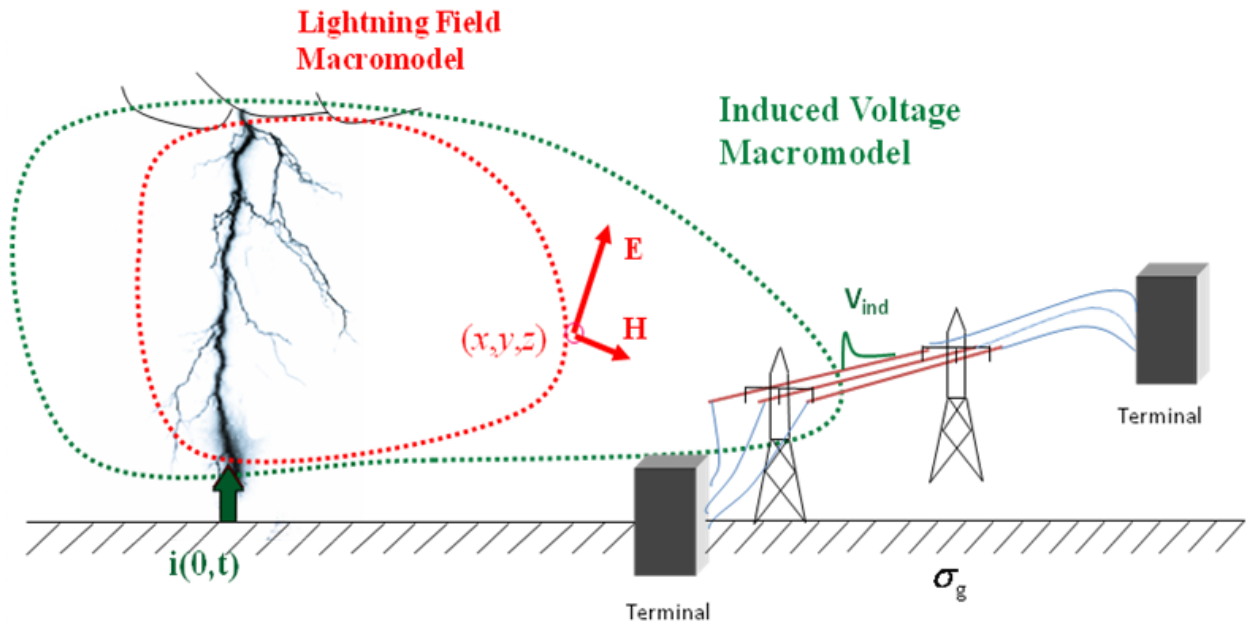
Figure 4.8: The Voltage macromodel of lightning RSC. Channel base current as input and induced overvoltage as its output.
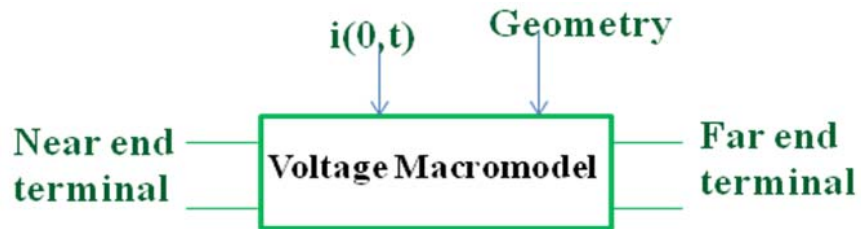
Figure 4.9: Equivalent block diagram representation of Figure 4.8.
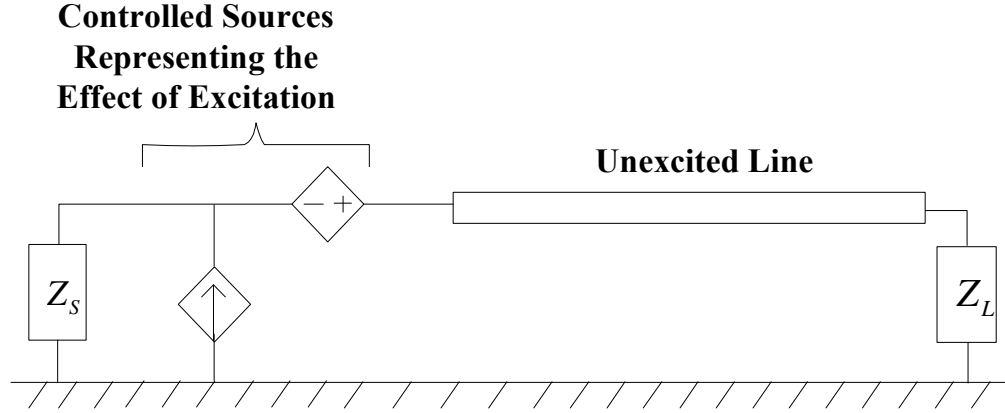
Figure 4.10: The equivalent representation of the Figure 4.8 with additional controlled sources representing the effects of excitation.

cal components in the time domain. In this work, this is done by using controlled voltage/current sources at the terminals of the transmission line. In this approach, we consider the transmission line as an unexcited transmission line. The advantage of this approach is that there are several already-developed models to analyze unexcited transmission line that can be employed. The main focus of this chapter is the efficient calculation of the controlled sources. We divide our problem into two categories. The first one is considering *two-conductor transmission lines* and the second one is considering *multiconductor transmission lines*. The former has a closed form solution for calculating forcing function integrals in the frequency domain and the later can be handled by proposed field macromodel efficiently which will be explained at follow.

4.2.1 The Voltage Macromodel for two-conductor Transmission Lines

Figure 4.10 shows the equivalent representation of Figure 4.8 for a two-conductor transmission line. In order to find a closed form solution for the controlled sources (or force

functions), we start with the integrals mentioned in 4.33 which are repeated below.

$$V'_{FT}(L) = \int_0^L \varphi_{11}(z)[E_z^{inc}(conductor\#1, z) - E_z^{inc}(ref, z)]dz$$

$$+[\int_0^h \mathbf{E}^{inc} \cdot \mathbf{dl}]|_{z=0} - \varphi_{11}(L)[\int_0^h \mathbf{E}^{inc} \cdot \mathbf{dl}]]|_{z=L}$$

$$= V_1 - V_2 + V_3 - V_4 \tag{4.47}$$

$$I'_{FT}(L) = -\int_0^L \varphi_{21}(z)[E_z^{inc}(conductor\#1, z) - E_z^{inc}(ref, z)]dz$$

$$+\varphi_{21}(L)[\int_0^h \mathbf{E}^{inc} \cdot \mathbf{dl}]|_{z=L} = -I_1 + I_2 + I_3 \tag{4.48}$$

where,

$$\varphi_{11}(z) = \cosh(\gamma z),$$

$$\varphi_{21}(z) = -\frac{1}{Z_c}\sinh(\gamma z),$$

$$\gamma = \alpha(\omega) + j\beta(\omega), \tag{4.49}$$

and,

$$V_1 = \int_0^L \varphi_{11}(z)E_z^{inc}(conductor\#1, z)dz,$$

$$V_2 = \int_0^L \varphi_{11}(z)E_z^{inc}(ref, z)dz,$$

$$V_3 = [\int_0^h \mathbf{E}^{inc} \cdot \mathbf{dl}]|_{z=0},$$

$$V_4 = \varphi_{11}(L)[\int_0^h \mathbf{E}^{inc} \cdot \mathbf{dl}]]|_{z=L}, \tag{4.50}$$
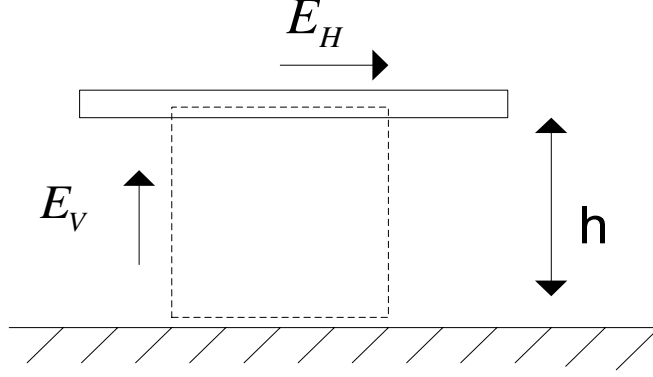
Figure 4.11: Vertical and horizontal electric field with respect to the line position.

and,

$$I_1 = \int_0^L \varphi_{21}(z) E_z^{inc}(\text{conductor}\#1, z) dz,$$

$$I_2 = \int_0^L \varphi_{21}(z) E_z^{inc}(ref, z) dz,$$

$$I_3 = \varphi_{21}(L) [\int_0^h \mathbf{E}^{inc} \cdot \mathbf{dl}]|_{z=L}. \tag{4.51}$$

Evaluation of the integrals mentioned in 4.50 is very similar to 4.51 and will suffice for this chapter. In 4.50, V_3 and V_4 are related to the vertical electric field which is shown in Figure 4.11 as E_V. According to our calculations, the variation of the vertical electric field from the ground level to the height of the wire, is negligible. Thus, we can assume that the vertical component of the electric field is constant and equal to its value at ground level. The above mentioned integrals can be calculated as,

$$V_3 \approx E_v(x = 0, z = 0) \times h,$$

$$V_4 \approx E_v(x = 0, z = l) \times h. \tag{4.52}$$

91

It is worth mentioning that these integrals in fact, for the case of a lossy ground, should be calculated from $-\infty$ to the height of the transmission line but according to Cooray [78], the vertical electric field from $-\infty$ to the ground level is negligible for the frequency range that is of interest in lightning studies and for typical values of the ground conductivity. Because of remarkable variation of the horizontal electric field along the Tline, the most controversial integrals in 4.50, are V_1 and V_2 which are in terms of the z component (or horizontal component) of the electric field and is shown in Figure 4.11 as E_H. As V_1 is similar to V_2, solving any of these integrals will provide the solution of other integral as well. Starting with V_1, we have,

$$V_1 = \int_0^L \varphi_{11}(z) E_H^{inc}(\text{conductor}\#1, z) dz. \tag{4.53}$$

We use the field macromodel results to simplify the above integral. We approximate the horizontal electric field data by using the Vector Fitting algorithm into M poles and residues in the form of,

$$E_H(j\omega) = \sum_{k=1}^M \frac{R_k(z)}{j\omega - P_k(z)}. \tag{4.54}$$

As it was shown in Chapter 3, we can approximate the trace of the poles and residues variation with distance by using 1st order and second order polynomial, respectively. We can rewrite 4.54 at any $\omega = \omega_0$ as,

$$E_H(j\omega_0) \cong \sum_{k=1}^M \frac{A_k z^2 + B_k z + C_k}{j\omega_0 - (F_k z + G_k)}, \tag{4.55}$$

where A_k, B_k, C_k, D_k, and F_k are the kth polynomials coefficients. By using 4.55 and 4.49, V_1 will be,

$$V_1 = \int_0^L \cosh(\gamma_0 z)[\sum_{k=1}^M \frac{A_k z^2 + B_k z + C_k}{D_k z + E_k}]dz, \tag{4.56}$$

where,

$$D_k = -F_k$$

$$E_k = j\omega_0 - G_k. \tag{4.57}$$

By dividing the nominator and denominator of the fraction and changing the order of the integral and summation in 4.56, we get,

$$V_1 = \sum_{k=1}^M \int_0^L \cosh(\gamma_0 z)\{\frac{A_k}{D_k}z + (\frac{B_k}{D_k} - \frac{A_k E_k}{D_k^2}) + \frac{C_k - \frac{B_k E_k}{D_k} - \frac{A_k E_k^2}{D_k^2}}{D_k z + E_k}\}dz. \tag{4.58}$$

The first and second terms inside the integral are easy to calculate. We need to just focus on the last term which we call it V_1' as,

$$V_1' = \sum_{k=1}^M \int_0^L \cosh(\gamma_0 z)\frac{A'_k}{D_k z + E_k}dz, \tag{4.59}$$

where,

$$A'_k = C_k - \frac{B_k E_k}{D_k} - \frac{A_k E_k^2}{D_k^2}. \tag{4.60}$$

There is a closed form solution for integral of 4.59 as,

$$V_1' = \sum_{k=1}^M \frac{A'_k}{D_k}\{\cosh(\frac{\gamma_0 E_k}{D_k})Chi(\frac{\gamma_0 E_k}{D_k} + \gamma_0 z)$$

$$- \sinh(\frac{\gamma_0 E_k}{D_k})Shi(\frac{\gamma_0 E_k}{D_k} + \gamma_0 z)\}, \tag{4.61}$$

93

where $Chi(.)$ and $Shi(.)$ functions are *hyperbolic cosine integral* and *hyperbolic sine integral*

functions, respectively, and are defined as,

$$Chi(z) = \gamma + \ln(z) + \int_0^z \frac{\cosh(t) - 1}{t} dt$$

$$Shi(z) = \int_0^z \frac{\sinh(t)}{t} dt, \tag{4.62}$$

where, $\gamma = 0.57721$ and is called the *Euler-Mascheroni constant.* So, by using 4.52- 4.61,

we are able to calculate the 4.47 and 4.48 in a closed form solution for a two-conductor line.

The coefficients of the poles and residues trace functions given by EM field macromodel,

are the only information needed for this purpose.

4.2.2 The Voltage Macromodel for multiconductor Transmission Lines

Figure 4.12 shows the equivalent representation of the Figure 4.8 for a multiconductor

transmission line. Each of the conductors has its own lumped sources at the terminals

connected to the loads. To calculate the forcing functions in the time domain, we start
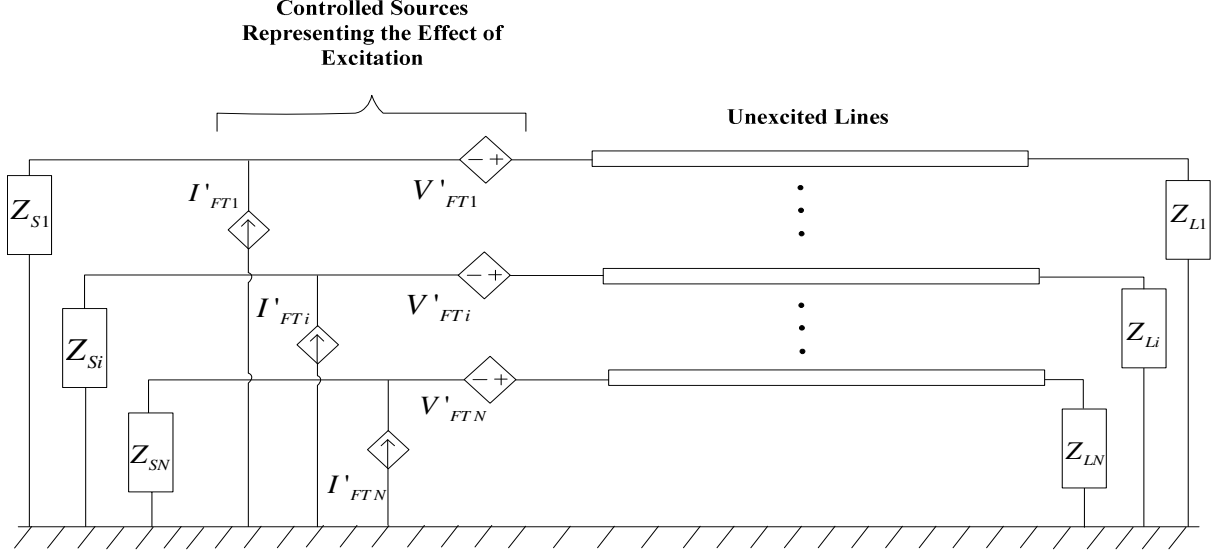
Figure 4.12: The equivalent representation of the Figure 4.8 for a multiconductor transmission line with additional controlled sources representing the effects of excitation.

with the integrals mentioned in 4.34 which are repeated below.

$$
\mathbf{V}'_{FT}(L) = \int_0^L \varphi_{11}(z) \begin{bmatrix} ... \\ E_z^{inc}(ith\,\text{conductor}, z) - E_z^{inc}(\text{reference}\,\text{conductor}, z) \\ ... \end{bmatrix} dz
$$

$$
+ \mathbf{I}_n \begin{bmatrix} ... \\ \int_0^{h_i} \mathbf{E}^{inc} \cdot \mathbf{dl} \\ ... \end{bmatrix} \Big|_{z=0} - \varphi_{11}(L) \begin{bmatrix} ... \\ \int_0^{h_i} \mathbf{E}^{inc} \cdot \mathbf{dl} \\ ... \end{bmatrix} \Big|_{z=L}
$$

$$
= \mathbf{V}_1 + \mathbf{V}_2 + \mathbf{V}_3 + \mathbf{V}_4 \tag{4.63}
$$

$$\mathbf{I}'_{FT}(L) = -\int_0^L \varphi_{21}(z) \begin{bmatrix} \cdots \\ E_z^{inc}(ith\text{conductor}, z) - E_z^{inc}(\text{reference conductor}, z) \\ \cdots \end{bmatrix} dz$$

$$+\varphi_{21}(L) \begin{bmatrix} \cdots \\ \int_0^{h_i} \mathbf{E}^{inc} \cdot \mathbf{dl} \\ \cdots \end{bmatrix} |_{z=L} = \mathbf{I}_1 + \mathbf{I}_2 + \mathbf{I}_3, \tag{4.64}$$

where, V_1, V_2, V_3, and V_4 have similar definition mentioned in 4.50. Unlike the two-conductor case, chain parameter matrix for a multiconductor transmission line is not in the form of a simple hyperbolic function and we need 4.27 to calculate it. Also, the nature of the elements of this matrix for MTL case is oscillatory and doesn't let us to map them into poles and residues. So the efficient way of calculating the integrals in 4.63 and 4.64 is to calculate them piece by piece by breaking them into several integrals. The developed EM field macromodel in chapter 3 can be employed then to calculate the EM fields in each of those integrals. Same as the two-conductor case, we can assume constant vertical electric field in different heights (to calculate V_3 and V_4) and apply the above mentioned method just for the integral which depends on the horizontal electric field (V_1 and V_2).

Using this method, V_1 will be,

$$\mathbf{V}_1 = \int_0^L \varphi_{11}(z) \begin{bmatrix} \cdots \\ \sum_{k=1}^{M} \frac{A_{ki}z^2+B_{ki}z+C_{ki}}{D_{ki}z+E_{ki}} \\ \cdots \end{bmatrix} dz$$

$$= \sum_{j=1}^{N_{seg}} \int_{z_j}^{z_{j+1}} \varphi_{11}(z) \begin{bmatrix} \cdots \\ \sum_{k=1}^{M} \frac{A_{ki}z^2+B_{ki}z+C_{ki}}{D_{ki}z+E_{ki}} \\ \cdots \end{bmatrix} dz, \qquad (4.65)$$

where N_{seg} is the number of the pieces which the original integral is broken into. Equation 4.65 can be calculated simply by knowing the coefficients of poles and residues trace (coming from the EM field macromodel) and chain parameter matrix using 4.27.

In the last part of this chapter, we will show a comparison between several experimental results and our proposed voltage macromodel.

4.3   Voltage Macromodel Results

In this section, we are showing the results of our voltage macromodel as presented in 4.47-4.65 and by using the concepts explained in the previous chapter. We chose PSCAD/EMTDC [52] to analyze the excited transmission lines as this power system simulation software has several pre-defined models for analyzing the unexcited frequency dependent transmission lines over lossy ground. Our job is to add the force functions to the Tline circuit as shown in Figure 4.12, and to obtain the induced voltages at the terminals. The incorporation of our MATLAB codes into the PSCAD is done by using the MATLAB to PSFAD interface [88].
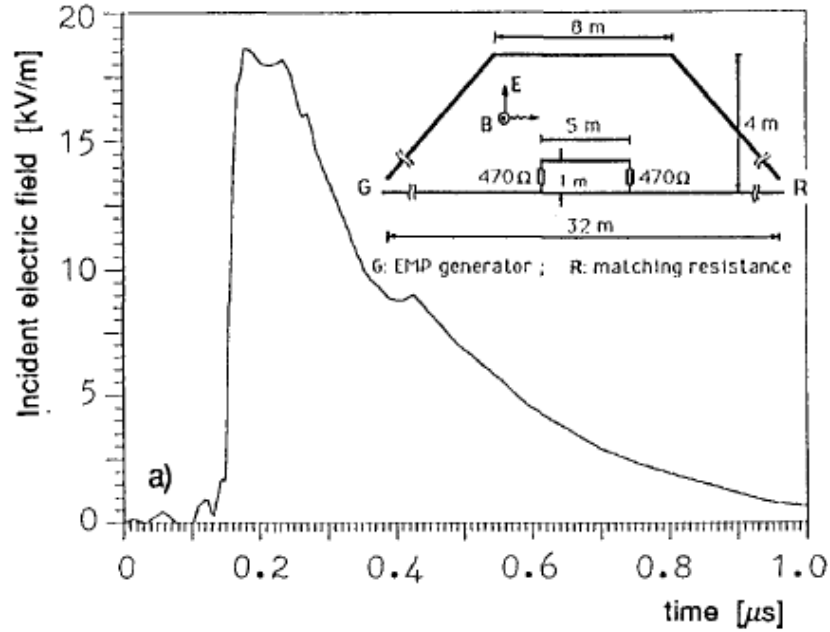
Figure 4.13:   The schematic layout of the experiment and incident electric field in an experimental test of a short line illuminated by a NEMP simulator. Adopted from [6].

The first test case to verify the accuracy of the voltage macromodel is adopted from [6].

Figure 4.13 shows the schematic of the test and the waveform of the incident electric field.

A 5m-long transmission line is terminated at matching loads and is illuminated by a tran-

sient electromagnetic field inside a NEMP simulator. The voltage macromodel results are

compared to the measured results in Figure 4.14. This figure shows the induced current

at the left terminal which we obtained by dividing the simulated induced voltage over the

resistor's value. Since the excitation EM wave is a plane wave in this experiment, we could

also use Paul's FDTD code [4], besides the measurement and macromodel results for the

sake of comparison. The results are in good agreement with measurement. Figure 4.15

shows the PSCAD software environment in where the simulations were done for this ex-

ample.

We simulated the same experiment configuration using a *Gaussian plane wave* with a
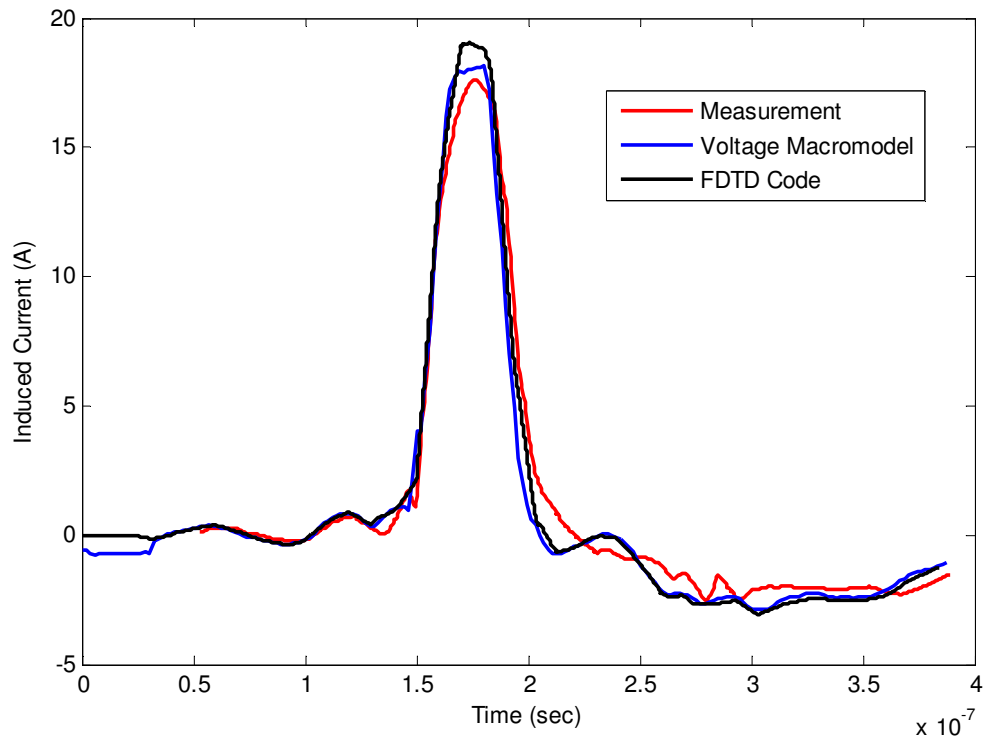
Figure 4.14: Induced current at the left termination of Figure 4.13.
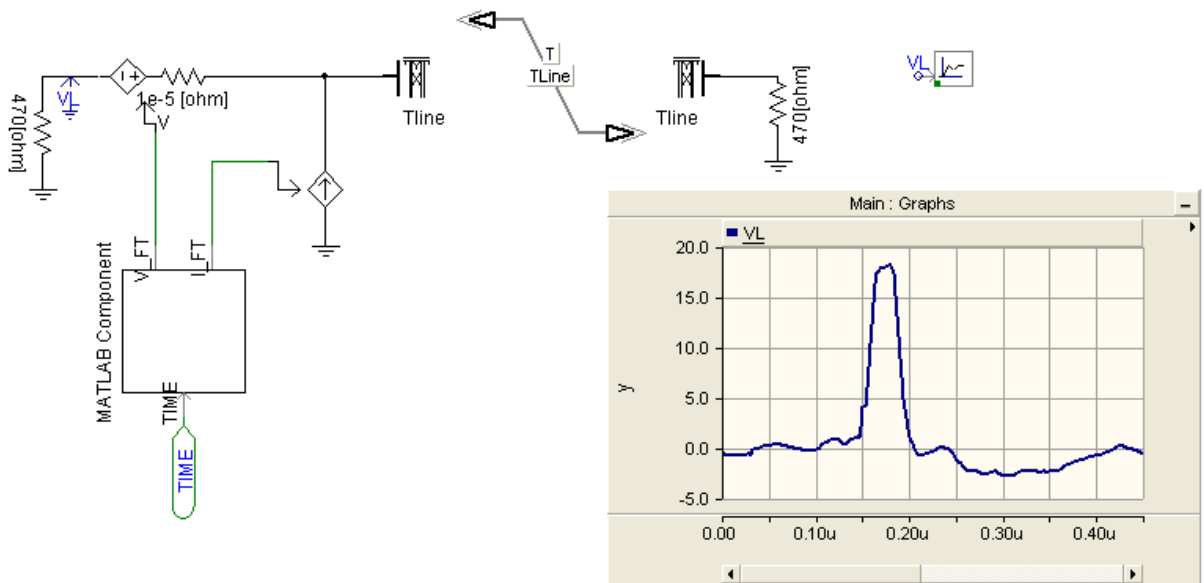
Figure 4.15: The PSCAD environment for the first example.
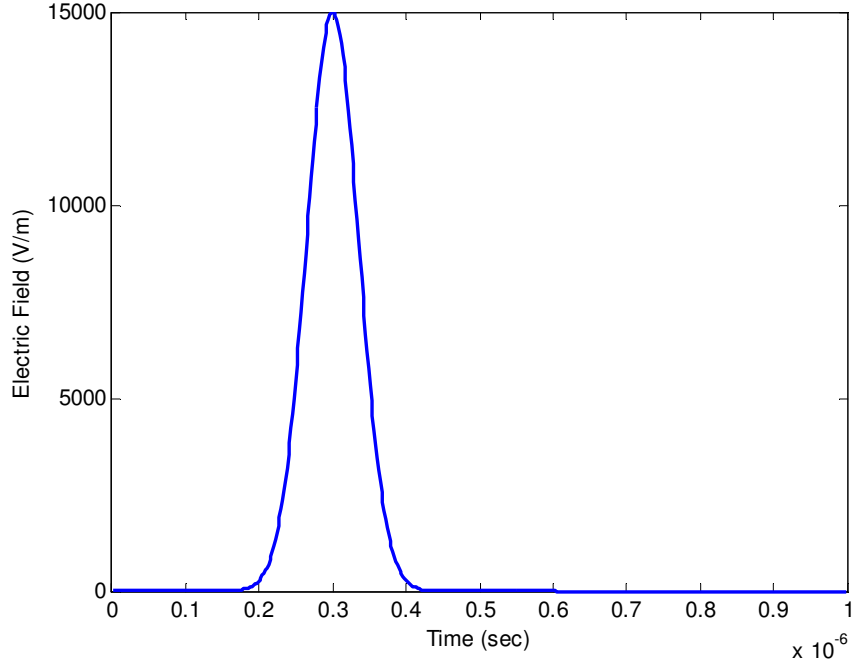
Figure 4.16: Gaussian plane wave illuminates the short line of the Figure 4.13 with the angle of 45 degree.

radiation angle of 45 degree, (see Figure 4.16). The macromodel result is compared to FDTD code in Figure 4.17. They are in good agreement too.

It should be noted that the field-to-line coupling equations mentioned in 4.17, are valid only at a frequency range in which the line cross section is much smaller the shortest wavelength of interest. If we increase the incident electric field's frequency up to, for example 600MHz, as shown in Figure 4.18, the obtained results for induced voltage are not reliable anymore, (see Figure 4.19). This is because the TEM approximation is not valid for transmission line formulas in high frequencies. In this case full-wave FDTD needs to be used for an accurate simulation of the problem.

The second example studied to verify the accuracy of the proposed voltage macromodel is adopted from [6]. Figure 4.20 shows the location of a transmission line and the lightning return stroke channel. This is the same example we used in chapter 3 to calculate the
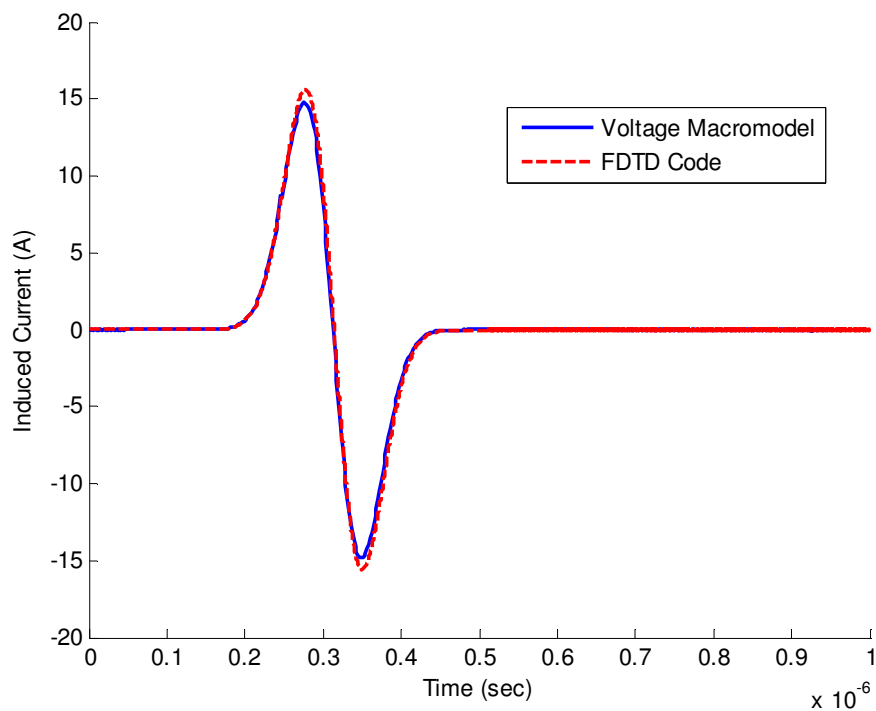
Figure 4.17: Induced current at the left termination due to Gaussian plane wave excitation with 45 degree angle of illumination.
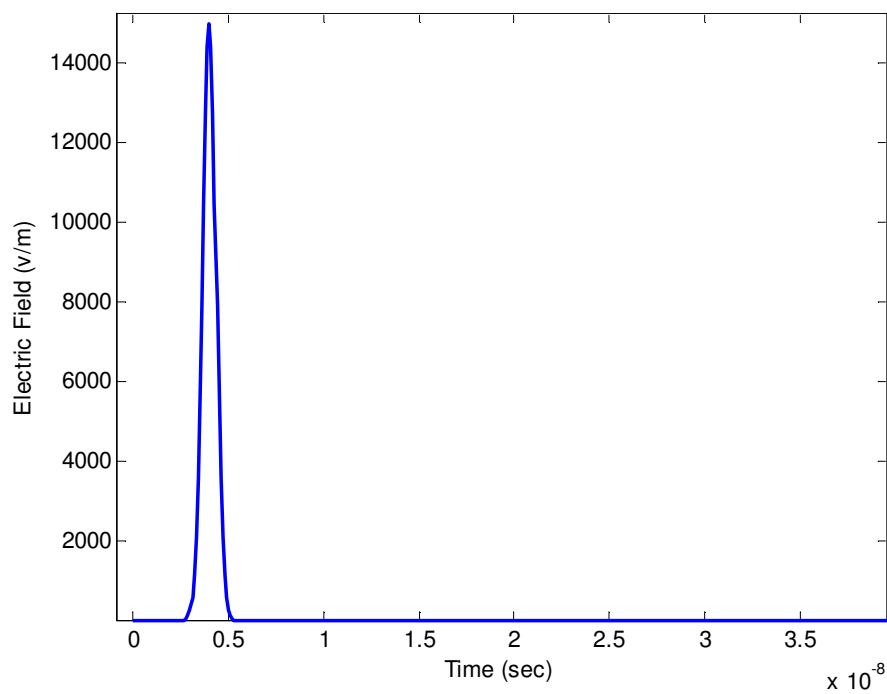
Figure 4.18: Sharp Gaussian plane wave illuminates the short line of Figure 4.13 with the angle of 45 degree.
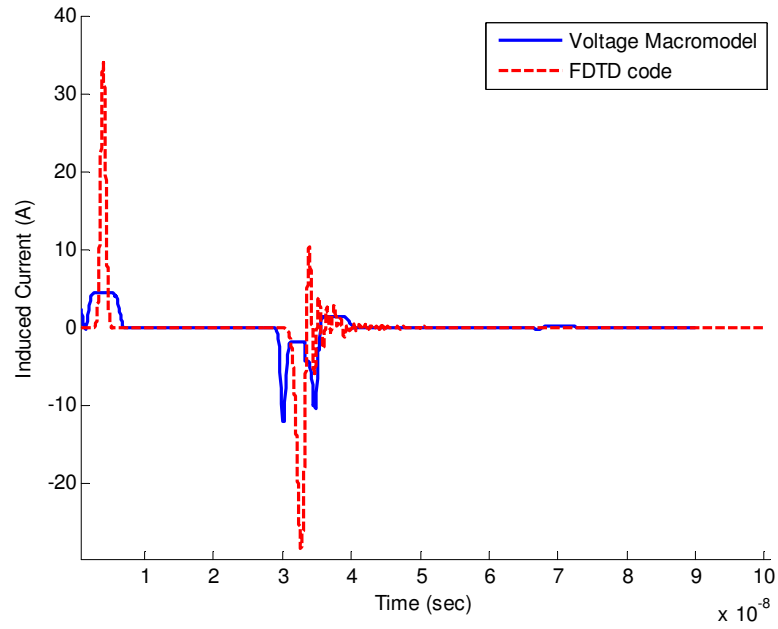
Figure 4.19: Induced current at the left termination due to sharp Gaussian plane wave excitation with 45 degree angle of illumination.
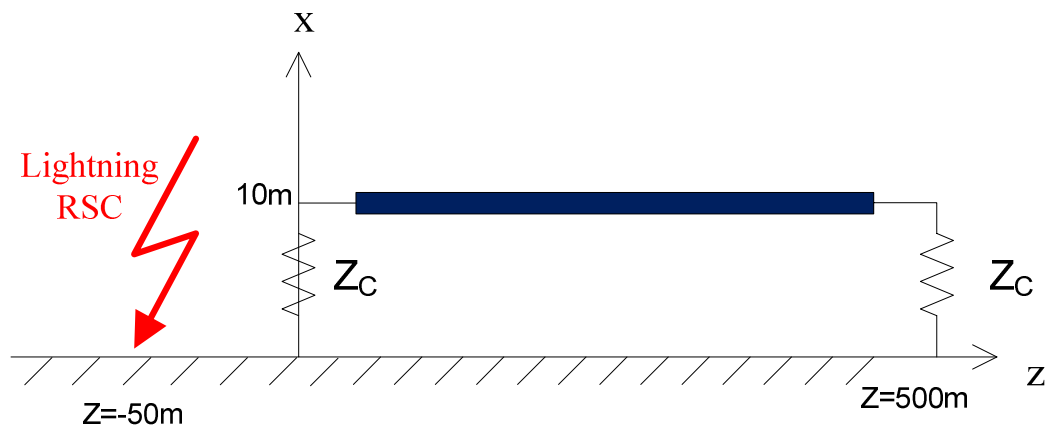
Figure 4.20: Geometry of the second example.
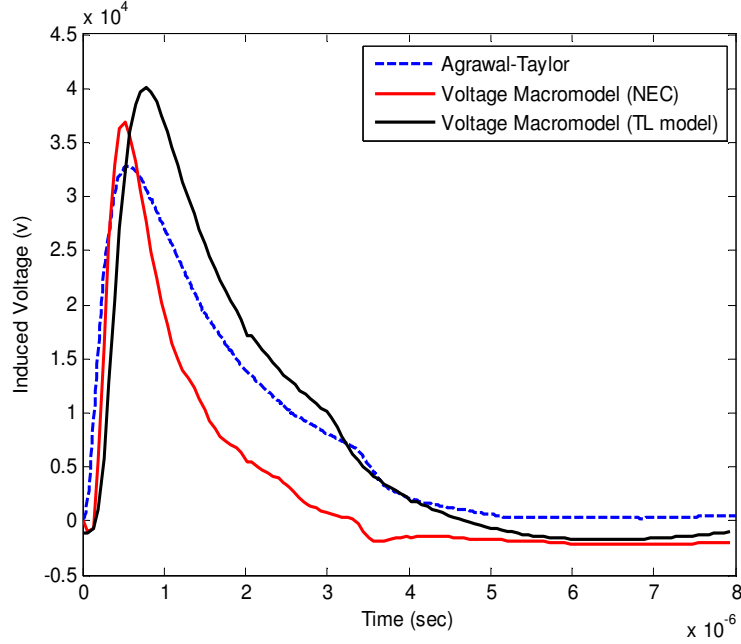
Figure 4.21:   Induced overvoltage at the left terminal of the transmission line of Figure 4.20.

electromagnetic fields of a 6-km RSC. A 500m transmission line, located at 10m above the ground, is terminated at matching load at its two terminals. The ground is assumed to be PEC. The field information is calculated by using both NEC and TL engineering models to be used in the voltage macromodel. In Figure 4.21, we are comparing the obtained induced voltage with the Agrawal-Taylor direct method. Although we have used 1st and 2nd order polynomial approximations for tracing the poles and residues, respectively, there is a very good agreement between the results. We used the same channel base current in Figure 3.27 for the macromodel's input.

The last experimental test is chosen for multiconductor transmission line case which was done by Barker *et al.* [2]. Figure 4.22 shows the configuration of this experiment. In Barker *et al.*'s experiment, a rocket-triggered lightning was the source of external excitation of the Tline at a distance of 145m from the center of a multiconductor overhead line. The line was 682m long, and the two conductors were vertically stacked with the separation be-
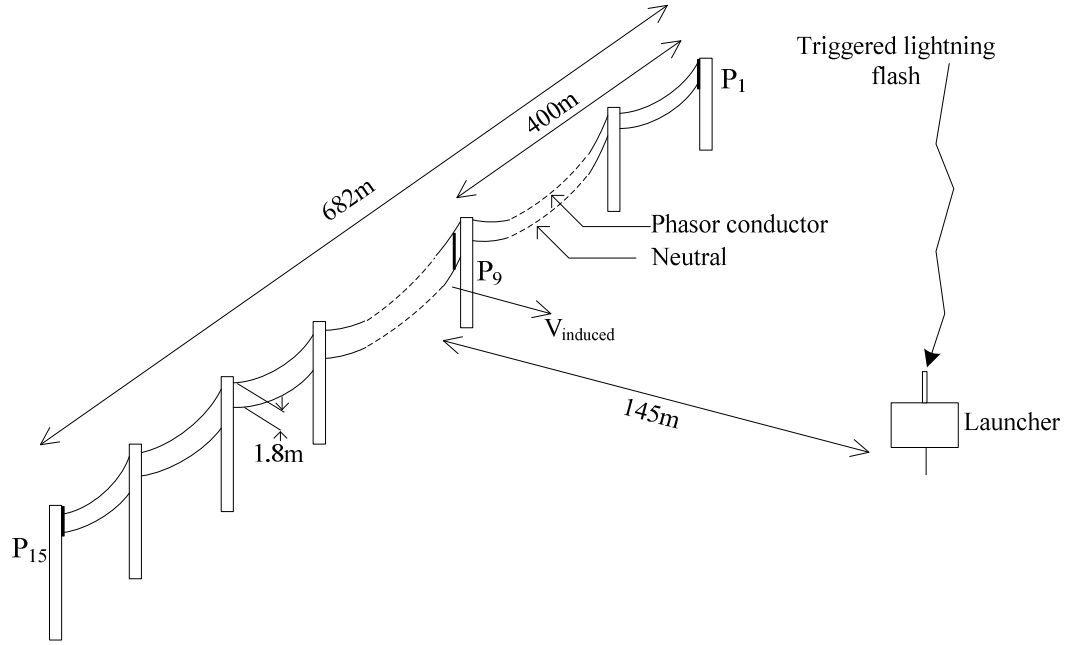
Figure 4.22: Experimental configuration. Adopted from Barker *et al.* [2].

tween them being 1.8m. The line was supported by 15 wooden poles spaced about 49m apart. The upper conductor was placed above the ground at a height of 7.5m and simulated the phase conductor. It was connected to the lower conductor by 455Ω resistors at the termination poles. The lower conductor which simulated the neutral, was grounded at both ends and at pole 9 (the grounding at pole 9 is considered in our model as a resistive load). The grounding resistance values were between 30 and 75Ω [89]. Figure 4.23 shows the channel base current, as measured by Barker *et al.*. We used the same current as the input of the voltage macromodel to calculate the induced voltage at pole 9. There is uncertainty about the ground conductivity. So we obtained the electromagnetic fields of a typical 5-km RSC at 50 and 110 m using different ground conductivities. Comparison of calculated results with measured electromagnetic fields by Barker *et al.*, determines the proper value for the ground conductivity. Figures 4.24 shows the vertical component of the electric field at distance of r=110m on the ground level for different choices of ground
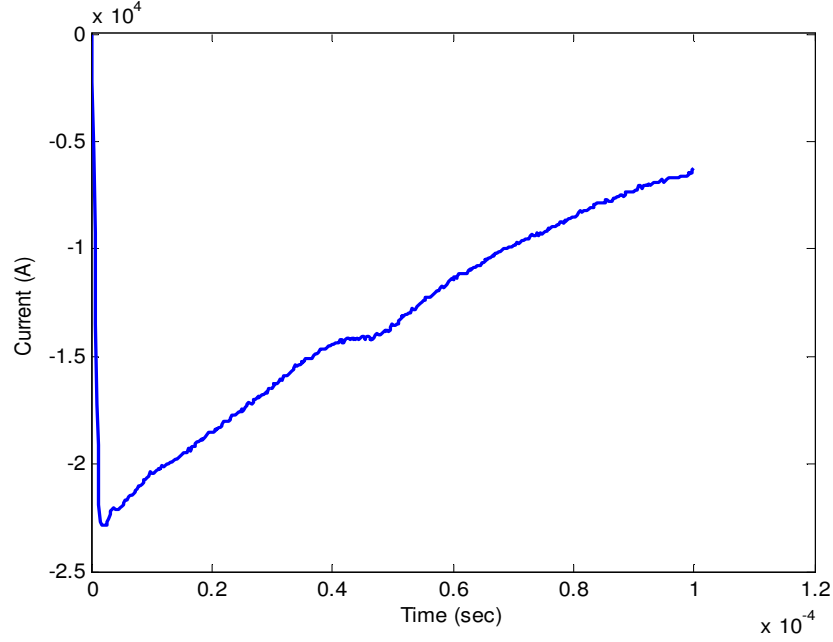
Figure 4.23: Channel base current in Barker *et al.*'s experiment.

conductivities. Figure 4.25 and 4.26 shows the simulation result for the horizontal component of the magnetic field on the ground level at distances of r=110m and 50m from the RSC, respectively. $\sigma = 3.5 \times 10^{-2} S/m$ seems to be a good choice to be used in our voltage macromodel as the ground conductivity. In our simulation, we used a ground with conductivity of $\sigma = 3.5 \times 10^{-2}$ and relative permittivity of 10 and NEC to simulate the lightning RSC. A 5-km channel length with the current velocity of $1.5 \times 10^8 m/s$ is used. The schematic of the transmission line and the added controlled sources for each of the wires is shown in Figure 4.27. We are comparing the macromodel result with measurement in Figure 4.28 for the induced voltage at pole 9. Again, they are in acceptable agreement.

In summary, in this chapter, starting with the field-to-line coupling equations, we introduced an efficient macromodel for the calculation of the induced voltages on transmission lines excited by external electromagnetic radiations such as lightning electromagnetic fields. The efficiency of the proposed macromodel is much more obvious when we see the only
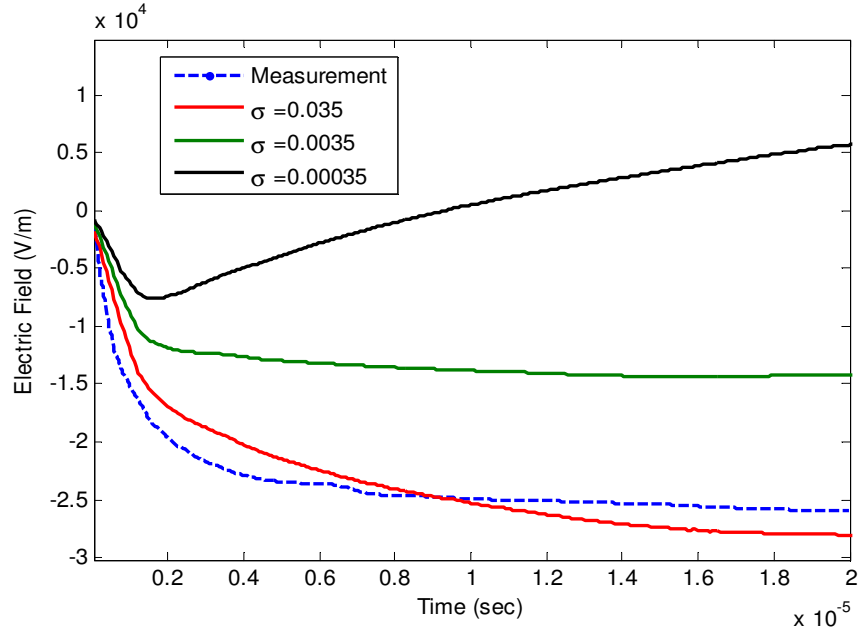
Figure 4.24: Comparison of the vertical electric field for different ground conductivities on the ground level and $r=110$m from the RSC.
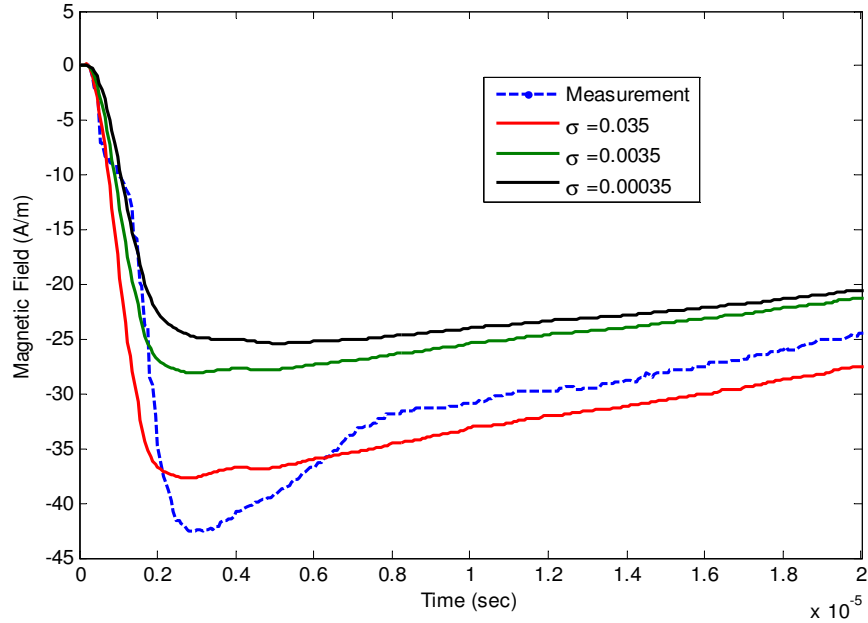
Figure 4.25: Comparison of the horizontal magnetic field for different ground conductivities on the ground level and $r=110$m from the RSC.
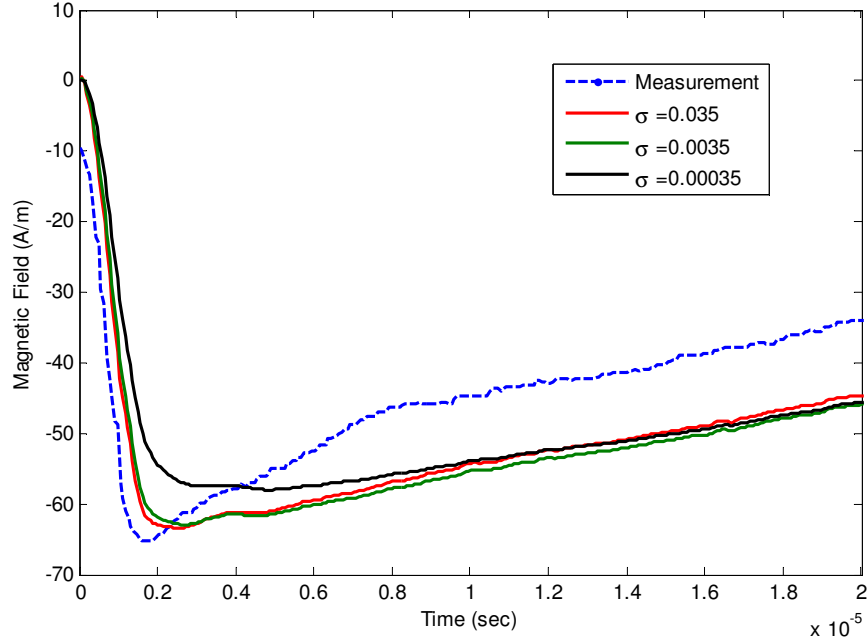
Figure 4.26: Comparison of the horizontal magnetic field for different ground conductivities on the ground level and r=50m from the RSC.
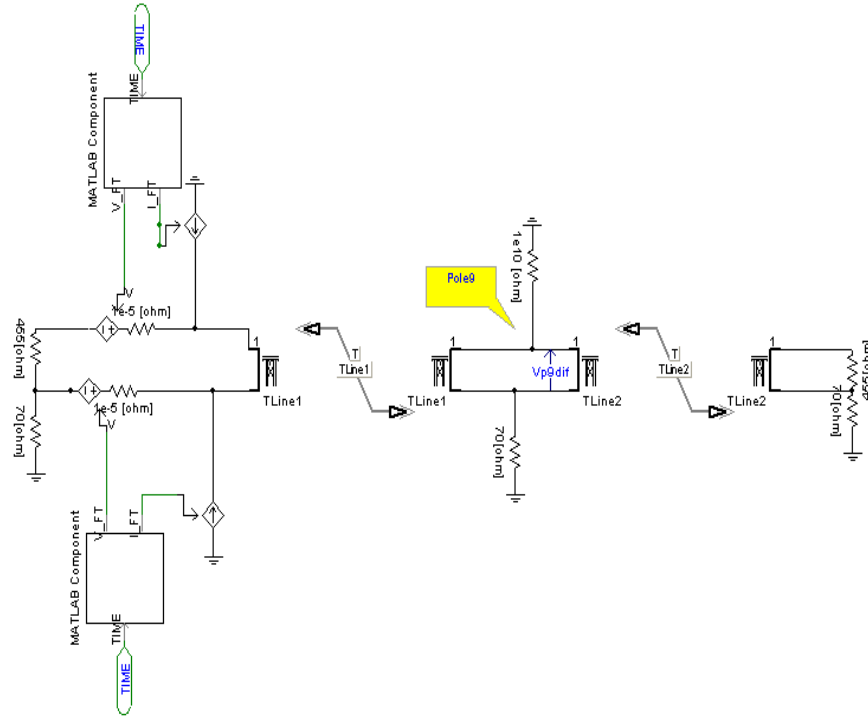
Figure 4.27: The schematic of the transmission line and the controlled sources inside the PSCAD software.
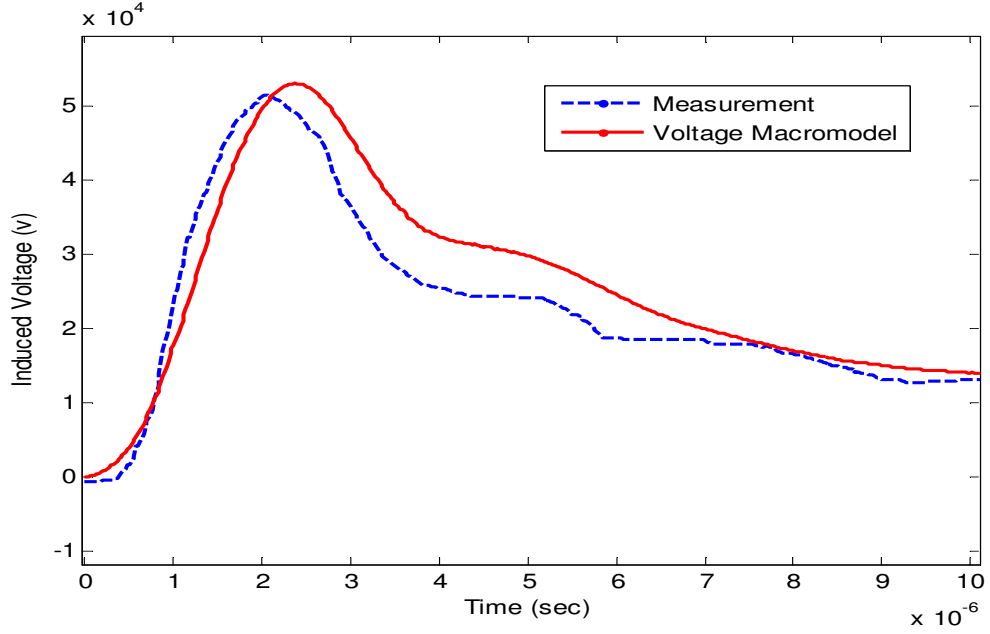
Figure 4.28: Induced voltage on pole 9 due to rocket triggered lightning excitation in Barker *et al.*'s experiment.

required data to calculate force functions, are the coefficients of the trace of poles and residues of the electric field. This information is in fact provided by field macromodel as the core of the voltage macromodel. Comparison between a number of simulation and measurement results with the macromodel results shows the accuracy of the proposed macromodel. One of the main advantages of using the voltage macromodel to calculate induced voltages on the transmission lines is that we can incorporate the frequency domain software into the time domain simulators to be able get advantage of both time and frequency domain specifications.

Chapter 5

Concluding Remarks

This chapter is describing the highlights of the thesis and discusses the obtained results in previous chapters along with possible future work.

5.1   Overview

The issue of mixed time-frequency modeling of excited lossy transmission lines was studied in this thesis. We introduced two kinds of macromodels. The first macromodel is called the field macromodel which is to calculate radiated electromagnetic fields at any arbitrary point around the radiation source efficiently with the knowledge of the EM field's information at few points in the space. The lightning return stroke channel as an important source of radiation to power transmission lines was studied. Different available models of RSC were discussed. The engineering models such as TL, MTLL, and MTLE as well as electromagnetic model were chosen to evaluate lightning RSC. The effect of ground conductivity on the vertical and horizontal electric field was discussed by using different approximations. It was concluded that vertical electric field, unlike the horizontal component, is almost in-

dependent of ground conductivity. For calculating the horizontal component of the electric field in this thesis, Cooray-Rubinstein formula was used. The well-known Vector Fitting algorithm is used to map frequency domain data into poles and residues. This is useful to be able to trace the location of poles and residues of the system transfer function at few points in the space and predict the poles and residues of any arbitrary point. This method makes us able to use recursive convolution in the time domain to save system memory and calculations time. Choosing a proper number of poles to be used in Vector Fitting algorithm is critical to have enough fitting accuracy. choosing a very few number of poles makes little accuracy and very large number leads to an unstable result.

To see the accuracy of the proposed macromodel, we obtained results for a typical lightning RSC in an example and compared it with direct time domain results. The criteria in selecting the time step and the RSC channel segment's length for engineering models as well as time step and frequency interval in NEC were discussed. We showed that there are very smooth variations in poles and residues positions in complex plane with respect to distance changing. This makes us able to find the functions which fit to their traces. In this example, we used both engineering model and NEC to obtain electric field in several points in the space. The poles and residues were fitted into 1st and 2nd order polynomials, respectively. The obtained electric fields for different distances were in a very good agreement with direct time domain results which is using analytic formulations.

Several parametric studies were considered to test the reliability of the field macromodel. We examined our macromodel by different engineering model, different ground conductivities, different number of space segmentations and fitting poles. In all cases, the field macromodel was able to predict the accurate electric field information. It was concluded that by using the field macromodel instead of direct time domain method, we are able to

get 30 times faster calculations beside saving lots of system memory.

The second macromodel is called voltage macromodel to calculate induced overvoltages on transmission lines due to electromagnetic radiation. Coupling equations were studied and the effect of radiation was summarized at the terminals of the transmission line with controlled current and voltage sources. There was closed form solution for these sources in plane wave excitation case already. By using the proposed voltage macromodel, we were able to calculate the force functions for nonuniform excitation in a closed form solution for two-conductor transmission lines and efficiently for muticonductor transmission lines. This was done by approximating the trace of poles and residues with 1st and 2nd order polynomials, respectively. After calculating the force functions in time domain by using Inverse Fourier Transform, we used PSCAD software to analyze the unexcited line with added controlled sources.

We tested the proposed voltage macromodel with several models and measurement cases. In first case the radiated electromagnetic field was plane wave. The comparison of the calculated induced current at the terminals, showed very good agreement with measurement and FDTD code results. At the second case, we compared the macromodel's result with Agrawal-Taylor's model for a 500m two-conductor transmission line excited by nonuniform fields of lightning RSC. The third test case was Barker's experiment. A 682m multiconductor transmission line excited with a 5-km lightning RSC. The obtained voltage was in a good agreement with measurement result.

By using the concept of system's transfer function and macromodeling, we made it possible to incorporate the frequency domain software's result into time domain simulators. Furthermore, the calculations were fast and efficient.

5.2 Future Work

The EM field macromodel developed in chapter 3, was verified by available lightning measurement data. Other sources of electromagnetic radiation may also be investigated by using this macromodel. As long as the radiated EM fields have smooth time variation, will guarantee us to be able to use the proposed algorithm and trace the poles and residues. The functions we used in this work, were chosen polynomial functions to trace the poles and residues of the EM field and at the same time, simplify the voltage macromodel. Other functions such as exponential functions may be employed for this purpose to get higher accuracy.

In this work we used 1-dimensional functions to interpolate and predict the poles and residues of the EM fields for any arbitrary point on a ground with an specific conductivity. An extension of this work is to use N-dimensional tracing function in which several ground and lightning RSC parameters are considered. Parameters such as distance, ground conductivity, propagation speed along the lightning RSC, channel height, etc. This can be done by building a proper bank of data for different parameters configuration and using multidimensional interpolation.

The closed form solution obtained for the voltage macromodel to include the force functions at the terminals of the transmission line is proposed for any two-conductor transmission line in which the chain parameters are in the form of hyperbolic functions. It will worth to consider the problem for multiconductor transmission lines in which the chain parameter matrix is oscillatory and it is not possible to map its poles and residues into analytic functions to be able to simplify the force functions. For this reason, using modal analysis seems to be useful. The problem with using modes in multiconductor transmission lines is that the propagation constant matrix is changing in different frequencies for different

modes. This is called *mode switching* in transmission line studies and one needs to trace these modes for different conductors as well, to be able to use the force functions formula along with the Vector Fitting algorithm.

In this work, we simplified the forcing functions to a closed form solution in the frequency domain. Inverse Fourier Transform then was applied to have the data in time domain. It will be a remarkable result to find a closed form solution for forcing function in the time domain by using the definition of the IFFT. This can be done by choosing a proper function for the trace of poles and residues of the EM field.

Finally, the whole focus of the proposed voltage macromodel was on the overhead transmission system. A similar procedure followed in this thesis can be employed to find the electromagnetic behaviour of buried power cables. This can be achieved by applying minor changes in the EM field macromodel derived in Chapter 3.

References

[1] V. Rakov and M. A. Uman, *Lightning: Physics and Effects.* Cambridge Univ. Press, 2003.

[2] P. Barker, T. Short, A. Eybert-Berard, and J. Berlandis, "Induced voltage measurements on an experimental distribution line during nearby rocket triggered lightning flashes," *Power Delivery, IEEE Transactions on*, vol. 11, no. 2, pp. 980 –995, April 1996.

[3] Y. Lin, M. Uman, J. Tiller, R. Brantley, W. Beasley, E. Krider, and C. Weidman, "Characterization of lightning return stroke electric and magnetic fields from simultaneous two-station measurements," *Geophys. Res*, vol. 84, p. 63076314, 1979.

[4] C. Paul, *Analysis of Multiconductor Transmission Lines*, 2nd ed. IEEE Press, 2008.

[5] F. Rachidi, "Formulation of the field-to-transmission line coupling equations in terms of magnetic excitation field," *Electromagnetic Compatibility, IEEE Transactions on*, vol. 35, no. 3, pp. 404 –407, aug. 1993.

[6] C. Nucci, F. Rachidi, M. Ianoz, and C. Mazzetti, "Comparison of two coupling models for lightning-induced overvoltage calculations," *Power Delivery, IEEE Transactions on*, vol. 10, no. 1, pp. 330 –339, jan. 1995.

[7] D. Ward, "Power quality and the security of electricity supply," *Proceedings of the IEEE*, vol. 89, no. 12, pp. 1830 –1836, dec. 2001.

[8] C. Nucci, M. Paolone, and M. Bernardi, "Use of lightning location systems data in integrated systems for power quality monitoring," vol. 1, oct. 2002, pp. 552 – 556.

[9] *NEC-2 Manual, Part III: Users Guide version. 0.92*, Formatted binary document (WDBN), September 1996.

[10] G. Burke, *Numerical Electromagnetic Code- NEC-4, Method of Moments*, January 1992.

[11] V. Rakov and M. Uman, "Review and evaluation of lightning return stroke models including some aspects of their application," *IEEE Transactions on Electromagnetic Compatibility*, vol. 40, no. 4, pp. 403 –426, nov. 1998.

[12] S. Rusck, *Protection of Distribution Systems.* Academic Press, 1977, vol. 2, ch. 23.

[13] *IEEE Guide for Improving the Lightning Performance of Electric Power Overhead Distribution Lines*, 1997.

[14] B. Franklin, *Experiment and Observation of Electricity Made at Philadelphia in America*, 5th ed. London: F. Newberry, 1774.

[15] E. Workman and R. Holzer, "A preliminary investigation of the electrical structure of thunderstorms," The National Advisory Committee on Aeronautics, Tech. Rep. 864, 1942.

[16] S. Reynold and H. Neil, "The distribution and discharge of thunderstorm charge center,," *METEOROLOGY*, vol. 12, 1955.

[17] M. Uman, *Understanding lightning.* Pittsburgh: Bek technical publication, 1971.

[18] S. Drabkina, "The theory of the development of the spark channel," *Experiment. Theoret. Phys*, vol. 21, p. 473483, 1951.

[19] S. Braginskii, "Theory of the development of a spark channel," *Sov. Phys. JETP*, vol. 34, p. 10681074, 1958.

[20] A. Agrawal, H. Price, and S. Gurbaxani, "Transient response of multiconductor transmission lines excited by a nonuniform electromagnetic field," *Electromagnetic Compatibility, IEEE Transactions on*, vol. EMC-22, no. 2, pp. 119 –129, may. 1980.

[21] V. Rakov, "Some inferences on the propagation mechanisms of dart leaders and return strokes," *Geophys. Res.*, vol. 103, p. 18791887, 1998.

[22] C. Baum and L. Barker, "Analytic return-stroke transmission-line model," *Lightning Electromagnetics*, pp. 17–40, 1990.

[23] C. Baum, "Return-stroke initiation," *Lightning Electromagnetics*, pp. 101–114, 1990.

[24] D. F. Strawe, *Non-linear modeling of lightning return strokes*, J. Robb, J. Cline, J. Raney, & J. Dunn, Ed. Florida Inst. of Technol, Mar. 1979.

[25] A. S. Podgorski and J. A. Landt, "Three-dimensional time domain modeling of lightning," *Power Engineering Review, IEEE*, vol. PER-7, no. 7, pp. 72 –73, jul. 1987.

[26] V. A. Rakov, "Lightning electromagnetic fields modeling and measurements," *Proc. 12th Int. Zurich Symp. Electromagn. Compat.*, pp. 59–64, Feb 1997.

[27] M. Uman and D. McLain, "Magnetic field of the lightning return stroke," *Geophys. Res.*, vol. 74, p. 68996910, 1969.

[28] V. Rakov and A. Dulzon, "Calculated electromagnetic fields of lightning return stroke," *Tekh. Elektrodinam*, no. 1, p. 8789, 1987.

[29] C. A. Nucci, C. Mazzetti, F. Rachidi, and M. Ianoz, "On lightning return stroke models for LEMP calculations," in *19th International Conference on Lightning Protection*, 1988.

[30] R. Anderson and A. Erikson, "Lightning parameters for engineering application," *Electra*, no. 69, pp. 65–101, 1980.

[31] K. Berger, R. Anderson, and H. Kroninger, "Parameters of lightning flashes," *Electra*, no. 41, pp. 23–37, 1975.

[32] R. Golde, *Lightning.* Academic Press, 1977.

[33] R. Jones, "On the use of tailored return-stroke current representations to simplify the analysis of lightning effects on systems," *Electromagnetic Compatibility, IEEE Transactions on*, vol. EMC-19, no. 2, pp. 95 –96, may. 1977.

[34] R. Gardner, L. Baker, C. Baum, and D. Andersh, "Comparison of lightning with public domain hemp waveforms on the surface of an aircraft," *6th Int. Symp. Electromagnetic Compatibility*, pp. 175–180, 1985.

[35] F. Heidler, J. Cvetic, and B. Stanic, "Calculation of lightning current parameters," *Power Delivery, IEEE Transactions on*, vol. 14, no. 2, pp. 399 –404, apr. 1999.

[36] V. Javor and P. Rancic, "On the choice of the lightning channel current decay constant in the modified transmission line model with exponential decay," in *17th International Conference on Software and Computer Networks*, October 2009.

[37] C. Yang and B. Zhou, "Calculation methods of electromagnetic fields very close to lightning," *Electromagnetic Compatibility, IEEE Transactions on*, vol. 46, no. 1, pp. 133 – 141, feb. 2004.

[38] R. Moini, B. Kordi, G. Rafi, and V. Rakov, "A new lightning return stroke model based on antenna theory model," *Geophysical Research*, vol. 105, no. 24, pp. 29 693–29 702, 2000.

[39] A. Sommerfeld, "ber die ausbreitung der wellen in der drahtlosen telegraphie," *Annalen der Physik*, vol. 28, p. 665, 1909.

[40] B. Djebari, J. Hamelin, C. Leteinturier, and F. J., "Comparison between experimental measurements of the electromagnetic field emitted by lightning and different theoretical models. influence of the upward velocity of the return stroke,," in *4th Int. Symp. Tech. Exhib. Electromag. Compat*, 1981.

[41] M. Rubinstein, "Voltages induced on a test power line from artificially initiated lightning: theory and experiment," Ph.D. dissertation, University of Florida, Gainesville, 1991.

[42] E. Thomson, P. Medelius, M. Rubinstein, M. Uman, J. Johnson, and J. Stone, "Horizontal electric fields from lightning return strokes," *Geophys. Res.*, vol. 93, pp. 2429–2441, 1988.

[43] V. Cooray, "Horizontal fields generated by retum strokes," *Radio Sci.*, vol. 27, pp. 529–537, 1992.

[44] M. Rubinstein, "An approximate formula for the calculation of the horizontal electric field from lightning at close, intermediate, and long range," *Electromagnetic Compatibility, IEEE Transactions on*, vol. 38, no. 3, pp. 531 –535, aug. 1996.

[45] M. Uman, V. Rakov, J. Versaggi, R. Thottappillil, A. Eybert-Berard, L. Barret, J. Berlandis, B. Bador, P. Barker, S. Hnat, J. Oravsky, T. Short, C. Warren, and R. Bernstein, "Electric fields close to triggered lightning,," in *EMC94 ROMA, Int. Symp. Electromagn. Compat., Rome, Italy*, Rome-Italy, September 1994, pp. 33–37.

[46] M. Uman, V. Rakov, K. Rambo, T. Vaught, M. Fernandez, D. Cordier, R. Chandler, R.M. Bernstein, and C. Golden, "Triggered lightning experiments at camp blanding, fl (19931995)," *Inst. Elect. Eng. Japan*, vol. 117, no. 4, p. 446452, 1997.

[47] V. Rakov, M. Uman, K. Rambo, M. Fernandez, R. Fisher, G. Schnetzer, R. Thottappillil, A. Eybert-Berard, J. Berlandis, P. Lalande, A. Bonamy, P. Laroche, and A. Bondiou-Clergerie, "New insights into lightning processes gained from triggered lightning experiments in florida and alabama," *Geophys. Res.*, vol. 102, pp. 14 117–14 130, 1998.

[48] J. Branin, F.H., "Transient analysis of lossless transmission lines," *Proceedings of the IEEE*, vol. 55, no. 11, pp. 2012 – 2013, nov. 1967.

[49] A. Budner, "Introduction of frequency-dependent line parameters into an electromagnetic transients program," *Power Apparatus and Systems, IEEE Transactions on*, vol. PAS-89, no. 1, pp. 88 –97, jan. 1970.

[50] J. Snelson, "Propagation of travelling waves on transmission lines - frequency dependent parameters," *Power Apparatus and Systems, IEEE Transactions on*, vol. PAS-91, no. 1, pp. 85 –91, jan. 1972.

[51] J. R. Marti, "Accurate modeling of frequency-dependent transmission lines in electromagnetic transient simulations," *Power Engineering Review, IEEE*, vol. PER-2, no. 1, pp. 29 –30, jan. 1982.

[52] *PSCAD Users Manual*, HVDC Research Center, Winnipeg, Manitoba, Canada, 2003.

[53] *Electromagnetic Transient Program (EMTP) Rule Book*, Bonneville Power Administration, Oregon, 1984.

[54] T. Noda, N. Nagaoka, and A. Ametani, "Phase domain modeling of frequency-dependent transmission lines by means of an arma model," *Power Delivery, IEEE Transactions on*, vol. 11, no. 1, pp. 401 –411, jan. 1996.

[55] A. Morched, B. Gustavsen, and M. Tartibi, "A universal model for accurate calculation of electromagnetic transients on overhead lines and underground cables," *Power Delivery, IEEE Transactions on*, vol. 14, no. 3, pp. 1032 –1038, jul. 1999.

[56] B. Gustavsen, G. Irwin, R. Mangelrod, D. Brandt, and K. Kent, "Transmission line models for the simulation of interaction phenomena between parallel ac and dc overhead lines," in *Int. Conf. on Power Systems Transients (IPST 99)*, Budapest, Hungary, June 1999, pp. 61–67.

[57] A. Djordjevic, T. Sarkar, and R. Harrington, "Time-domain response of multiconductor transmission lines," *Proceedings of the IEEE*, vol. 75, no. 6, pp. 743 – 764, jun. 1987.

[58] A. Orlandi and C. Paul, "Fdtd analysis of lossy, multiconductor transmission lines terminated in arbitrary loads," *Electromagnetic Compatibility, IEEE Transactions on*, vol. 38, no. 3, pp. 388 –399, aug. 1996.

[59] G. Antonini, A. Orlandi, and C. Paul, "An improved method of modeling lossy transmission lines in finite-difference, time-domain analysis," *Electromagnetic Compatibility, 1999 IEEE International Symposium on*, vol. 1, pp. 435 –439, 1999.

[60] D. Mardare and J. LoVetri, "The finite-difference time-domain solution of lossy mtl networks with nonlinear junctions," *Electromagnetic Compatibility, IEEE Transactions on*, vol. 37, no. 2, pp. 252 –259, may. 1995.

[61] B. Kordi, J. LoVetri, and G. Bridges, "Finite-difference analysis of dispersive transmission lines within a circuit simulator," *Power Delivery, IEEE Transactions on*, vol. 21, no. 1, pp. 234 – 242, jan. 2006.

[62] I. Erdin, A. Dounavis, R. Achar, and M. Nakhla, "Circuit simulation of incident field coupling to multiconductor transmission lines with frequency-dependent losses," *Electromagnetic Compatibility, 2001. EMC. 2001 IEEE International Symposium on*, vol. 2, pp. 1084 –1087 vol.2, 2001.

[63] G. Shinh, R. Achar, N. Nakhla, M. Nakhla, and I. Erdin, "Simplified macromodel of mtls with incident fields (simmif)," *Electromagnetic Compatibility, IEEE Transactions on*, vol. 50, no. 2, pp. 375 –389, may. 2008.

[64] R. Achar and M. Nakhla, "Simulation of high-speed interconnects," *Proceedings of the IEEE*, vol. 89, no. 5, pp. 693 –728, may. 2001.

[65] H. Xie, J. Wang, R. Fan, and Y. Liu, "A hybrid fdtd-spice method for transmission lines excited by a nonuniform incident wave," *Electromagnetic Compatibility, IEEE Transactions on*, vol. 51, no. 3, pp. 811 –817, aug. 2009.

[66] G. Shinh, N. Nakhla, R. Achar, M. Nakhla, and I. Erdin, "Fast emc analysis high-speed interconnects with frequency-dependent parameters," *Electromagnetic Compatibility, 2006. EMC 2006. 2006 IEEE International Symposium on*, vol. 2, pp. 556 –559, aug. 2006.

[67] I. Erdin, A. Dounavis, R. Achar, and M. Nakhla, "A spice model for incident field coupling to lossy multiconductor transmission lines," *Electromagnetic Compatibility, IEEE Transactions on*, vol. 43, no. 4, pp. 485 –494, nov. 2001.

[68] G. Shinh, N. Nakhla, R. Achar, M. Nakhla, A. Dounavis, and I. Erdin, "Efficient spice macromodel for emi analysis of electronic packages and high-speed interconnects," *Electrical Performance of Electronic Packaging, 2004. IEEE 13th Topical Meeting on*, pp. 277 – 280, oct. 2004.

[69] N. Nakhla, A. Dounavis, R. Achar, and M. Nakhla, "Depact: delay extraction-based passive compact transmission-line macromodeling algorithm," *Advanced Packaging, IEEE Transactions on*, vol. 28, no. 1, pp. 13 –23, feb. 2005.

[70] G. Shinh, N. Nakhla, R. Achar, M. Nakhla, A. Dounavis, and I. Erdin, "Fast transient analysis of incident field coupling to multiconductor transmission lines," *Electromagnetic Compatibility, IEEE Transactions on*, vol. 48, no. 1, pp. 57 –73, feb. 2006.

[71] G. Antonini, "A spectral formulation for the transient analysis of plane-wave coupling to multiconductor transmission lines," *Electromagnetic Compatibility, IEEE Transactions on*, vol. 51, no. 3, pp. 792 –804, aug. 2009.

[72] C. Taylor, R. Satterwhite, and J. Harrison, C., "The response of a terminated two-wire transmission line excited by a nonuniform electromagnetic field," *Antennas and Propagation, IEEE Transactions on*, vol. 13, no. 6, pp. 987 – 989, nov. 1965.

[73] C. Paul, "Frequency response of multiconductor transmission lines illuminated by an electromagnetic field," *Electromagnetic Compatibility, IEEE Transactions on*, vol. EMC-18, no. 4, pp. 183 –190, nov. 1976.

[74] F. Rachidi, C. Nucci, M. Ianoz, and C. Mazzetti, "Influence of a lossy ground on lightning-induced voltages on overhead lines," *Electromagnetic Compatibility, IEEE Transactions on*, vol. 38, no. 3, pp. 250 –264, aug. 1996.

[75] M. Master and M. Uman, "Lightning induced voltages on power lines: Theory," *Power Apparatus and Systems, IEEE Transactions on*, vol. PAS-103, no. 9, pp. 2502 –2518, sep. 1984.

[76] H. Koga, T. Motomitsu, and M. Taguchi, "Lightning surge waves induced on overhead lines," *Trans. ZECE Japan*, vol. E62, no. 04, April 1979.

[77] F. de la Rosa, R. Valdivia, H. Perez, and J. Loza, "Discussion about the inducing effects of lightning in an experimental power distribution line in mexico," *Power Delivery, IEEE Transactions on*, vol. 3, no. 3, pp. 1080 –1089, jul. 1988.

[78] V. Cooray and V. Scuka, "Lightning-induced overvoltages in power lines: validity of various approximations made in overvoltage calculations," *Electromagnetic Compatibility, IEEE Transactions on*, vol. 40, no. 4, pp. 355 –363, nov. 1998.

[79] B. Gustavsen and A. Semlyen, "Rational approximation of frequency domain responses by vector fitting," *Power Delivery, IEEE Transactions on*, vol. 14, no. 3, pp. 1052 –1061, jul. 1999.

[80] B. Gustavsen, "Improving the pole relocating properties of vector fitting," *Power Delivery, IEEE Transactions on*, vol. 21, no. 3, pp. 1587 –1592, jul. 2006.

[81] D. Deschrijver, M. Mrozowski, T. Dhaene, and D. De Zutter, "Macromodeling of multiport systems using a fast implementation of the vector fitting method," *Microwave and Wireless Components Letters, IEEE*, vol. 18, no. 6, pp. 383 –385, jun. 2008.

[82] B. Gustavsen, *User's guide for Vecfit3.m (Fast, Relaxed Vector Fitting) for Matlab*, SINTEF Energy Research, August 2008.

[83] M. Ishii and Y. Baba, "Advanced computational methods in lightning performance the numerical electromagnetics code (nec-2)," *IEEE Power Engineering Society*, vol. 4, pp. 2419 – 2424, 2000.

[84] Y. Baba and M. Ishii, "Numerical electromagnetic field analysis of lightning current in tall structures," *Power Delivery, IEEE Transactions on*, vol. 16, no. 2, pp. 324 –328, apr. 2001.

[85] L. Rickets, S. Bridges, and M. Mileta, *EMP Radiation and Protective Techniques*. New York: Wiley, 1976.

[86] M. Ianoz, C. A. Nucci, and F. M. Tesche, "Transmission line theory for field-to-transmission line coupling calculations," *Electromagnetics*, vol. 8, no. 2-4, pp. 171 – 211, 1988, field-to-Transmission Line Coupling;EMP-Power Lines Interaction;Excitation Sources;Validity Limits;Overhead Wires;Nuclear EMP Excitation;.

[87] F. Rachidi, "Lightning electromagnetic effects on overhead transmission lines. modelling and simulation," Ph.D. dissertation, Swiss Federal Institute of Technology, Laussane, December 1991.

[88] A. Gole and A. Daneshpooy, "Towards open systems: A pscad/emtdc to matlab interface," in *International Conference on Power Transients*, Seattle, 1997.

[89] H.-M. Ren, B.-H. Zhou, V. Rakov, L.-H. Shi, C. Gao, and J.-H. Yang, "Analysis of lightning-induced voltages on overhead lines using a 2-d fdtd method and agrawal coupling model," *Electromagnetic Compatibility, IEEE Transactions on*, vol. 50, no. 3, pp. 651 –659, aug. 2008.